(12)

NSWC TR 85-360

AD-A177 885

THE PROPERTIES OF CONDENSED EXPLOSIVES FOR ELECTROMAGNETIC ENERGY COUPLING

BY DOUGLAS G. TASKER

RESEARCH AND TECHNOLOGY DEPARTMENT

15 OCTOBER 1985

Approved for public release; distribution is unlimited.

DTIC
ELECTE
MAR 1 1 1987
S E

NAVAL SURFACE WEAPONS CENTER

Dahlgren, Virginia 22448-5000 • Silver Spring, Maryland 20903-5000

DTIC FILE COPY

UNCLASSIFIED
SECURITY CLASSIFICATION OF THIS PAGE

ADA177885

REPORT DOCUMENTATION PAGE

1a. REPORT SECURITY CLASSIFICATION Unclassified	1b. RESTRICTIVE MARKINGS
2a. SECURITY CLASSIFICATION AUTHORITY	3 DISTRIBUTION/AVAILABILITY OF REPORT Approved for public release; distribution is unlimited.
2b. DECLASSIFICATION/DOWNGRADING SCHEDULE	
4. PERFORMING ORGANIZATION REPORT NUMBER(S) NSWC TR 85-360	5. MONITORING ORGANIZATION REPORT NUMBER(S)
6a. NAME OF PERFORMING ORGANIZATION Naval Surface Weapons Center 6b. OFFICE SYMBOL (If applicable) R13	7a. NAME OF MONITORING ORGANIZATION
6c. ADDRESS (City, State, and ZIP Code) 10901 New Hampshire Avenue Silver Spring, Maryland 20904-5000	7b. ADDRESS (City, State, and ZIP Code)
8a. NAME OF FUNDING/SPONSORING ORGANIZATION Naval Sea Systems Command 8b. OFFICE SYMBOL (If applicable)	9. PROCUREMENT INSTRUMENT IDENTIFICATION NUMBER
8c. ADDRESS (City, State, and ZIP Code) Department of the Navy Washington, D. C. 20362	10. SOURCE OF FUNDING NUMBERS PROGRAM ELEMENT NO.: 6R21AC422, 6R19BB581 PROJECT NO: SR024-03, RF33-327 TASK NO: 61153N, PE62633N WORK UNIT ACCESSION NO.

11 TITLE (Include Security Classification)
The Properties of Condensed Explosives for Electromagnetic Energy Coupling (U)

12. PERSONAL AUTHOR(S)
Douglas G. Tasker

13a. TYPE OF REPORT	13b. TIME COVERED FROM TO	14. DATE OF REPORT (Year, Month, Day)	15. PAGE COUNT
		85/10/15	106

16. SUPPLEMENTARY NOTATION

17 COSATI CODES			18. SUBJECT TERMS (Continue on reverse if necessary and identify by block number)
FIELD	GROUP	SUB-GROUP	

19. ABSTRACT (Continue on reverse if necessary and identify by block number)

The principal objective of this work is to intensify and tailor the detonation wave output of condensed high explosives (HE's) through the use of electromagnetic energy coupling (EMEC) or augmentation. This results in the enhancement of the explosive's energy release properties.

The reasons for studying EMEC phenomena in a detonating explosive, are to improve the safety, performance and understanding of explosives. The technique would allow the use of low performance, yet safe explosives, in high performance applications.

From the beginning of 1985, the research has been divided into two parallel efforts. These are research into the fundamental physics of EMEC phenomena and applications of the physics to obtain measurable enhancements. Within the basic research program, the electrical properties of HE's are being studied. The spacial and temporal distributions of conductivity are being determined experimentally and compared with theoretical predictions. These, in turn, will be used to examine models of chemical reaction pathways within the detonation zone

20. DISTRIBUTION/AVAILABILITY OF ABSTRACT	21 ABSTRACT SECURITY CLASSIFICATION
☐ UNCLASSIFIED/UNLIMITED ☐ SAME AS RPT ☐ DTIC USERS	
22a. NAME OF RESPONSIBLE INDIVIDUAL	22b. TELEPHONE (Include Area Code) / 22c. OFFICE SYMBOL

DD FORM 1473, 84 MAR — 83 APR edition may be used until exhausted. All other editions are obsolete.

SECURITY CLASSIFICATION OF THIS PAGE

0102-LF-014-6602

UNCLASSIFIED

FOREWORD

This report describes recent research studies designed to understand and obtain the enhancement of the performance of detonating high explosives by electrical means. The improved performance is obtained by the deposition of electrical energy into the reaction zone of the detonating explosive. This leads to improved safety and also expands our understanding of the detonation process itself.

This work was performed for and funded by two programs. The Naval Sea Systems Command Task 61153N, SR 024-03 supported the majority of the work, especially in the 6.1 category. The Office of Naval Research under PE62633N, Subproject RF33-327, provided the support for the 6.2 effort.

J. Goforth (LANL) has made many valuable contributions to the programs through research and numerous helpful discussions related to the pulse power research. He shared in the experimental effort reported in Chapter 4, and performed the experimental work reported in Chapter 5. The author is indebted to H. Gillum, W. Freeman, J. Roscher, R. Baker and the late C. Sorrels for the excellence of their experimental support. M. Ginsberg (LANL) deserves credit for his support and many helpful discussions. Thanks are due to D. Demske for his contributions at the beginning of the 6.1 Program. R. J. Lee deserves great credit for the excellence of his recent work in both programs. Special thanks are due to J. W. Forbes who has made significant contributions with his technical expertise, his enthusiasm, and his contributions to the theory. Last, but by no means least, Connie Cronin and Marie Incarnato are to be applauded for their efforts in the formidable task of preparing this manuscript.

Accession For
NTIS GRA&I
DTIC TAB
Unannounced
Justification
By
Distribution /
Availability Codes
Dist | Avail and/or Special
A-1

DTIC COPY INSPECTED

Approved by:

KURT F. MUELLER, Head
Energetic Materials Division

CONTENTS

Chapter		Page
1	INTRODUCTION	1-1
2	COAXIAL ELECTRODE CONDUCTIVITY MEASUREMENT	2-1
3	COINCIDENCE OF ARRIVAL OF THE DETONATION WAVE AND THE CONDUCTION ZONE	3-1
4	CONDUCTIVITY/ENHANCEMENT EXPERIMENTS IN PARALLEL ELECTRODE GEOMETRIES	4-1
5	ANOMALIES IN THE MEASUREMENT OF THE RESISTANCE OF PBX 9501	5-1
6	PLASTICS CONDUCTIVITY MEASUREMENTS	6-1
7	PULSED POWER EQUIPMENT, DESIGN AND DEVELOPMENT	7-1
8	SHOCK AIR RESISTANCE EFFECTS	8-1
9	SUMMARY	9-1

Appendix		Page
A	VOLTAGE MEASUREMENTS	A-1
B	COAXIAL FUSE, THEORY AND DESIGN	B-1
C	ROGOWSKI COIL CURRENT MONITORS, ERROR ANALYSIS AND IMPROVEMENTS	C-1

ILLUSTRATIONS

Figure		Page
2-1	COAXIAL EXPLOSIVE ASSEMBLY	2- 2
2-2	ELECTRICAL CIRCUIT	2- 4
2-3	V-I DATA, PBX-9404, EARLY DATA	2- 6
2-4	ELECTRICAL CIRCUIT	2- 9
2-5	VOLTAGE ACROSS COAXIAL EXPLOSIVE ASSEMBLY	2-11
2-6	PBX-9404 DATA WITHOUT AIR EFFECTS	2-12
3-1	ALIGNMENT OF PIEZOELECTRIC AND IONIZATION PINS	3- 2
3-2	COINCIDENCE EXPERIMENT	3- 2
3-3	COAXIAL COUPLING OF CIRCUITRY	3- 3
3-4	OSCILLOSCOPE RECORD	3- 4
4-1	PARALLEL PLATE EXPERIMENT	4- 2
4-2	GUARD-RAIL MODIFICATION TO PARALLEL PLATE EXPERIMENT	4- 3
4-3	TOP VIEW OF GUARD-RAIL MODIFICATION	4- 4
4-4	PRODUCT GAS BREAKDOWN, DC18	4- 6
5-1	RESISTANCE MEASUREMENT OF DETONATING PBX-9501	5- 2
5-2	VARIATION OF RESISTANCE WITH THICKNESS	5- 3
5-3	CROSS-SECTION OF DETONATING PBX-9501 BETWEEN ELECTRODES	5- 4
5-4	RADIAL EXPANSION OF DETONATION	5- 5
5-5	ACTUAL AND CALCULATED VARIATION OF RESISTANCE WITH TIME	5- 7
5-6	VOLTAGE AND CURRENT WAVEFORMS	5- 8

ILLUSTRATIONS (Cont.)

Figure		Page
6-1	ELECTRODE/PLASTIC ASSEMBLY	6- 2
6-2	EXPERIMENTAL ARRANGEMENT	6- 3
6-3	MEASUREMENT CIRCUIT	6- 3
6-4	VOLTAGE AND CURRENT RECORDS, LEXAN, E 495B	6- 5
7-1	INTERMEDIATE STORAGE INDUCTOR CIRCUIT, SCHEMATIC	7- 2
7-2	VOLTAGE AND CURRENT DATA, EC17	7- 4
7-3	NEW 40kV CAPACITOR SYSTEM	7- 7
8-1	EFFECTS OF AIR GAP	8- 2
8-2	COAXIAL CONDUCTIVITY MEASUREMENT	8- 3
8-3	PBX-9404 DATA WITHOUT AIR EFFECTS	8- 4
A-1	VOLTAGE PROBE CIRCUIT	A- 2
A-2	VOLTAGE PROBE EQUIVALENT CIRCUIT	A- 3
A-3	VOLTAGE PROBE CIRCUIT	A- 6
B-1	INTERMEDIATE STORAGE INDUCTOR CIRCUIT, SCHEMATIC	B- 2
B-2	CROSS SECTION OF LINEAR FUSE ASSEMBLY	B- 4
B-3	EACB AND LINEAR FUSE RESPONSE	B- 5
B-4	CURRENT - TIME INTEGRAL	B- 6
B-5	EACB/FUSE INTERACTION	B- 8
B-6	NSWC COAXIAL FUSE ASSEMBLY	B-10
B-7	COAXIAL FUSE RESPONSE	B-11
C-1	TOROIDAL COIL	C- 2
C-2	ROGOWSKI COIL	C- 5
C-3	ROGOWSKI COIL INTEGRATOR	C- 6

ILLUSTRATIONS (Cont.)

Figure		Page
C-4(a)	ROGOWSKI COIL MEASUREMENT CIRCUIT	C- 8
C-4(b)	EQUIVALENT CIRCUIT	C- 8
C-5	COAXIAL CABLE CONNECTIONS	C-11
C-6	OPTIMIZED COMPLETE CIRCUIT	C-12

TABLES

Table		Page
2-1	COAXIAL APPARATUS DIMENSIONS	2- 3
4-1	SUMMARY OF "GUARD-RAIL" EXPERIMENTAL RESULTS	4- 8
C-1	NSWC ROGOWSKI COIL PARAMETERS	C- 9
C-2	INDUCTANCE CALCULATION DATA	C-14

CHAPTER 1

INTRODUCTION

OBJECTIVE

The principal objective of this work is to intensify and tailor the detonation wave output of condensed high explosives (HE's) through the use of electromagnetic energy coupling (EMEC) or augmentation. This results in the enhancement of the explosive's energy release properties.

The reasons for studying EMEC phenomena in a detonating explosive are to improve the safety, performance and understanding of explosives. The technique would allow the use of low performance yet safe explosives in high performance applications. The performance would be improved by the redirection of the available explosive's chemical energy to enhance its power at the prescribed time and place. A significant fraction of the chemical energy would be converted to electromagnetic energy using devices such as Compressed Magnetic Flux Generators. This energy would then be redirected into the detonation zone towards the latter stages of its travel, thereby improving its performance.

ELECTRICAL POWER IN DETONATING HIGH EXPLOSIVES

The concept depends on the excellent electrical properties of detonating HE's. The unreacted HE and the detonated product gases both possess good dielectric breakdown properties comparable with polyethylene in performance. The reaction zone of the HE, on the other hand, has an electrical conductivity of the order of 10^4 mhos/m. If the HE is subjected to an electric field then current flows only in the reaction zone which may be no more than 0.1mm wide; the subsequent power density may be very high. It can be shown that P_{elec}, the electrical power deposited per unit area in the HE, is:

$$P_{elec} = \sigma \Delta E^2$$

where σ is the electrical conductivity, Δ the conduction zone width and E the applied electric field. This electrical power can be very large (circa 10^{15} W/m^2) so that the resultant improvements in performance can be significant.

RESEARCH PROGRAMS

From the beginning of 1985 the work has been divided into two parallel efforts. These are research into the fundamental physics of EMEC phenomena and application of the physics to obtain measurable enhancements. Within the

basic research program, the electrical properties of HE's are being studied. The spacial and temporal distributions of conductivity are being determined experimentally and compared with theoretical predictions. These in turn will be used to examine models of chemical reaction pathway; within the detonation zone.

MEASUREMENT OF ELECTRICAL PROPERTIES OF EXPLOSIVES

In this report the various measurements of electrical conductivity in detonating HE's at very high current densities (circa 10^9 to 10^{11} A/m^2) are described. These measurements are made extraordinary difficult by the combination of large rapidly changing electrical currents (and voltages) with the already hostile environment of a detonating explosive. The difficulties imposed by these conditions are described as well as the techniques that have been developed to surmount them.

DIELECTRIC PROPERTIES OF EXPLOSIVES

The dielectric properties of unreacted HE's and product gases are also under study, these are reported in a separate report.[1] This work is proving itself to be of great benefit to the hazards community as it is improving our knowledge of electrostatic phenomena in energetic materials.

STRUCTURE OF THE REPORT

Conductivity of Detonating Explosives

Conductivities have been measured for a number of explosives although these studies have concentrated on just two: PBX-9404 and PBX-9501; the results for these are reported here. They have been measured in coaxial and parallel electrode geometries. The products of conductivity and conduction zone width are typically 1-2 mhos. consequently conductivities may be as high as 2×10^4 mhos/m.

Coincidence of Arrival of the Detonation Wave and the Conduction Zone

The coincidence of arrival of the pressure wave and conduction front has been measured to be within 0.5 nsecs. This measurement is described together with its relevance for Energy Coupling theory.

Performance Enhancement of PBX-9501

Measurable performance enhancements of PBX-9501 have been obtained which demonstrate that the technique is viable. Moreover, these measurements are in good agreement with calculations. The progress in this work is reported together with plans to obtain larger enhancements.

Anomalies Attributed to Conduction in Gases and Plastics

Anomalies due to conduction within shocked gases and plastics have been observed. The measurement of the electrical conductivities of shocked

plastics and air are, therefore, of great importance to the program; this work is also reported.

Apparatus and Instrumentation

Three appendixes are included to cover some of the more detailed aspects of the apparatus and instrumentation developed for this program. These include the measurements of voltage in rapidly changing magnetic fields, the design of coaxial fuses for large magnetic fields and the use of Rogowski cost current monitors.

Outlook

The future for EMEC looks bright; no fundamental difficulties can be identified that would mitigate against the successful application of the technique. The physics of the enhanced detonation phenomena are fascinating; irrespective of the success of the program, our understanding of detonation physics as a whole will be substantially improved by this work.

CHAPTER 2

COAXIAL ELECTRODE CONDUCTIVITY MEASUREMENT

BACKGROUND

It has long been known that the reaction zone between the shock front and the CJ plane of a detonating explosive is an electrical conductor, whereas the gaseous detonation products and the unreacted explosive are insulators.[2-4]

The rate of dissipation of electrical energy, the electric power dissipation, is the fundamental parameter which determines the efficacy of Energy Coupling by Joule heating. When an electric field E is applied, the Joule heat dissipated in a unit cross section is expressed as P watts,

$$P = \sigma E^2 \Delta$$

where σ is electrical conductivity, Δ is the effective conduction zone thickness parallel to the detonation velocity vector.

It is assumed that the detonation wave is planar and that the electric field, to which the unreacted explosive is subjected, is not limited by conduction in the reaction zone behind it or in the product gases beyond. Clearly, the magnitude of the conductivity is of fundamental importance.

Measurements of the conductivity of PBX-9404 at currents up to 10kA have been reported in the open literature.[2] This early work is described below.

EXPERIMENTS

The resistance of the conduction zone in PBX-9404 was measured in the coaxial configuration shown in Figure 2-1. Two sizes of apparatus were used; both were point initiated at one end with a CH-6 booster pellet and an RP80 detonator. The explosive was confined within a brass or copper tube which served as the ground electrode. Dimensions of the two assemblies are given in Table 2-1.

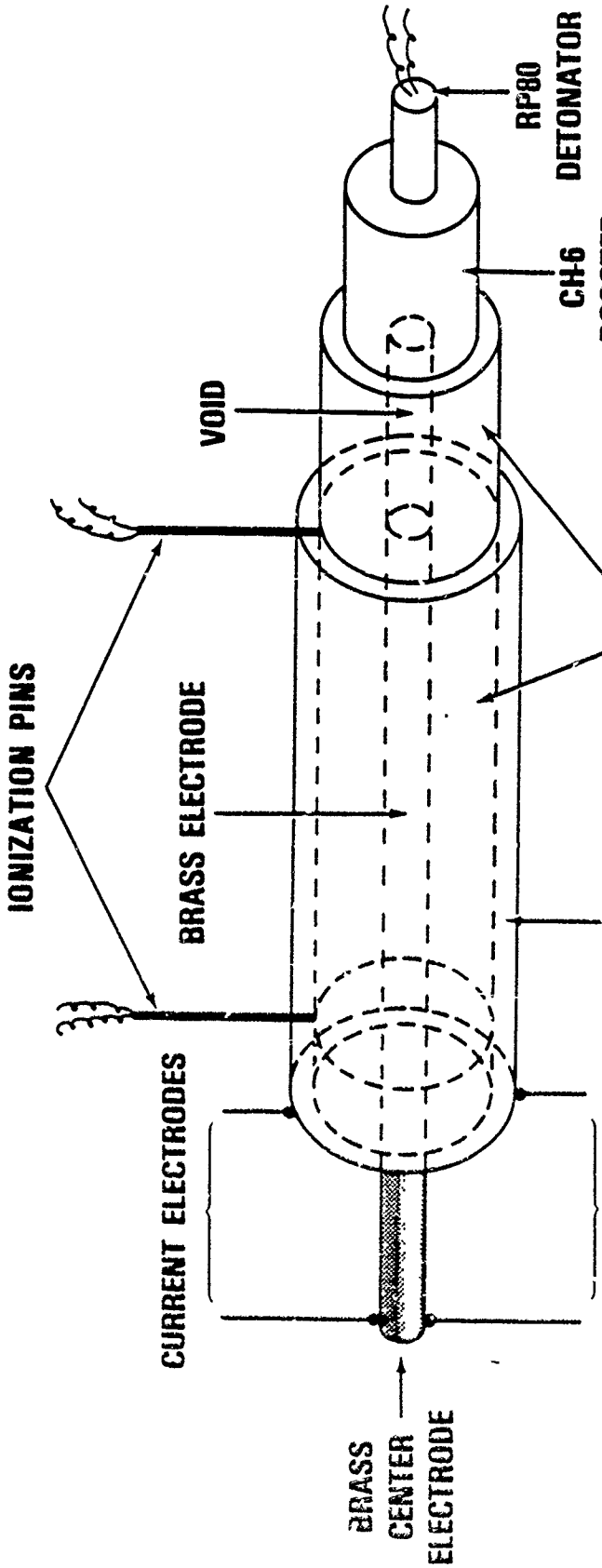

FIGURE 2-1. COAXIAL EXPLOSIVE ASSEMBLY

TABLE 2-1. COAXIAL APPARATUS DIMENSIONS

Explosive Diameters Inside (mm)	Outside (mm)	Explosive Weights (g)	Copper Tube Length (mm)	Wall Thickness (mm)
3.1	14.0	33	100	1.5
11.5	30.2	140	75	1.5
Explosive length 127 mm Explosive density 1.82 g/cm^3				

IONIZATION PINS

Two ionization pins were used to establish the position of the detonation front; they were positioned carefully in contact with the outer surface of the explosive by insertion through the copper tube wall; each was 0.8 mm in diameter. One pin was placed 0.4 mm away from the detonator end of the tube; the other was precisely aligned with the rear end of the charge. The latter was recessed 0.4 mm inside the tube to facilitate insulation of the electrodes; the cavity was filled with a silicone rubber insulator (Dow Corning 3145) and thus premature surface breakdown was prevented.

ELECTRICAL CIRCUIT

The electrical circuit is shown in Figure 2-2. A 57 μF, paper capacitor was charged to 5 kV via a large resistor. The capacitor was discharged at the appropriate time by a hydrogen thyratron (5C22). Thus a 5 kV potential difference was presented across the explosive, the current was zero, prior to the time of entry of the detonation wave into the copper tube. Note that the unreacted explosive behaves like a good insulator.

CURRENT AND VOLTAGE MEASUREMENT

Current in the reaction zone was measured with a Pearson 301X current transformer; it was positioned around the ground lead of a coaxial cable (RG213) connecting the thyratron to the explosive. Voltage probe leads were connected separately in a four-probe arrangement so as to avoid contact errors. In view of the difficulties associated with measuring high voltages, especially in an explosive environment, the voltage between electrodes was measured using several independent voltage probes. These probes were of two types. The first was a pair of Tektronix P6015 1000X, 100MΩ, 20kV probes used in differential mode and coupled direct to the oscilloscopes; no ground connection was made to the equipment. The second was manufactured from a TRW high voltage potential divider of 26.5kΩ resistance. This was modified by the addition of a Tektronix P6042 current probe which facilitated the measurement of current in the divider without connection to the ground. Consequently both probes were devoid of ground loop errors.

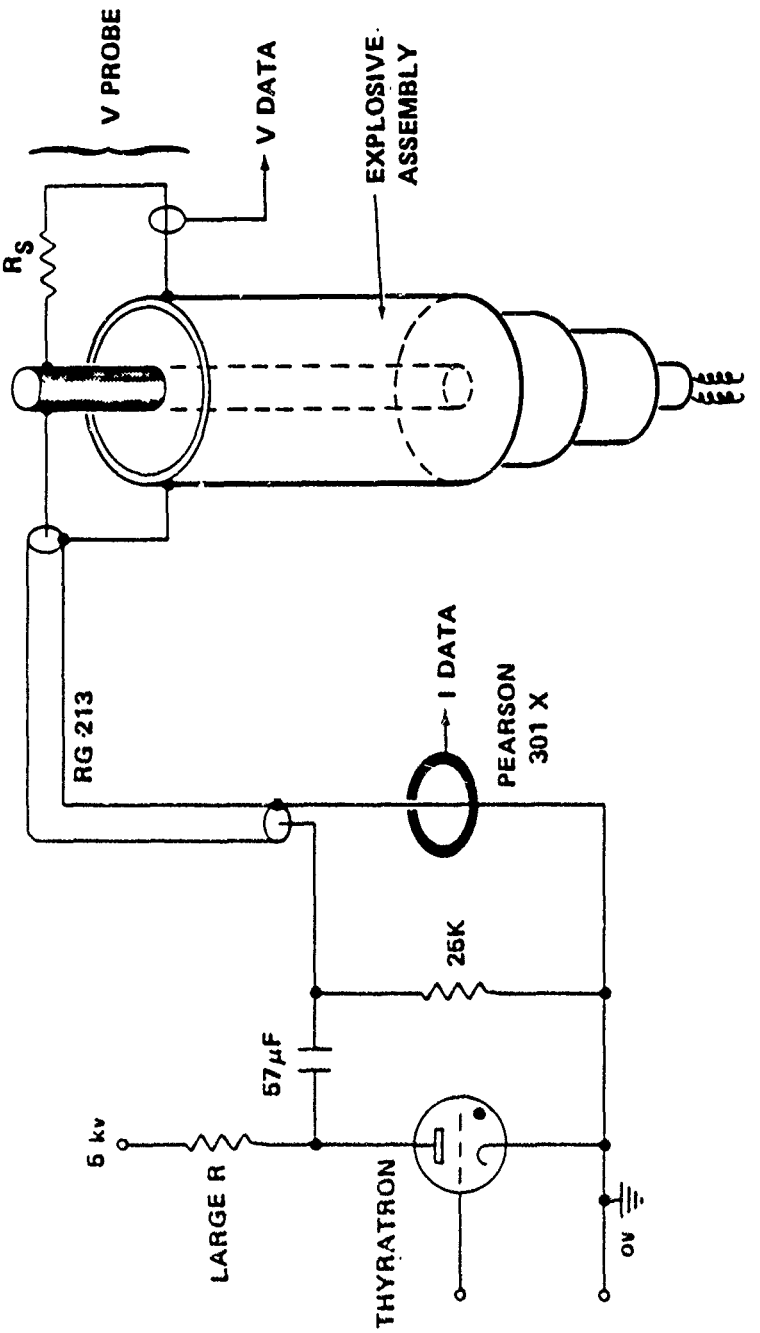

FIGURE 2-2. ELECTRICAL CIRCUIT

Current and voltage data were recorded on Nicolet series III transient recording oscilloscopes and a Tektronix 7633 storage oscilloscope.

EQUIVALENT CIRCUIT

The equivalent circuit of the thyratron, capacitor and coaxial cable was characterized prior to each shot by short-circuiting the cable, at the load end, and discharging the capacitor through the short-circuit. The current flow i(t) can accurately be described by a damped sine wave of the form:

$$i(t) = i_0 \sin w_0' t \; e^{-Rt/2L}$$

where

$$w_0' = w_0 \sqrt{1 - 1/4q^2} \;, \quad q = \frac{w_0 L}{R} \;,$$

$$w_0 = \sqrt{\frac{1}{LC}} \;, \quad i_0 = \frac{V_0}{w_0 L}$$

and V_0 is the initial voltage on the capacitor.

SEQUENCE OF EVENTS

When the explosive is detonated, the current begins to flow when the wave enters the copper tube, but is limited by the inductance of the circuit as described above. Current and voltage therefore rise gradually during the course of the experiment. The initial rate of current rise is 1.2×10^9 A/sec; the current rises to 8kA in 10μsecs. Thus a graph of voltage versus current can be obtained for a range of currents, from zero to 8kA, by monitoring current and voltage with time.

EARLY RESULTS

One set of voltage-current data is shown in Figure 2-3. At time t = 0 the thyratron was triggered. Several microseconds later the detonation wave reached the copper tube, the explosive began to conduct current and the voltage across it fell from 5 kV to near zero.

The voltage and current then increased gradually. For the duration of the transit of the detonation wave in the tube the voltage-current (V-I) relationship was observed to be linear, thus obeying Ohm's law. When the wave exited the tube the current rapidly dropped to zero and the voltage rose towards 5 kV. Re-strike often occurred a few microseconds later, caused by shock wave initiated conduction of the silicone rubber insulator.

The ionization pin switching times are superimposed on Figure 2-3; they confirm that the linear ohmic portion of the V-I plot truly corresponds to the detonation wave transit inside the copper tube. Detonation wave curvature and

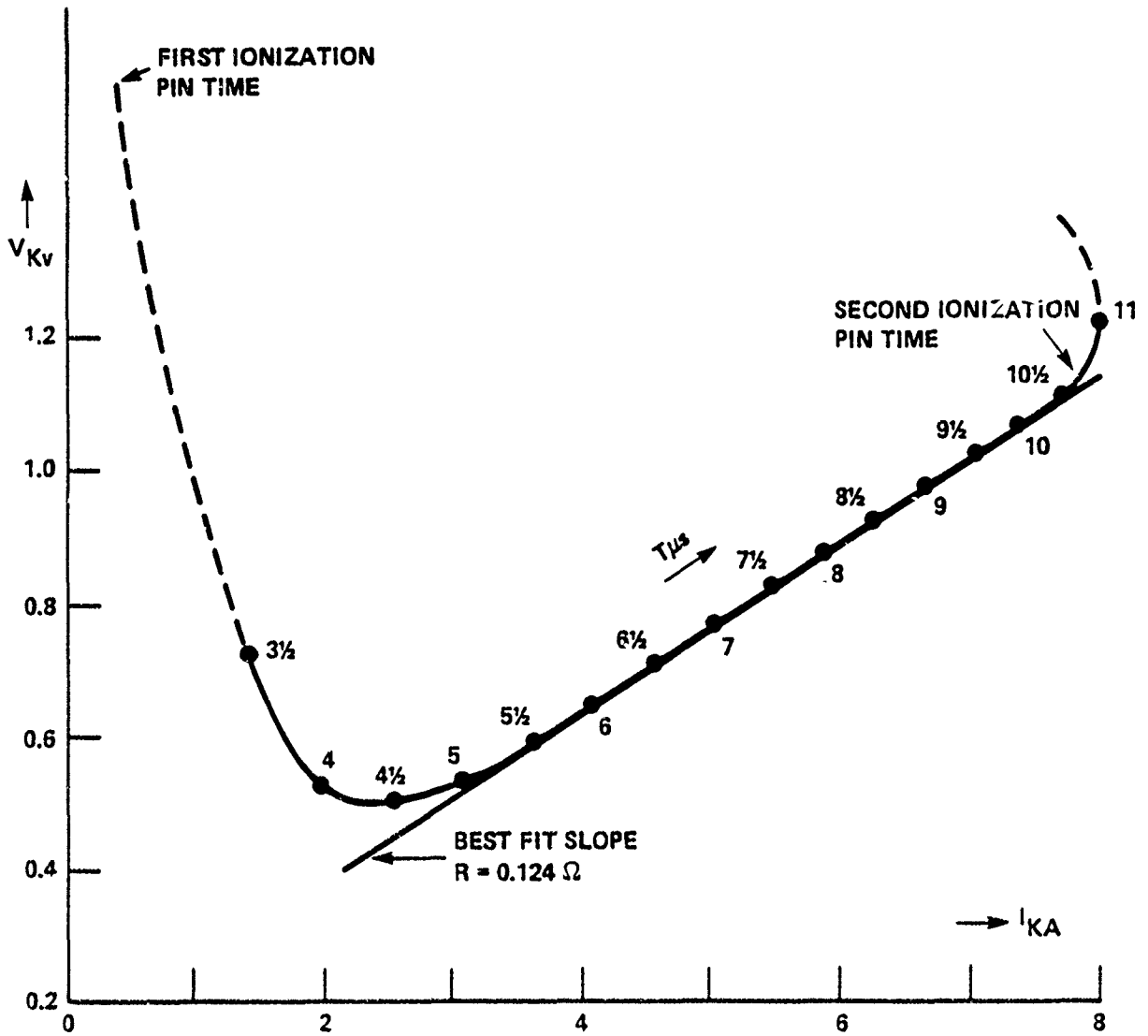

FIGURE 2-3. V-I DATA, PBX-9404, EARLY DATA

dropping instantaneously upon entry of the detonation wave into the tube. These limitations are discussed in Appendix A. At the time of detection of exit, however, the shock curvature cannot limit the response, and the voltage rise and ionization pin times matched closely (within the precision of the experiment). The current record did not suffer the same limitations; current switch-on and switch-off times matched the ionization pin records.

The characteristics of the original voltage probes were such that they did not operate at frequencies below 100 Hz. As a consequence, the linear V-I data did not extrapolate through the origin, and a voltage error existed at zero current. However, the voltage probes gave identical linear slopes despite differences in voltage errors. Moreover, these errors varied randomly, from experiment to experiment, whereas the slopes did not. Voltage data calculated from the equivalent circuit model of equation (2) also closely matched the linear slopes; this gave added confidence in the validity of the V-I data.

In a coaxial geometry with internal radius r_1, external charge radius r_2, the resistance R will be, for a plane conduction front:

$$R = \frac{\ln r_2/r_1}{2\pi\sigma\Delta}, \qquad (3)$$

where σ is the average conductivity and Δ the effective conduction zone width product. The measured resistances of the larger apparatus had a mean value of 0.127Ω and for the smaller apparatus 0.206Ω. Incorporating these results into equation (3), we find that the calculated products, $\sigma\Delta$, are not significantly different at the 99% level of significance. Incorporating all results for both configurations, we obtain a mean product for PBX-9404 of:
$\sigma\Delta$ = 1.246 mho with a computed standard error of the mean of 0.017 mho based on 32 degrees of freedom.

The current and ionization pin switching times matched to within the precision of the experiment (0.1 μs) so that the effective conduction zone width is less than 1 mm. Consequently, the current density is of the order of $\sim 10^9$ A/m^2 and the conductivity $\sigma > \sim 10$ mho/cm. Little precision can be assumed for these separate estimates of σ and Δ because no allowances have been made for shock wave curvature and spatial dependence.

RECENT EXPERIMENTS

Sufficient improvements have been made in the precision of voltage measurements (Appendix A) and in time resolution to warrant further tests (the time resolution has been improved to 50 nsecs for current and voltage measurements).

The resistance of the conduction zone was measured in a coaxial configuration similar to that of the earlier experiments. In such high current experiments unwanted capacitive and inductive effects can be significant. To minimize inductive effects a new stripline configuration was employed for electrical connection to the explosive. A significant

employed for electrical connection to the explosive. A significant contribution to resistance due to shocked air between the explosive and the outer cylindrical electrode has been observed. This has been reduced to a minimum by careful machining of the explosive and tube so that they have matching tapers of approximately 1 μm diameter per mm length. The explosives are forced into the tubes; thus, intimate contact between explosive and tube is achieved. It has not been possible to taper the center electrode although it is tightly fitted into the explosive (see Chapter 8).

CURRENT MEASUREMENT

Current flow in the conduction zone was measured at the source end of the circuit, using a calibrated current transformer, Pearson Model 110A. The equivalent circuit of the capacitor, cables and stripline was obtained prior to each shot by discharging the capacitor through a short circuit as in the earlier experiments. These data were used to verify the validity of the V-I data as described previously.

VOLTAGE MEASUREMENT

The accurate measurement of voltage in these high current experiments is extremely difficult. A detailed discussion of these problems and solutions is given in the Appendix A. The voltage probe was manufactured from a copper sulphate resistor (500Ω to 1000Ω) and a Pearson current transformer, model 411. Thus, no ground loops existed in the measurement circuits. The resistance of the copper sulphate R_{CuSO_4} was measured using a

Hewlett Packard LCZ bridge, model HP 4227A, over a range of frequencies between 10KHz and 1MHz. From this resistance and the sensitivity of a Pearson 411, the sensitivity of the probe could be calculated. It was typically 11.5 kV/V. This sensitivity was verified at the time of firing by comparison of the known capacitor bank charging voltage and the voltage signal measured by the probe. These data always agreed to within 1%.

MEASUREMENT CIRCUIT

The apparatus for measuring the resistance of detonating explosives is shown schematically in Figure 2-4. The stripline was 1m long with an inductance from input to load of 4nH. Coaxial high voltage connectors joined the capacitor bank and the voltage probe to the stripline. The explosive was fitted into a brass tube of 14.0 mm internal diameter and had a 3.175 mm diameter brass central electrode. Brass plumbing compression fittings were adapted to connect the electrodes to the stripline, and metal to metal contact resistances were less than 10 μΩ throughout.

In one series of experiments, a 57μF paper capacitor was charged to 5kV via a large resistor. The capacitor was subsequently switched by a hydrogen thyratron, 4C35, to the explosive load. In another series of experiments current was switched to the load via an intermediate storage inductor from a 5kV, 8.6 mF capacitor bank (see Chapter 7 for details of the pulsed power experiment). When the detonation wave entered the coaxial assembly, current and voltage data were obtained as the wave swept the length of the explosive.

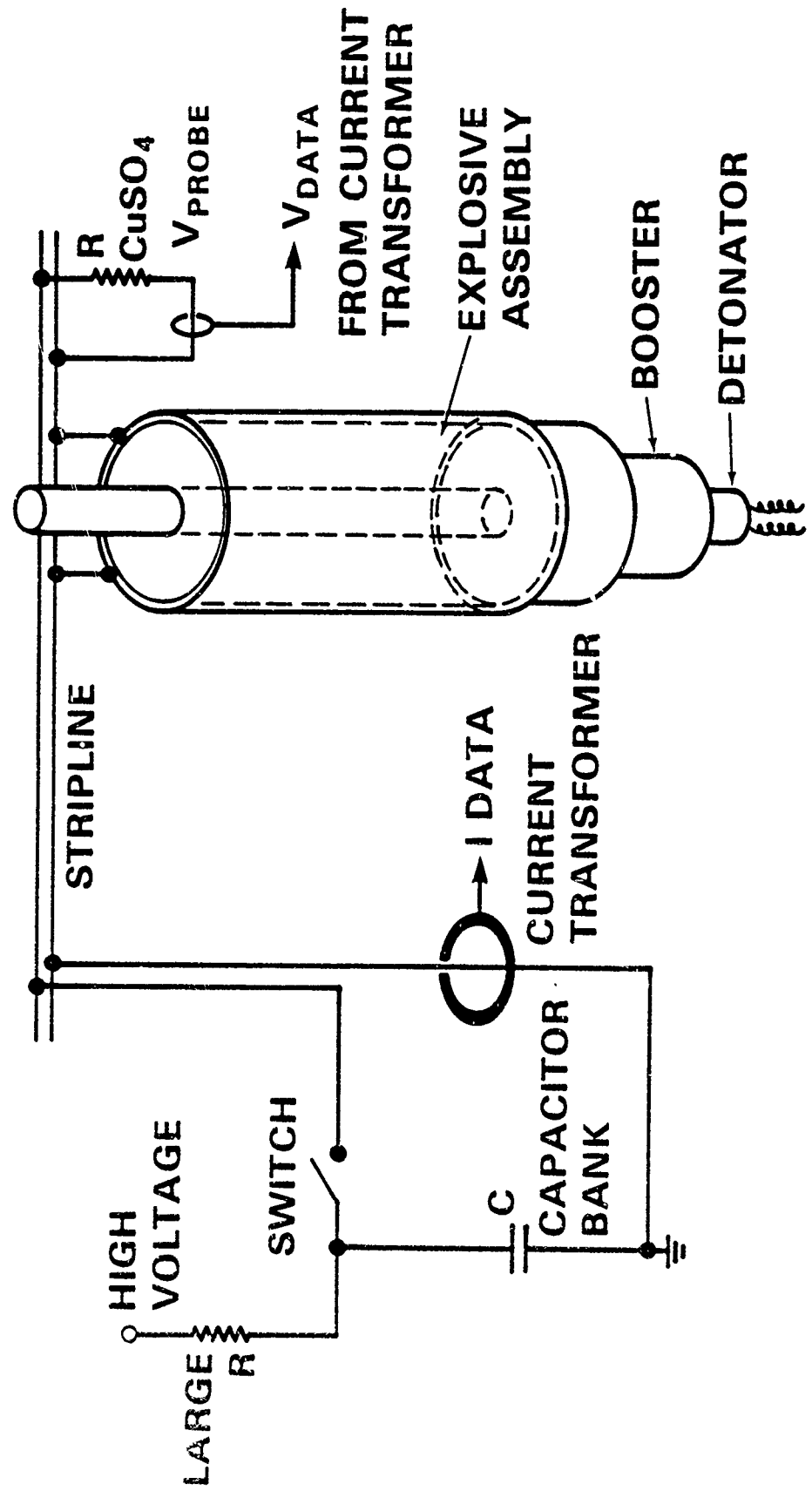

FIGURE 2-4. ELECTRICAL CIRCUIT

INDUCTIVE EFFECTS IN THE EXPLOSIVE TUBE

The magnetic flux, ϕ, stored between the coaxial electrodes introduces a voltage, $d\phi/dt$. As the detonation wave progresses, the inductance between them diminishes from 34 nH to zero. These effects cannot be eliminated but have been accurately quantified by calculation and direct measurement; all voltage records are corrected for this effect which is always less than 10% of the true data. Consider the circuit of Figure 2-5. Here the voltage V measured across the coaxial explosive assembly comprises two parts:

$$V = r_x + \frac{d}{dt}(Li)$$

where the first part is the desired potential difference across the explosive load ir_x and $\frac{d}{dt}(Li)$ is the voltage change due to the change in flux ϕ in the tube. Now

$$\frac{d}{dt}(Li) = L\frac{di}{dt} + i\frac{dL}{dt}.$$

The inductance L diminishes with time as the detonation wave travels towards the stripline. Thus:

$$L = \frac{\mu_o}{2\pi}(l - Dt)\ln r_2/r_1,$$

where μ_o is the permittivity of free space; r_2 and r_1 are the radii, l the original length of the tube between the point of detonation entry in the explosive to the stripline, D the detonation velocity and t the time. Hence:

$$V = ir_x + \frac{\mu_o}{2\pi}\ln\frac{r_2}{r_1}\left[(l - Dt)\frac{di}{dt} - iD\right].$$

Note that the effective resistance is reduced by δr even when $\frac{di}{dt} = 0$, where

$$\delta r = D\frac{\mu_o}{2\pi}\ln r_2/r_1 ;$$

δr is typically 2.6 mΩ.

This expression is evaluated numerically for each record. The validity of the original effective length, l, has been tested by a direct measurement of inductance in a calibration fixture. The fixture was an identical coaxial electrode configuration with the detonation zone represented by a sliding metal piston. By measuring the inductance with the HP 4227A bridge, for different piston positions an accurate r_2/r_1 ratio, and any equivalent stray inductance due to end effects, could be obtained. The measured data agreed

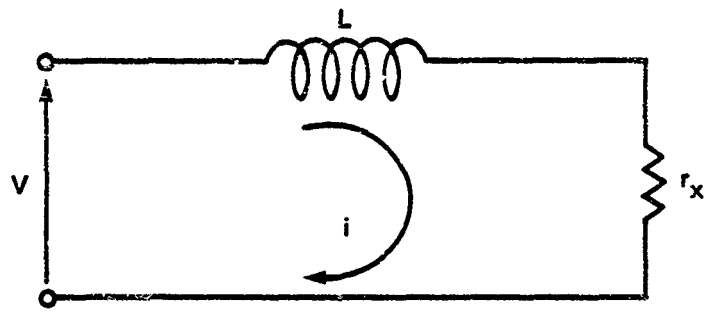

FIGURE 2-5. VOLTAGE ACROSS COAXIAL EXPLOSIVE ASSEMBLY

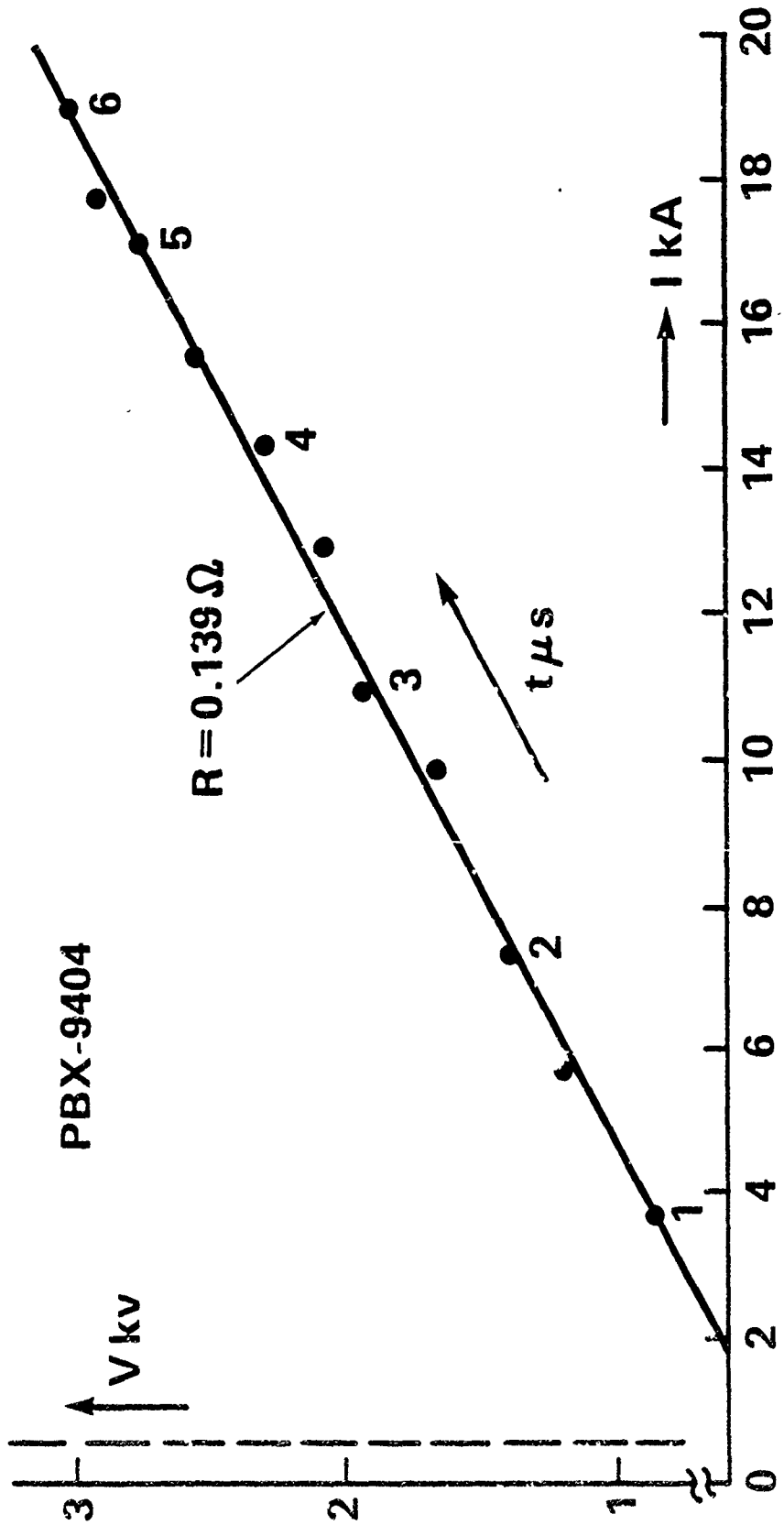

FIGURE 2-6. PBX-9404 DATA WITHOUT AIR EFFECTS

with calculation to within 0.1%. End effects were less than 1nH.

Results for PBX-9404. The results for the tapered coaxial assembly are shown in Figure 2-6. Corrections have been made for the inductive effects, $d\phi/dt$, described above. The Voltage-Current plot shows excellent linearity. Here R = 0.139 Ω with a standard error of 0.003 Ω. Using

$$R = \frac{\ln r_2/r_1}{2\pi\sigma\Delta} ,$$

we find the conductivity conduction zone width product to be $\sigma\Delta$ = 1.70 mho (with an estimated standard error of 0.05 mho) which is higher than previously reported, i.e. 1.25 mho.[5] In the earlier work no taper was used and the explosive had to be made with an air gap of approximately 10 μm to facilitate assembly. From the work presented in Chapter 8, a 10 μm gap would increase the resistance by approximately 0.06 Ω which is in excellent agreement with the data, i.e. previously R = 0.206 Ω and not 0.139 Ω as above. The early work incorporated no corrections for the effects described previously due to flux changes in the coaxial electrodes. Moreover, the instrumentation at that time suffered from the effects due to mutual inductance and capacitance described in Appendix A. The use of the tapered electrodes has clearly eliminated the air resistance problem.

SUMMARY

From the results of the electrical resistance measurements a number of important conclusions can be drawn.

(1) The electrical conductivity zone x width product, $\sigma\Delta$, is 1.70 mhos.

(2) From these data the voltage-current plot is linear. Hence, for currents from zero to 20KA, Ohm's law applies. This current range can be translated to a current density for the electrode diameters of 14.0 mm and 3.175 mm and a conduction zone width of 0.1 mm (this width is based on estimated detonation zone widths[6]). The current density at the surface of the center electrodes thus ranges from zero to 2.2×10^{10} A/m^2. (The maximum current density achievable before dielectric breakdown of the explosive is of the order of 10^{11} A/m^2).

(3) Within the precision of the experiment, the current flow starts and stops abruptly as the detonation wave enters and exits the coaxial electrode assembly. Moreover, the resistance is constant for the duration of the detonation wave transit.

There is, therefore, strong evidence that conduction is confined to a narrow zone coincident with the reaction zone. These findings are further supported by measurements of coincidence between the shock wave and conduction waves, Chapter 3.

(4) Using $\sigma\Delta = 1.70$ mhos and a dielectric strength of PBX-9404 of 2.2×10^7 V/m, the maximum attainable electrical power dissipation can be calculated for PBX-9404,[5] to be

$$P = \sigma\Delta E^2 = 8.2 \times 10^{14} \text{ W/m}^2.$$

CHAPTER 3

THE COINCIDENCE OF ARRIVAL OF THE DETONATION WAVE AND THE CONDUCTION ZONE

The coincidence of arrival of the detonation wave (strictly the Von-Neumann Spike) and the conduction zone has not been previously reported. This information is crucial to a complete understanding of the physical processes of conduction in detonating explosives. Previous experiments have used ionization pins in the side of the explosive to monitor shock wave arrival times, see Chapter 2. However, high resolution timing data can only be obtained with ionization pins aligned normal to direction of wave travel so that the detonation wave impacts across the total surface of the pins simultaneously (see Figure 3-1). The measurement was made under zero enhancement conditions.

EXPERIMENT

An ionization pin and a piezoelectric (PZT) pin, to monitor the arrival of the conduction and shock fronts respectively, were placed at the end of the coaxial explosive assembly described in Chapter 2, Figure 3-2; here again PBX-9404 was the explosive. The pins were supported in a polycarbonate (Lexan) insulator (not shown) in closely fitting holes; thus, the pins were constrained to lie on exactly the same radius from the center of the explosive and errors due to shock wave curvature were minimized. Signal reflection times for the open circuited pins were adjusted to match as closely as possible. All leads were exactly matched in length; short links were added to obtain coincidence in reflections within 0.2 nsecs, the resolution of the oscilloscope. All components were carefully assembled in a coaxial network as shown in Figure 3-3. The signals were observed using a Tektronix 400 MHz oscilloscope, 7844, with 7A16A plug-ins. Calibration experiments were performed using small exploding bridgewire detonators with small discs of aluminum foil on their ends; consequently, a simultaneous arrival of shock and conduction fronts was simulated. Other experiments were performed to determine the degradation of signal risetime with cable length. Cable lengths were adjusted to give optimum risetimes. Consequently, the two circuits were matched as closely as possible in terms of signal delay and signal risetime. In some experiments a 9.0 nsecs delay was added to the PZT pin cable to facilitate triggering from the ionization pin circuit. This delay must be subtracted from the oscilloscope traces to restore the traces of two records to apparent coincidence.

RESULTS AND DISCUSSION

Within the resolution of the experiment, coincidence was measured to within 0.6 nsecs for PBX-9404, see Figure 3-4. This corresponds to a

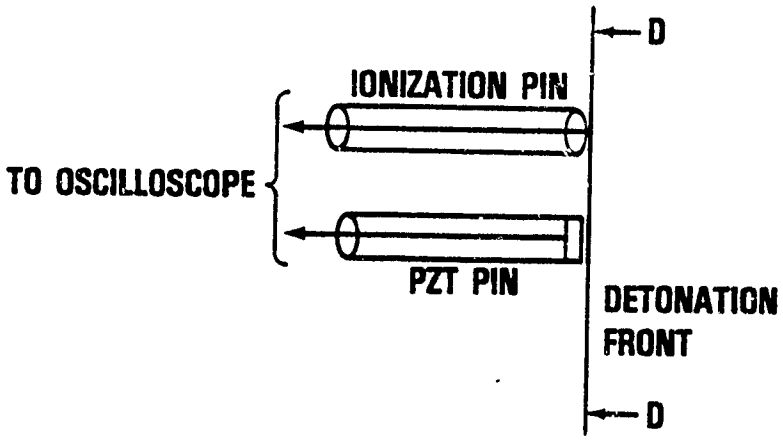

FIGURE 3-1. ALIGNMENT OF PIEZOELECTRIC (PZT) AND IONIZATION PINS

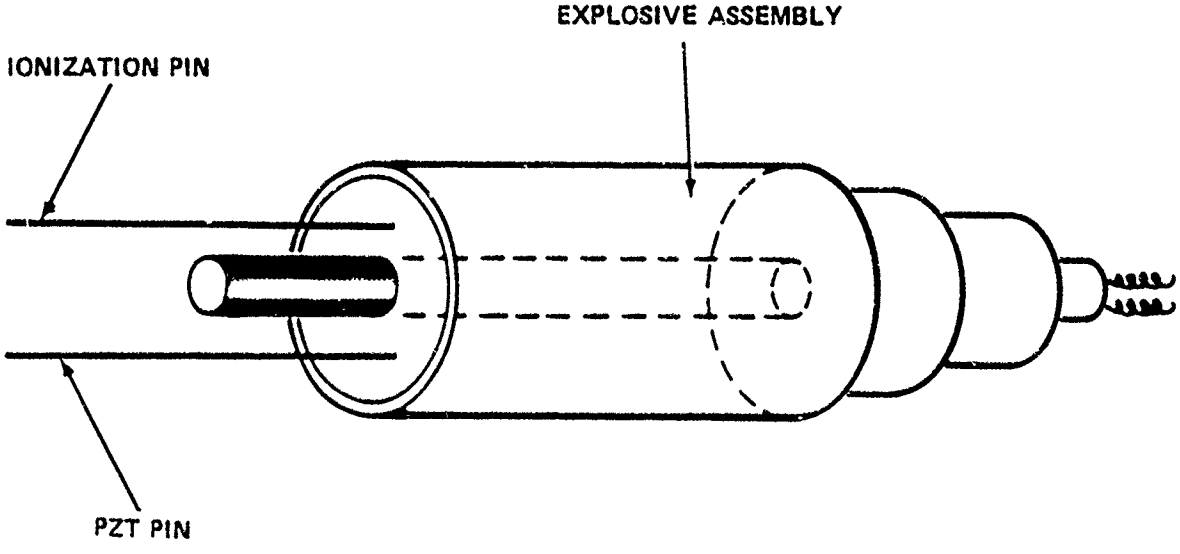

FIGURE 3-2. COINCIDENCE EXPERIMENT

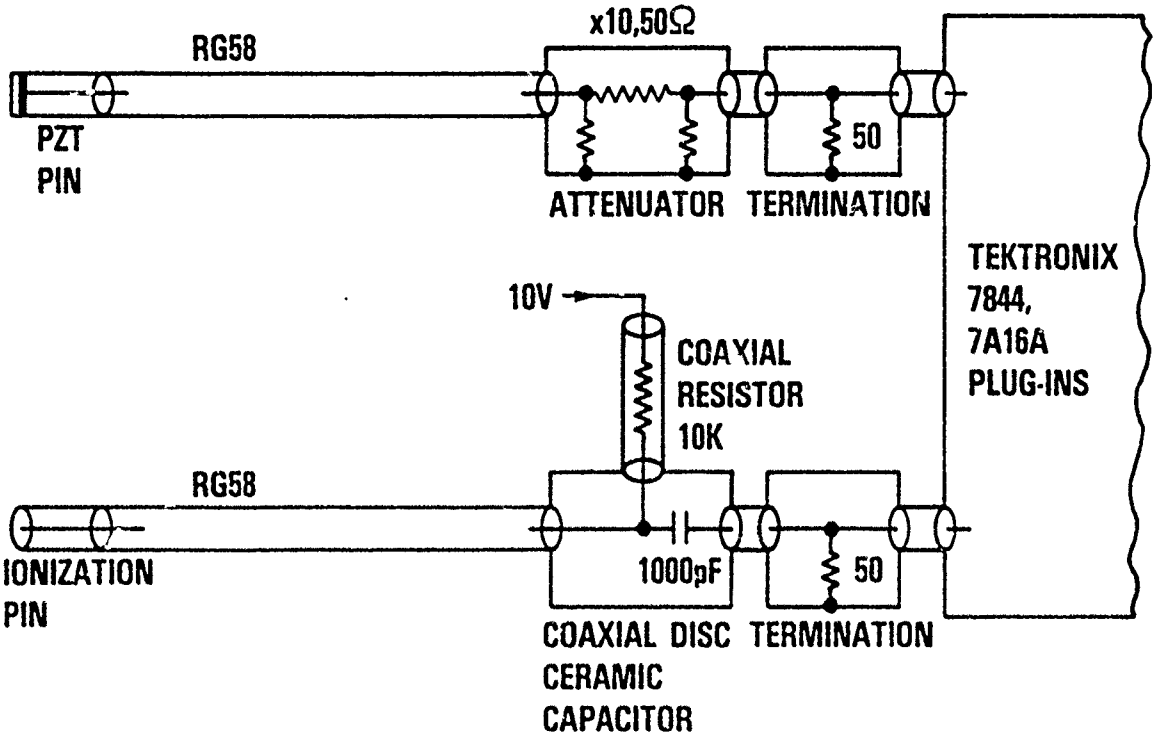

FIGURE 3-3. COAXIAL COUPLING OF CIRCUITRY

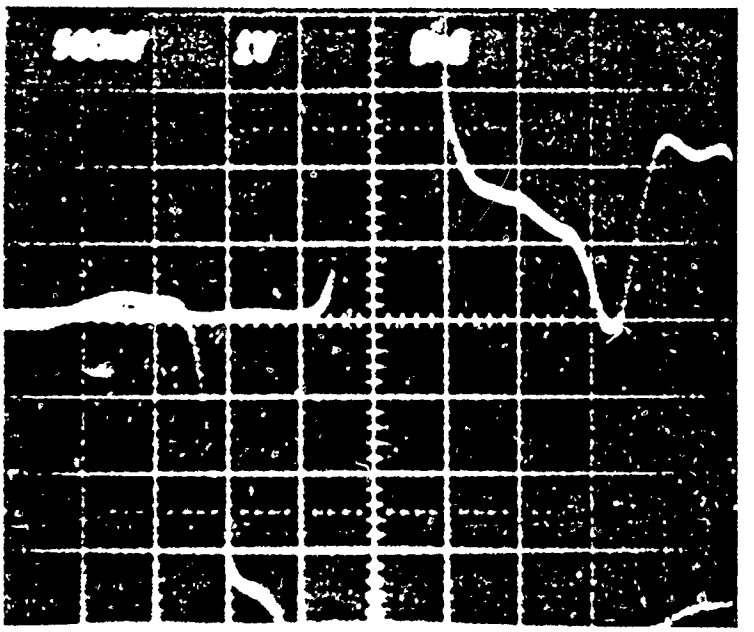

ACTUAL RECORD

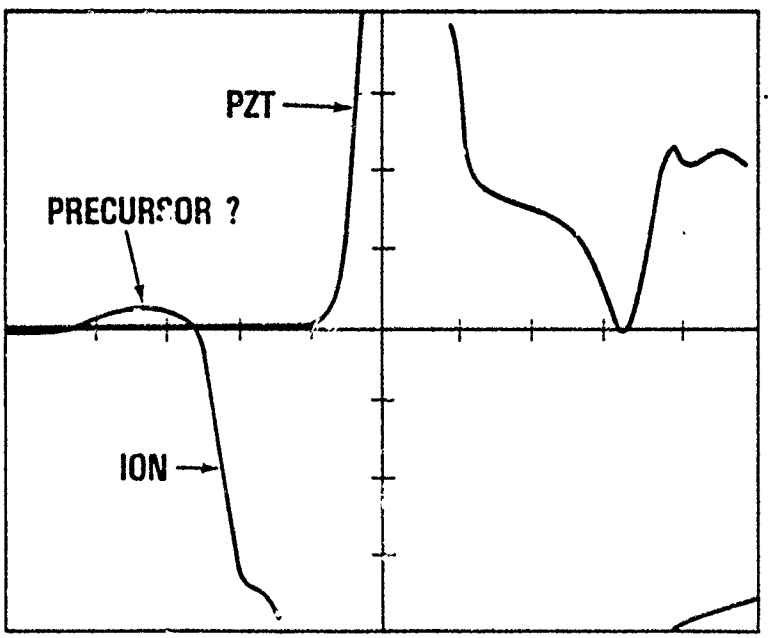

TRACING OF OSCILLOSCOPE RECORD, EC 17

5ns/DIV
PZT RECORD DELAYED BY 9.0ns

FIGURE 3-4. OSCILLOSCOPE RECORD

detonation wave travel of approximately 4.5 μm. Such a separation is comparable with the smallest particle size of the PBX-9404, this may be the best resolution possible. When observing such small time differences, great care must be exercised. For example, the piezoelectric pin is comprised of a thin piezoelectric disc with silver plating on the top and the bottom. Shock transit times through the plating must be considered as well as electromagnetic signal transit times through the crystal to the upper electrode. The crystal has a high dielectric constant, ε_r, hence the velocity of an electromagnetic wave will be reduced by $\sqrt{\varepsilon_r}$; this will affect the time resolution of the circuit. Electronic resolution could be improved by the use of 400 MHz plug-ins instead of the 250MHz 7A16A plug-ins that were used. In this way, the 10% to 90% risetimes would be improved from 1.5 nsecs to 0.9 nsecs; the time resolution would increase by a similar factor. The records did show a small precursor to the arrival of the shock front. This could be an observation of a region of ejecta into the porous explosive traveling ahead of the shock front.[7] However, further work is necessary to ensure that this was not due to anomalies in either the behavior of the ionization pin or the behavior of the internal delay lines of the oscilloscope.

CONCLUSIONS

Preliminary estimates of the coincidence between the arrival time of the shock front of the detonation wave and the conduction zone front gave a difference of less than 0.5 nsecs. Such a small time is comparable to the transit time of the smallest particle size of explosive PBX-9404 and may not be significant. However, further work is required to better characterize delay times in the piezoelectric crystals. Flyer plate studies are proposed which, together with faster electronic plug-ins, will improve the confidence of the coincidence measurement. Evidence of ejecta ahead of the detonation front may have been observed.[7] The close coincidence of the shock front and conduction front is particularly interesting. It has been estimated that the width of the reaction zone in PBX-9404 is of the order of 0.1mm.[8] If that is so, then the CJ plane must travel approximately 11 nsecs behind the shock front (the Von-Neumann spike). Provided that the PZT pin is fast enough, and all our studies suggest that it is, then conduction starts long before reaction is complete. Such evidence favors shock induced conduction of the unreacted explosive and conduction by chemical species present early in the processes of reaction, rather than coalescence of condensed carbon products, as the conduction media.[9] However, carbon product conduction may predominate later in the reaction zone.

CHAPTER 4

CONDUCTIVITY/ENHANCEMENT EXPERIMENT IN PARALLEL ELECTRODE GEOMETRIES

The results of an experiment performed on thick sheets of PBX-9501 caused doubts about the reliability of conductivity data obtained in parallel plate experiments. Anomalous data were obtained when the electrical conductivity of these thicker sheets was measured. These anomalies were ascribed to conduction in shock-compressed plastics insulation and to field divergence; see Chapter 5. No plastic can behave as an insulator at high pressures; one of the best materials is PTFE (Teflon) which has a conductivity as high as 0.01mho/m at a shock stress of 50GPa. Moreover, transparent plastics such as polycarbonate (Lexan) or PMMA (Plexiglas) have been shown to exhibit the largest shock induced conduction, as shown in Chapter 5. In order to measure any change of detonation velocity that may occur, as during the course of conductivity measurement under high power conditions, transparent insulators are employed. The problem is apparently insurmountable because no plastic, transparent, high pressure insulators exist. However, a novel guard-rail concept has been designed at NSWC which neatly circumvents this problem. The apparatus required for this concept was manufactured at NSWC; subsequently, the guard-rail experiments were performed at LANL with the collaboration of J. Goforth who provided the experimental facilities and manpower.

GUARD-RAIL EXPERIMENTS

These experiments are designed on the basis of parallel plate experiments fired previously; see Chapter 5. In those experiments, a thin sheet of explosive was studied; on opposing faces of the sheet two electrodes were attached and the sheet was line-initiated as shown in Figure 4-1. Voltages of up to 20kV were applied across the electrodes, thereby generating electric fields in the thin explosive sheet, approaching those necessary to obtain measurable detonation velocity enhancements.

The experiments were modified by the addition of guard-rails to either side of the electrodes (see Figures 4-2 and 4-3). The guard-rails were electrically connected to the center rail so they were all at the same voltage. However, the connections between guard-rails and center rails were made in such a way that the current between the center rails could be isolated and measured separately from currents between the guard-rails. The currents that caused the anamolous results, described above, flowed from the guard-rails and not the center rails. Consequently, measurements were made in a parallel field region between the center rails; all problems resulting from conducting plastics had been circumvented rather than eliminated. Moreover, the detonation wave was observed in the electrically enhanced region between a guard-rail and a center rail; this gap acted as the objective slit for streak

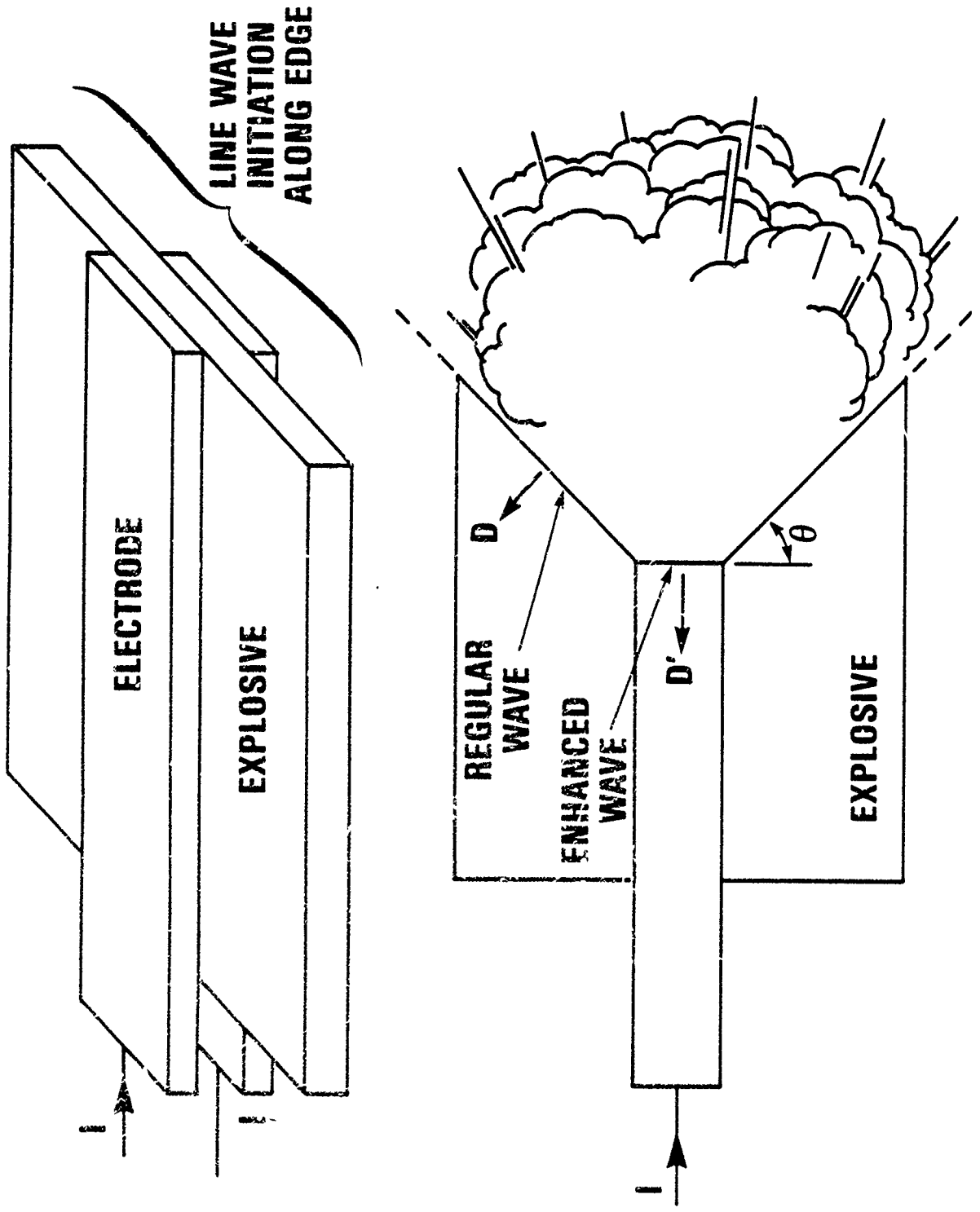

FIGURE 4-1. PARALLEL PLATE EXPERIMENT

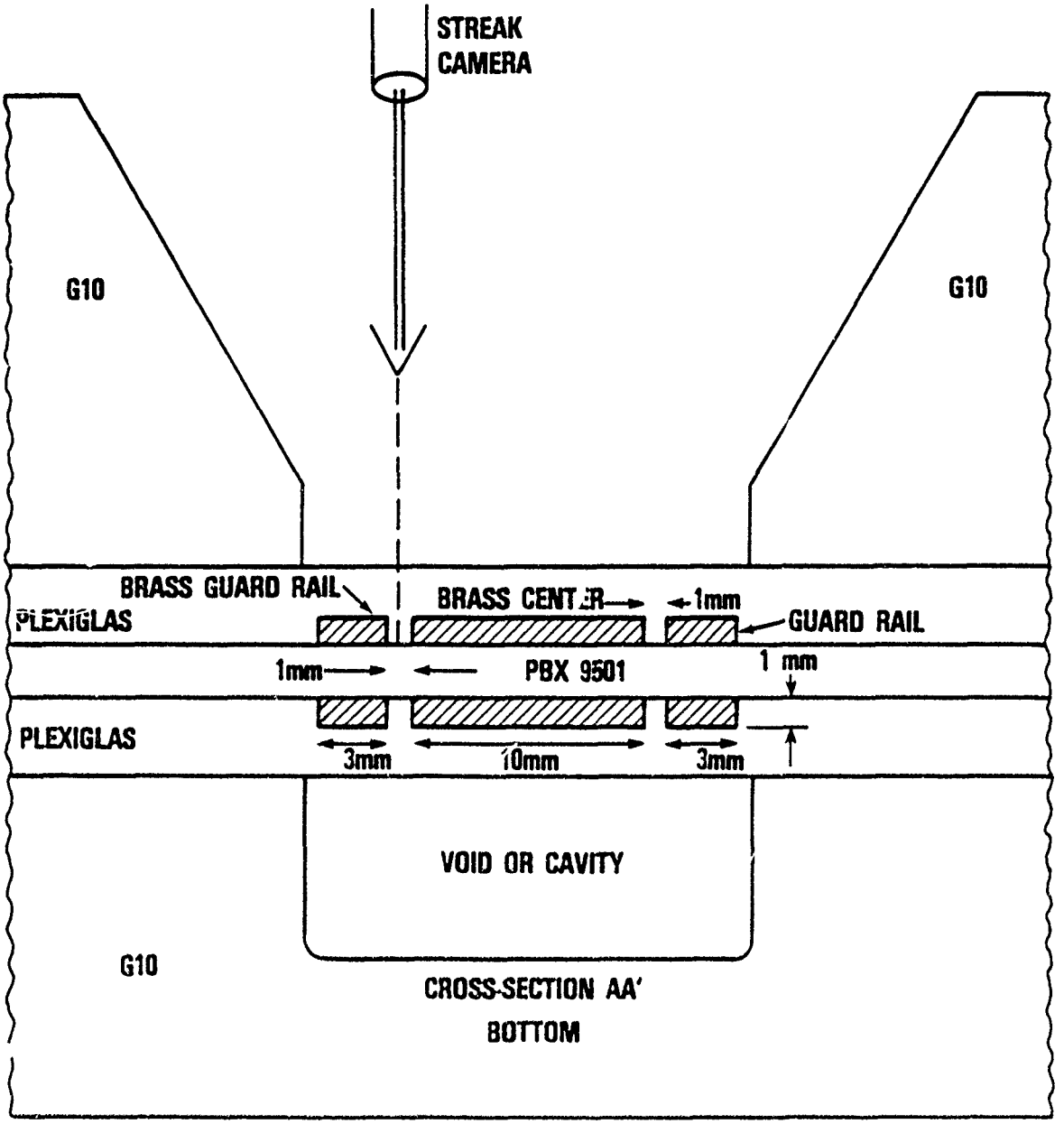

FIGURE 4-2. GUARD-RAIL MODIFICATION TO PARALLEL PLATE EQUIPMENT

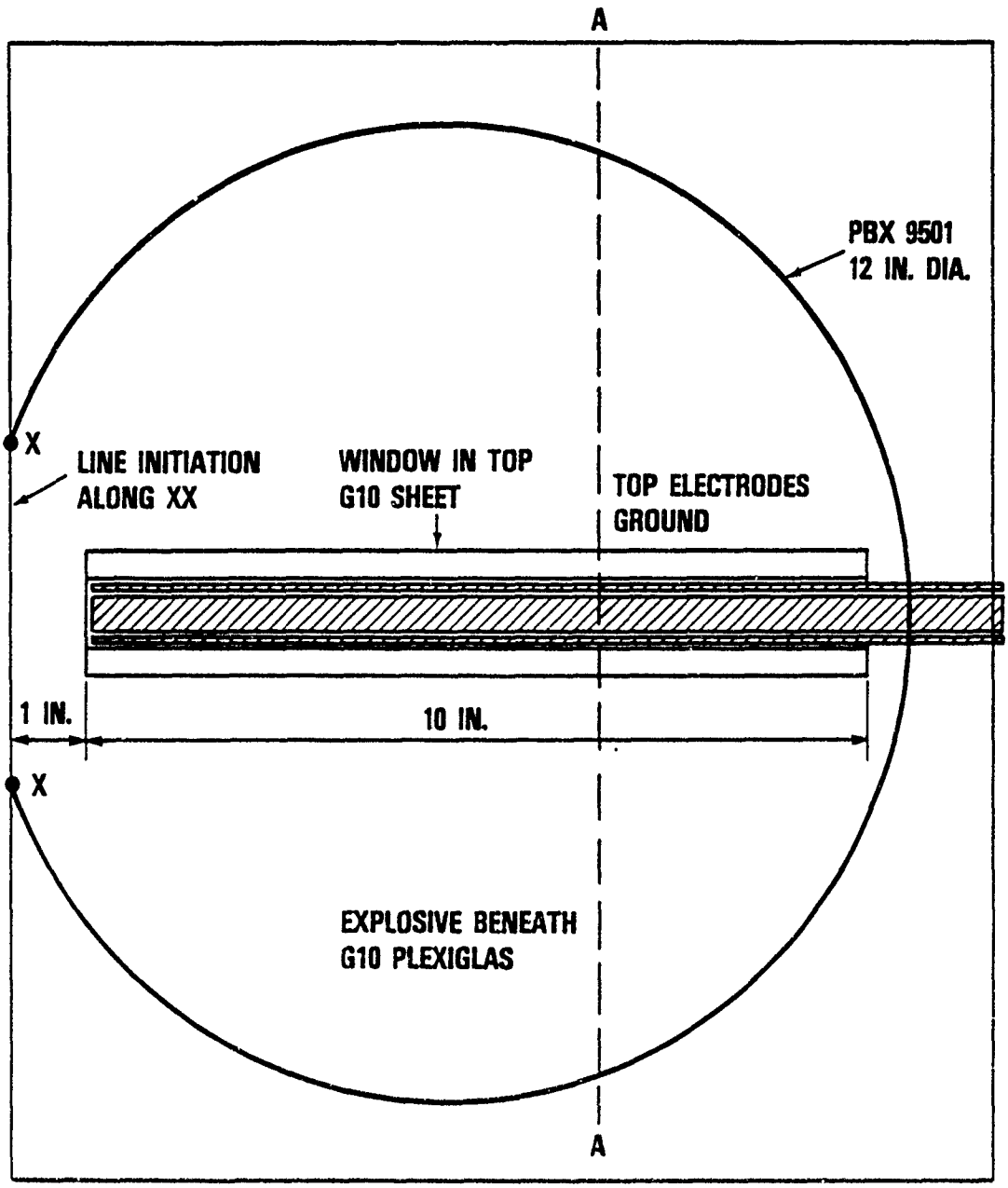

FIGURE 4-3. TOP VIEW OF GUARD-RAIL MODIFICATION

camera photography. The electrodes were pressed against the explosive surfaces by thick G10 epoxy/ fiberglass blocks as shown. Cut-away sections in the G10 allowed for the rapid separation of the electrodes after detonation. This was done with the intention of minimizing the electric field behind the conduction zone, thereby reducing the possibility of breakdown in the product gases. This minimization of confinement led to the rapid decay of the pressure in the product gases behind the detonation front; the effects of this are described below. The experiment was performed with several different sheet thicknesses.

RESULTS

Predetonation Breakdown Phenomena

In shots DC 15 and DC 16, the explosive broke down in a field of 10KV/mm prior to the arrival of the detonation wave. No useful data could be attained. Similarly, the charge of DC 17 broke down, although this time it was tested with a high voltage insulation tester before the charge was connected to the high energy capacitor bank. (Subsequently, this charge was fired under zero field conditions to establish the baseline detonation velocity for a 1.5 mm thick sheet.)

It was postulated that breakdown was due to the presence of small, translucent regions or imperfections, approximately 1-3mm in diameter, in the PBX-9501 explosives sheet. To prove that breakdown occurred at these points, a sheet of PBX-9501 was selected which had no such flaws in the center of the charge, DC 18. This central region was placed adjacent to the electrodes without insulation, whereas those areas that were translucent were insulated with a film of 60μm polymide (Kapton). The charge withstood the field without premature breakdown. However, the 60μm air gap, that resulted from insulating the explosive at points and thereby raising it from the electrodes, caused resistive arcing when the sheet was detonated, thus reducing the current flow below enhancement levels.

Recent dielectric breakdown studies[1] have demonstrated that the design of the conductors used here was poor; a significant field enhancement would exist at the edges. The edges were not well rounded and dielectric mismatching also existed at the explosive/plexiglas/brass interfaces. Consequently, the ultimate dielectric strength of the explosive would not be realized.

Product Breakdown Phenomena

Experiment DC 18 was particularly interesting in that the first measurements of post detonation breakdown in product gases were obtained, see Figure 4-4. The figure shows the voltage across the center electrodes as a function of time or distance after the wave entered the electrodes. Breakdown occurred 3 1/2 μs or 30mm behind the detonation front, and no breakdown was observed on the streak camera record. If breakdown had occurred ahead of the front it would have been observed on the camera record. The dielectric breakdown strength of the product gases is expected to obey Paschen's law in that the dielectric strength E_{br} is directly proportional to pressure P, i.e. $E_{br} \propto P$. Now, in the Taylor wave behind the CJ plane of the explosive, the

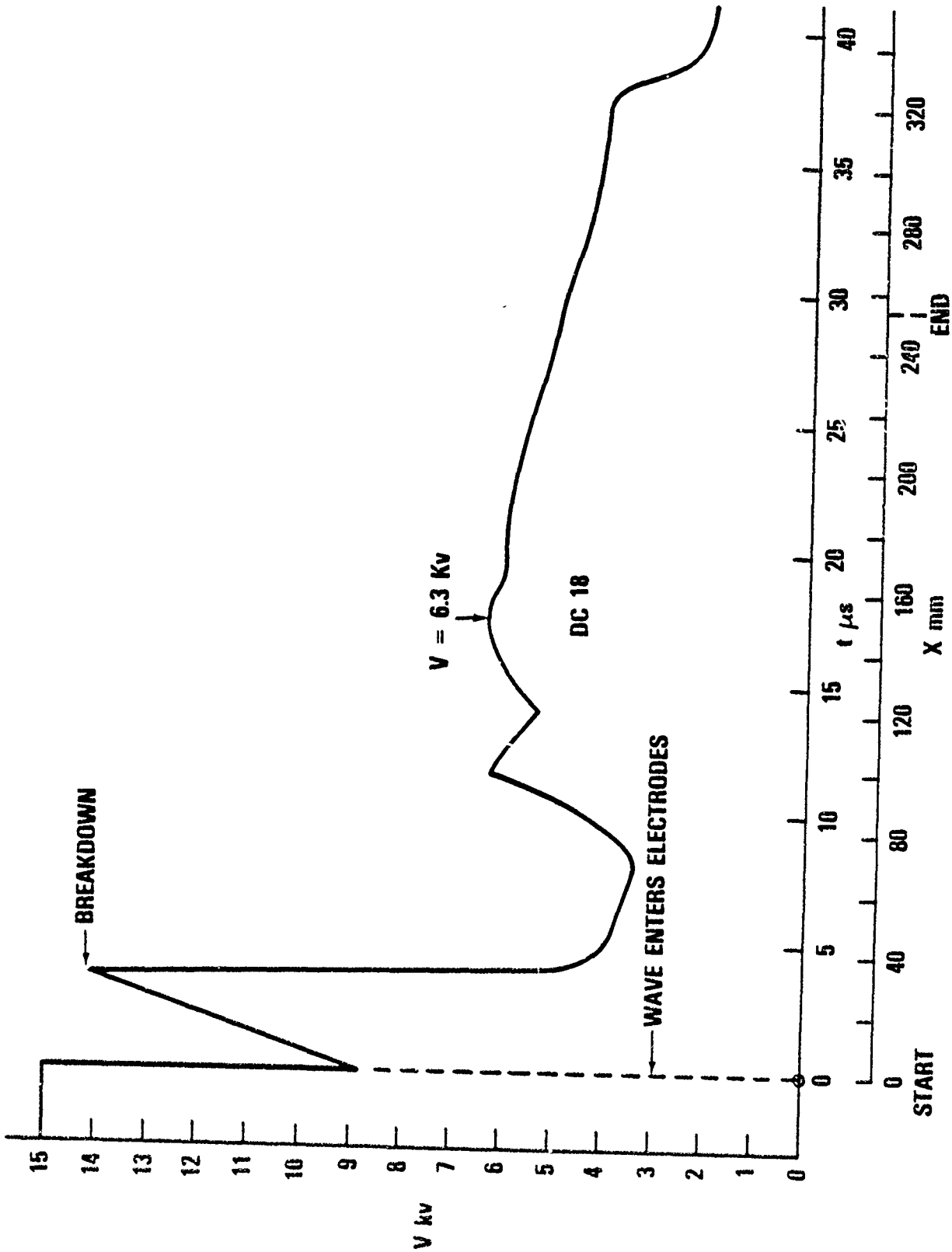

FIGURE 4-4. PRODUCT GAS BREAKDOWN, DC 18

product gas pressure decays rapidly as the gases expand, and by Paschen's law the dielectric strength will decay rapidly also. There is therefore a critical pressure P_{crit}, that corresponds to E_{br}, below which the gases will break down and conduct if the applied electric field exceeds E_{br}. In the case of experiment DC 18, the gases broke down 30 mm behind the detonation front when the dielectric strength fell below 7 kV/mm.

With hindsight it is clear that the decay of the Taylor wave should be minimized. Instead of minimizing confinement around the electrodes, as was done with these shots, the confinement should be as large as is practically possible; in this way rarefactions from the free surfaces would arrive later behind the detonation front, and gas product breakdown would be delayed. Clearly product breakdown reduces the time in which conductivity and enhancement measurements can be made. Future experiments will be designed to maximize the measurement time. Note that these product breakdown phenomena will have no effect on the applications of Energy Coupling. It is not necessary for the time duration of the enhancement to exceed 2μs; the product gases cannot break down in so short a time as the pressures will be too high, and no problems due to product breakdown are anticipated.

In the last two shots the voltage was reduced to 10 kV so as to avoid both post detonation and predetonation breakdown. Difficulty was experienced with DC 19 in maintaining a good contact between the brass electrodes and the explosive. Consequently arcing occurred which generated electrical noise on the current and voltage data. The separation of the electrodes from the explosive was prevented in shot DC 20 by better electrode preparation, and good data were obtained. Table 4-1 summarizes the results.

SUMMARY AND DISCUSSION

The guard-rail design allowed the measurements of $\sigma\Delta$ (the conductivity conduction width product) to be made with greater confidence. The measurements were devoid of errors due to field divergence and plastic conduction, and the technique was thus successful. The mean results gave $\sigma\Delta$ = 0.45 mho which is lower than previously estimated ($\sigma\Delta$ = 0.60 mho) and suggests that plastic conduction and field divergence had some effect on previous measurements. Using this data, the velocity enhancement can be estimated using the Kamlet-Jacobs equation of state.[9]

Table 4-1 shows that the detonation velocity enhancements measured were modest. They were limited by the experimental difficulties described above, and there is no indication that they were limited by the Energy Coupling technique per se. However, the measured velocities show excellent agreement with the predictions, and they are identical within experimental error. Note that these data are not based on the Abel equation of state, used by Toton, which gives more optimistic predictions.[10]

CONCLUSIONS

The guard-rail experiments were successful. Much has been learned from them. Future work will seek to establish the reasons for breakdown in the translucent areas of PBX-9501. This work will be part of a detailed program

TABLE 4-1. SUMMARY OF "GUARD-RAIL" EXPERIMENTAL RESULTS

Shot DC	Explosive Thickness mm	Capacitor Voltage KV	Power Enhancement	Predicted Velocity Enhancement ΔD/D	Measured Velocity Enhancement ΔD/D	Remarks
15	2.0	20	0	0	0	Explosive broke down before detonation
16	2.0	20	0	0	0	Explosive broke down before detonation
17	1.5	0	0	0	0	Measurement of velocity of detonation under zero field conditions, baseline reference
18	2.0	15	0	0	0	Measurement of conductivity using kapton insulation, product breakdown monitored
19	2.5	10	3.5%	1%	0.9%	Reduced E field measurement to avoid breakdown, air arcing detected
20	2.0	10	10%	2.4%	1.93%	Reduced E field measurement

of research into dielectric breakdown phenomena in explosives.[1] Further experiments are planned to obtain conductivity data and enhancement data under conditions of higher power enhancement. Based on what is presently known, these high power enhancement experiments should be very successful. This has provided additional motivation to install a new 40kV capacitor bank at NSWC, see Chapter 7. The dielectric breakdown of product gases will be researched later in the program. Excellent agreement between theory and experiment was obtained for the enhancement measurements. Measurements of $\sigma\Delta$ (the products of conductivity and conduction zone width) were improved by the use of the guard-rail technique; $\sigma\Delta$ = 0.45mho for PBX-9501. The resistive behavior, and arcing, caused by thin layers of air between electrodes and explosives, was unexpected. It has also been observed in other conductivity experiments (Chapter 8). Greater care will be taken to exclude air in future experiments.

CHAPTER 5

ANOMALIES IN THE MEASUREMENT OF THE RESISTANCE OF PBX-9501

During a series of experiments, performed at LANL by J. Goforth, measurements were made of the variation of resistance of detonating PBX-9501 with explosive sheet thickness. A schematic of the experiment is shown in Figure 5-1. Conductivity data obtained for thinner sheets (see Chapter 4) gave $\sigma\Delta = 0.6$ mho; the product of the conductivity σ and the detonation zone width Δ. However, when resistances of PBX-9501 were measured in thicker sheets $\sigma\Delta$ appeared to vary, i.e. the resistance did not vary with thickness in a manner predicted by

$$R = \frac{T}{\sigma \Delta W} ,$$

where T is the sheet thickness and W the electrode width. The results indicated the trend shown in Figure 5-2. There was, therefore, serious concern that these results indicated a departure from the theory,[11] that conductivity was being influenced by factors hitherto overlooked.

However, it was postulated that the results could be explained by a combination of shock induced conductivity in the plastic insulation and shock wave curvature.

ANALYSIS OF EXPERIMENT

The experiment was constructed as shown in Figure 5-3. Two brass electrodes, 1/2 in. wide and 3/4 in. high, were inset into a polycarbonate (Lexan) block as shown. In the actual experiment analyzed, DC 14, the explosive sheet of PBX-9501 was circular, 12 in. in diameter and 2 in. thick. The sheet was point initiated as shown in Figure 5-4, and the electrodes were clamped firmly to the explosive surface so that air resistance effects could be discounted.

It was postulated that.

a) The conductivity conduction zone width product, $\sigma\Delta$, remains constant.

b) The effective resistance of the sheet would be reduced by shock induced conduction in the plastic insulation.

c) Field divergence may further increase current flow.

A simple test of (c) was performed by J. Goforth at LANL in which a copper sulphate analog of the circuit was used. No significant field divergence effects were observed.

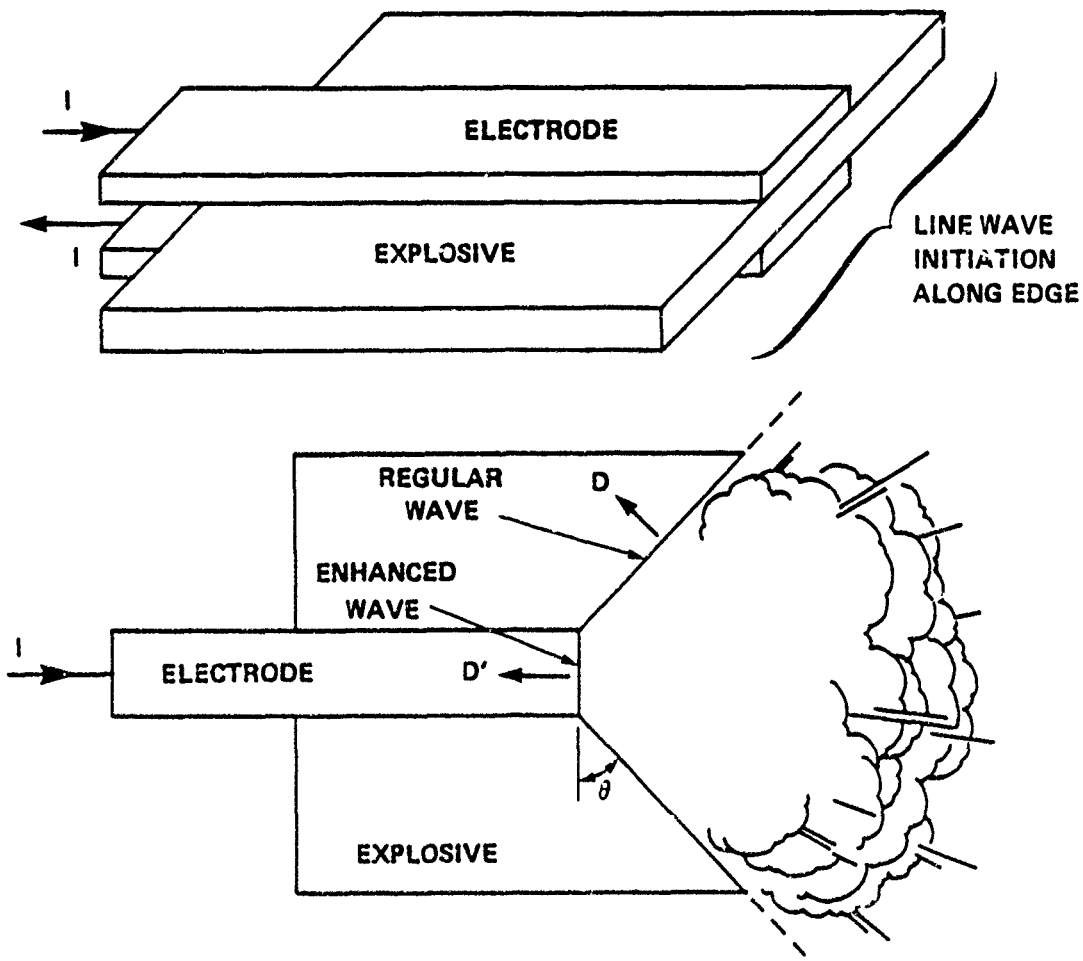

FIGURE 5-1. RESISTANCE MEASUREMENT OF DETONATING PBX 9501

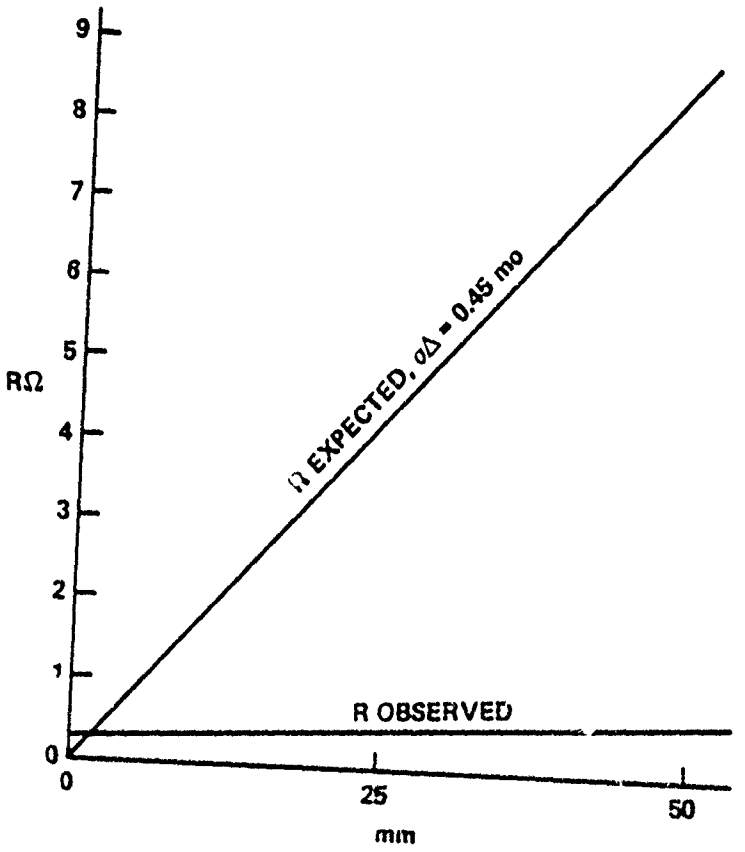

FIGURE 5-2. VARIATION OF RESISTANCE WITH THICKNESS

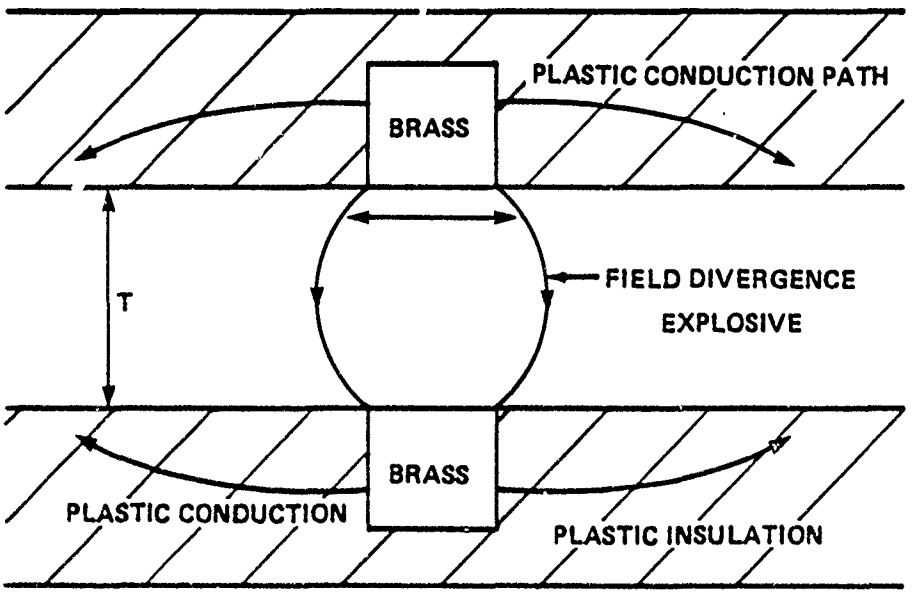

FIGURE 5-3. CROSS-SECTION OF DETONATING PBX 9501 BETWEEN ELECTRODES

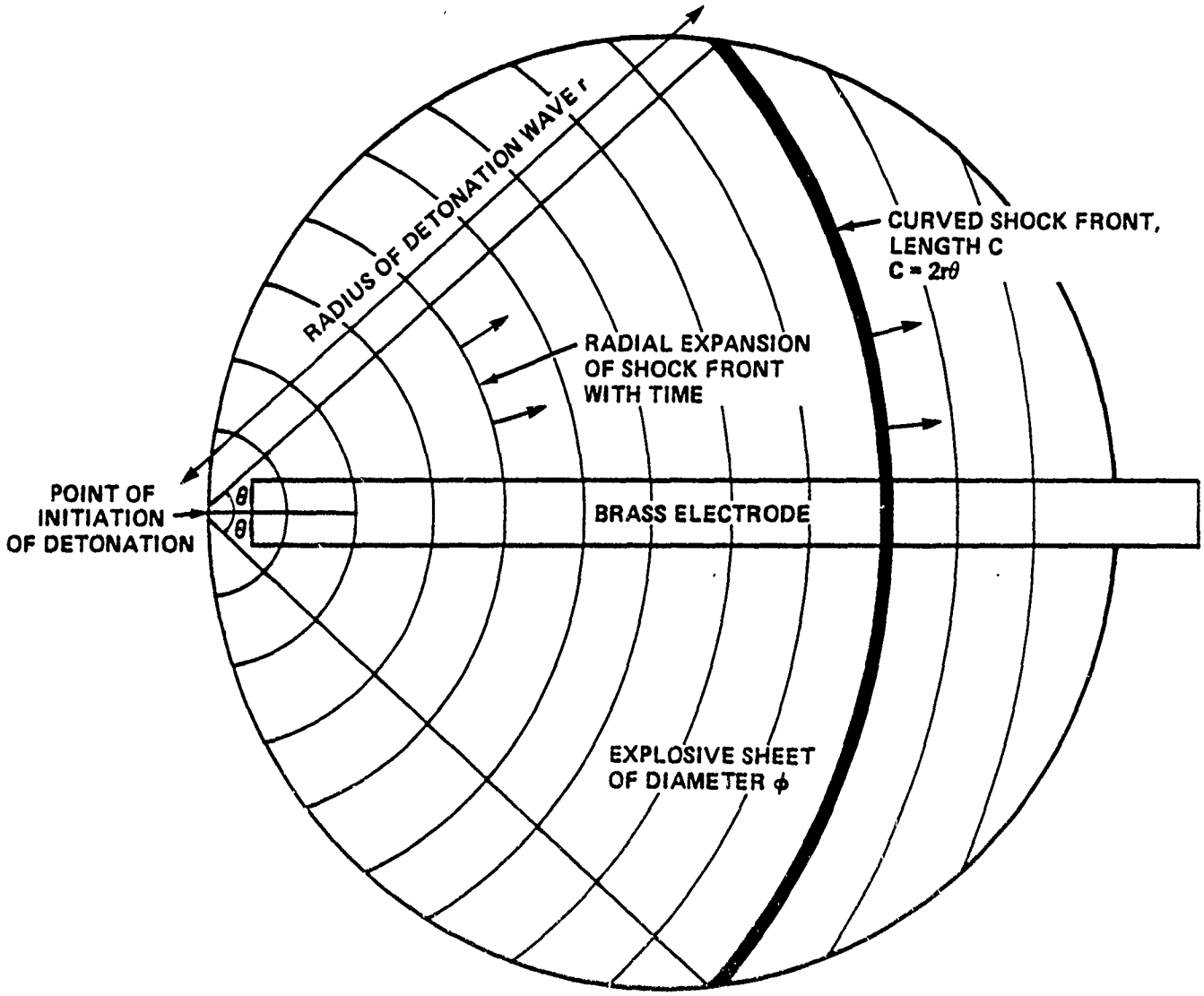

FIGURE 5-4. RADIAL EXPANSION OF DETONATION

It was assumed that:

a) $\sigma\Delta$ = 0.45 mho, from previous measurements (Chapter 4).

b) The shock induced conduction in the plastic produced a negligible resistance (Chapter 6),

c) Perturbations of shock wave curvature due to edge rarefactions could be ignored.

d) The resistance could be calculated on the basis that the effective electrode width was not W, but the length of an arc C extending across the sheet as shown. This follows directly from assumption (b).

Then the resistance R becomes

$$R = \frac{T}{C\sigma\Delta} \quad ,$$

and C increases as the wave expands like ripples on a pond (see Figure 5-4). It can be shown that

$$C = 2r \cos^{-1} \left(\frac{r}{\phi}\right) \quad ,$$

where r is the radius of the detonation wave, assuming Huygen propagation, and ϕ is the diameter of the sheet.

Now r = Dt the product of the detonation velocity D and the time t.

$$\text{Hence } C = 2Dt\cos^{-1} \left(\frac{Dt}{\phi}\right) .$$

The resistance becomes

$$R = \frac{T}{2DT\cos^{-1}\left(\frac{Dt}{\phi}\right)\sigma\Delta} \text{ ohms} .$$

This expression has been calculated as a function of time and drawn in Figure 5-5. Superimposed on the graph is a plot of the actual resistance measured in experiment DC 14 (the actual current and voltage data for this shot are shown in Figure 5-6).

The agreement is excellent, both in shape and magnitude. Clearly the assumption that the plastic conductivity was infinite would be wrong; the finite resistivity of the sheet will serve to increase the resistance slightly above that calculated, see Chapter 6.

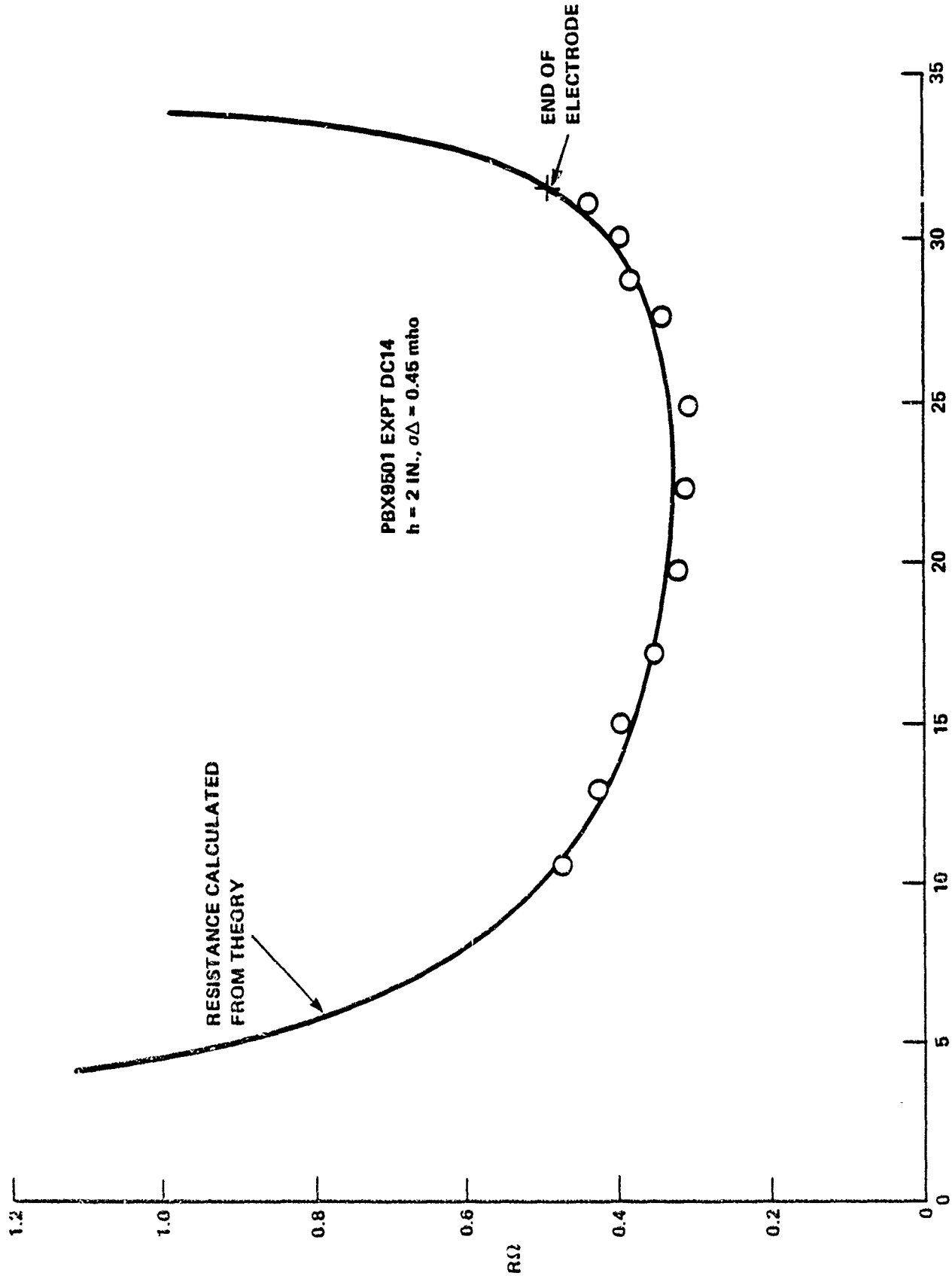

FIGURE 5-5. ACTUAL AND CALCULATED VARIATION OF RESISTANCE WITH TIME

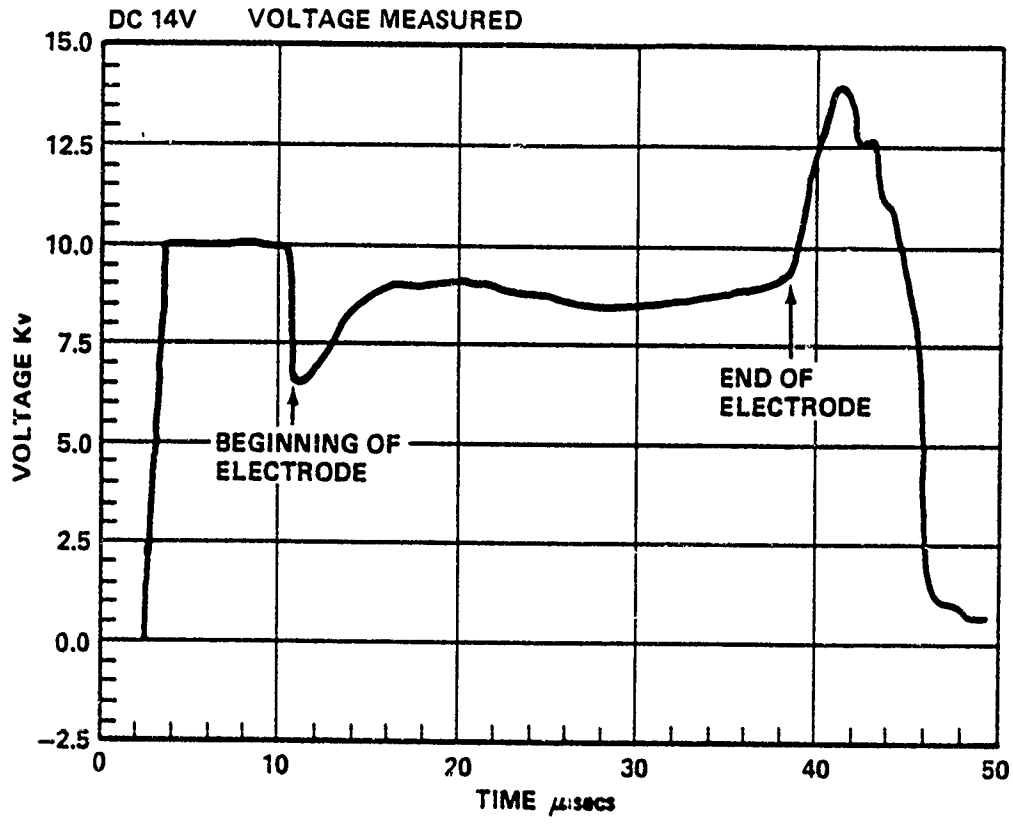

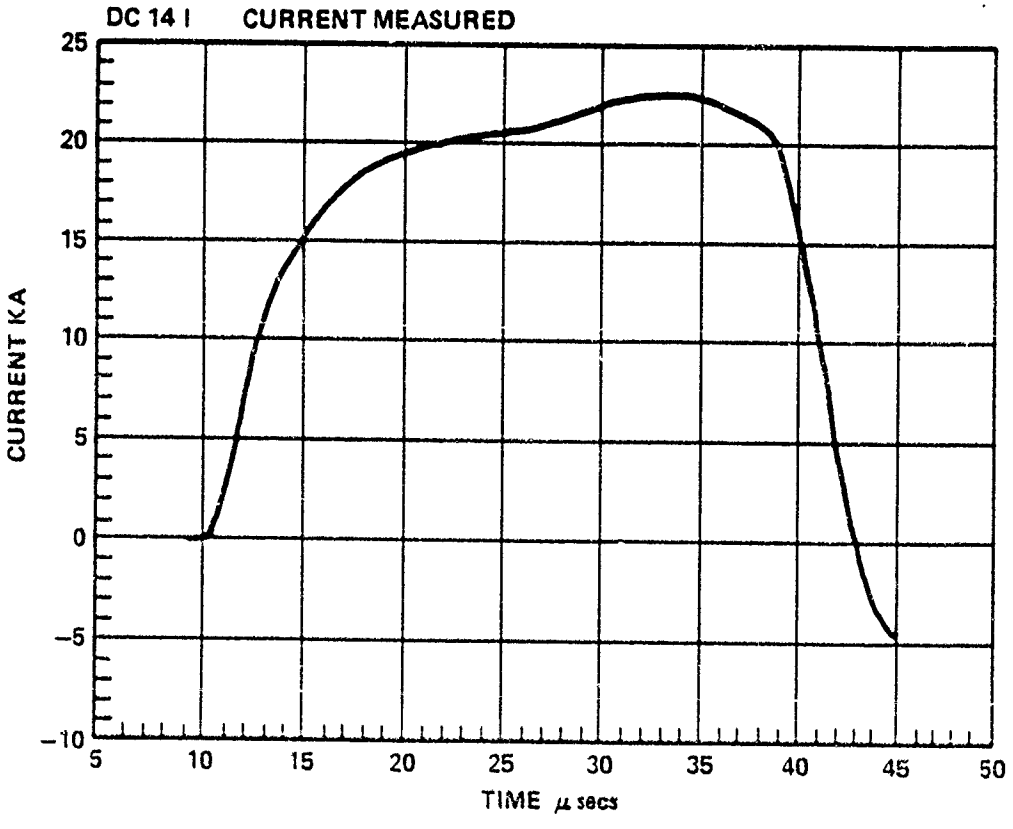

FIGURE 5-6. VOLTAGE AND CURRENT WAVEFORMS

CONCLUSIONS

Agreement between theory and experiment is excellent, therefore the assumption of a constant $\sigma\Delta$ is considered vindicated. The conductivity of shocked Lexan is shown in Chapter 6 to be large. This supports the hypothesis that current was increased by the effective widening of the metal electrodes by conduction in the plastic.

CHAPTER 6

PLASTICS CONDUCTIVITY MEASUREMENTS

A series of experiments was performed at LANL on thick sheets of PBX-9501 (see Chapter 5). The results of these experiments were analyzed and an anomalous relationship between explosive sheet thickness and resistance was identified. This behavior could be completely explained by electrical current flow in shock-compressed plastic insulation. Shock compresion conductivity data, for the plastics in question, was inadequate for the purposes of this high voltage study. Experiments were designed and performed at NSWC, White Oak, to provide this information.

The plastics polycarbonate (Lexan), polyethylene, PTFE (Teflon), and PMMA (Plexiglas) were studied; these materials are most commonly used as insulators in shock wave experiments. A definitive study would have necessitated the use of a gas gun flyer plate apparatus to produce flat one-dimensional shocks of known amplitude and duration. Such a study is planned for the future. This present study was designed to simply and quickly demonstrate that the plastic insulation was responsible for the anomalous results and to obtain order of magnitude data under conditions comparable to the LANL experiment.

EXPERIMENT

After some preliminary experimentation, the design of Figure 6-1 was used. The experimental arrangement is shown in Figure 6-2. The electrode assembly
was placed on top of a sheet of explosive (Detasheet), 1/4 in. thick. The sheet was detonated from one end and the detonation wave swept along the electrode assembly as shown. The electrode block was weighted to ensure good contact with the explosive.

The electrical circuit is shown in Figure 6-3 . A 57μF, 5kV capacitor C, charged to 3kV, was connected via a thyratron switch S and its associated stray circuit inductances and resistances (L and r) to the electrode block E. Current flow I through the plastic P was monitored with a Pearson current transformer CTI. The voltage across the plastic was measured by a four point probe technique using a copper sulphate voltage probe. The probe, comprised a copper sulphate resistor, R_{CuSO_4}, of 1kΩ and a Pearson current transformer CTV. The problems associated with high voltage measurements in the presence of rapidly changing electric currents and the $CuSO_4$ probe are discussed in the Appendix A. Piezoelectric pins, not shown, were used to correlate the observed voltage and current waveforms with the progress of the detonation wave along the explosive sheet and electrode block.

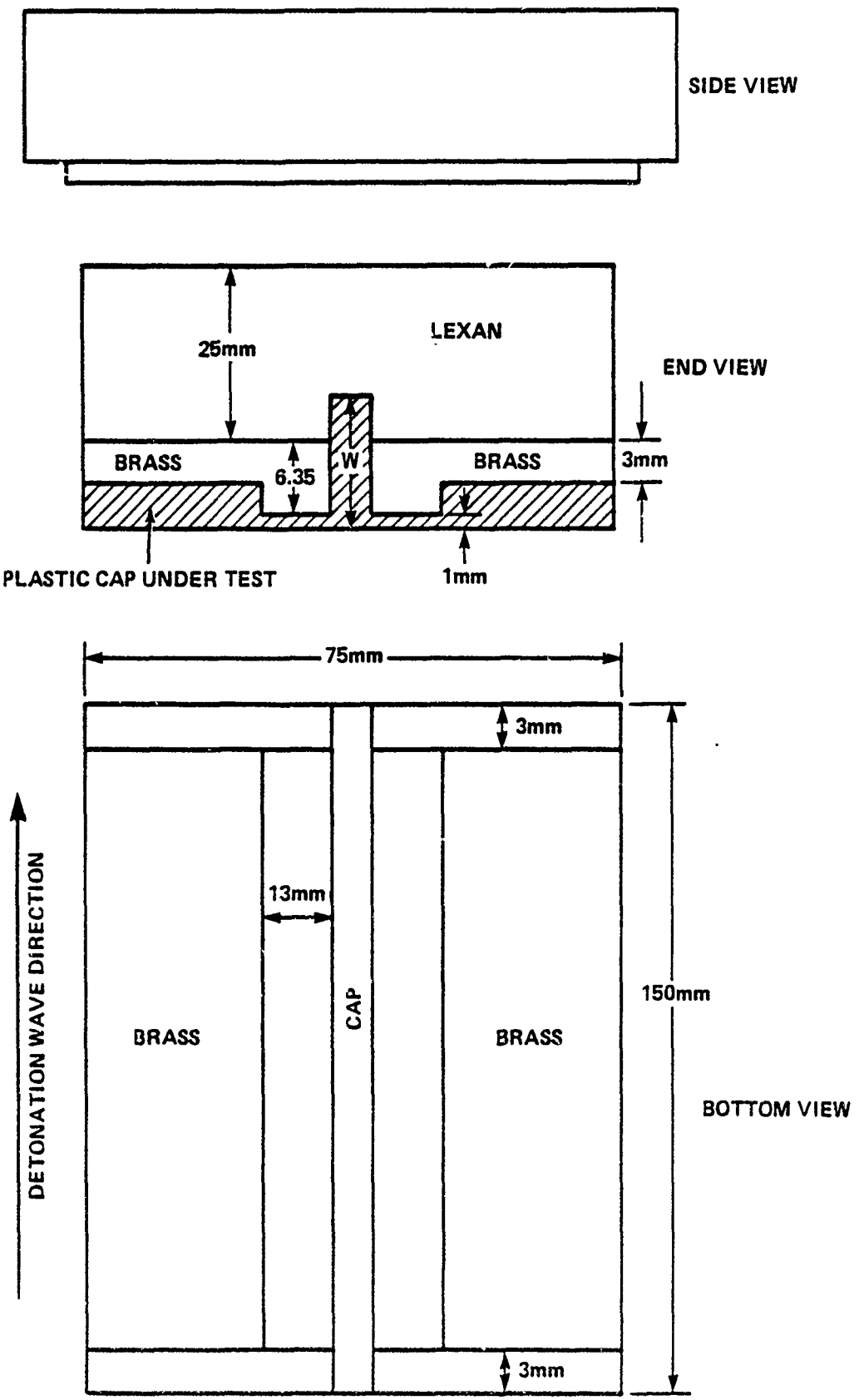

FIGURE 6-1. ELECTRODE/PLASTIC ASSEMBLY

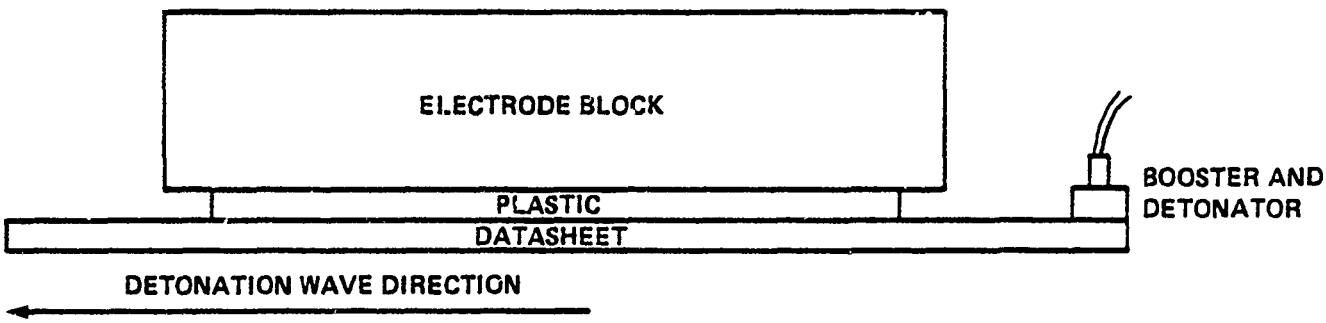

FIGURE 6-2. EXPERIMENTAL ARRANGEMENT

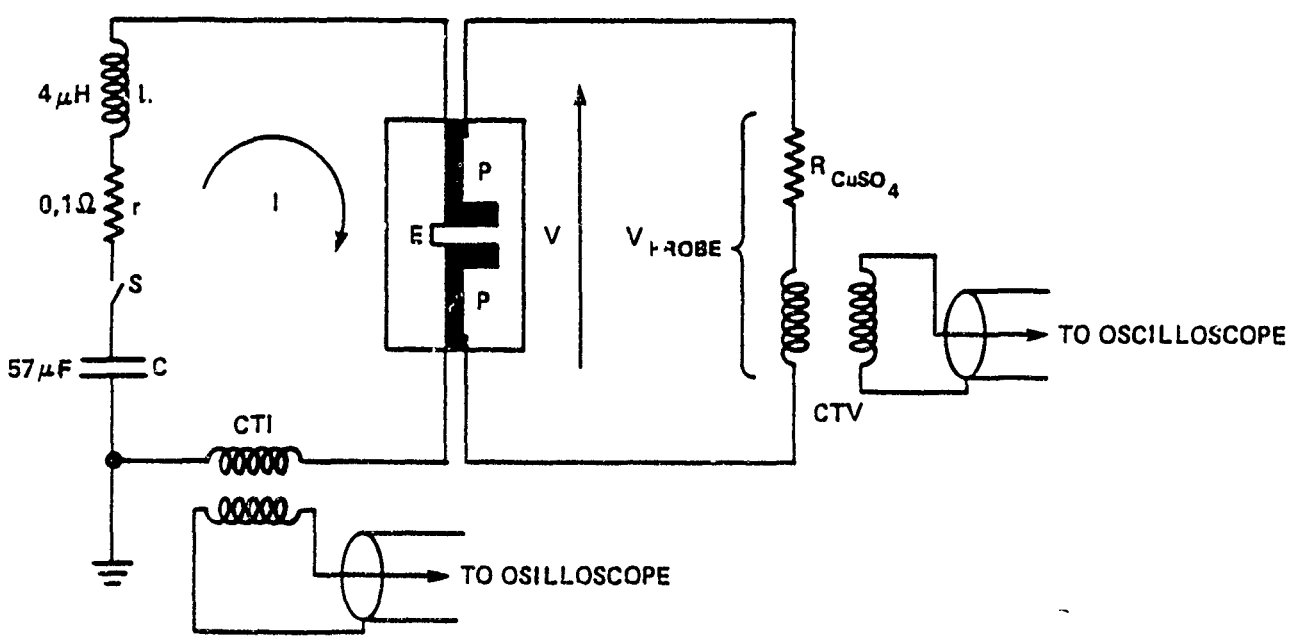

FIGURE 6-3. MEASUREMENT CIRCUIT

RESULTS AND CONCLUSIONS

Due to the 3-dimensional nature of the experiment, multiple reflections occurred within the electrode block during the course of the experiment. The subsequent waveform structure was complicated and tedious to interpret. Typical results are shown in Figure 6-4 for Lexan (experiment E395B).

The records of voltage and current show the following details:

(A) Entry of the shock wave into the electrodes;
(B) Exit of the shock wave from the electrodes;
(C) and (D) These are interpreted as the arrivals of rarefactions, at the electrode/plastic interface, from the brass/block and block/air interfaces. These rarefactions cause electrode separation and arcing;
(E) Breakdown in the air or gas products after the wave has left the block.

The current continued for a significant time after the wave exit at B; it appears that the shocked, conducting plastic continued to conduct long after the detonation wave had passed. Note that this is in contrast to the behavior of a detonating, conducting explosive which "turns off" after the detonation wave has passed because the product gases cannot support conduction. The data thus obtained are not conducive to an exact analysis. The results are approximate at best; however, the results indicate that the conductivities of the plastics measurement are sufficient to account for the anomalous behavior reported and analyzed in Section 5. Order of magnitude estimates suggest that the products of conductivity (σ) and effective conduction zone widths (Δ) are as follows:

Material	$\sigma\Delta$
Polycarbonate (Lexan)	~ 1 mho
PMMA (Plexiglas)	~ 1/2 mho
Polyethylene	~ 0.05 mho
PTFE (Teflon)	~ 0.01 mho

Note that the slow "turn off" of conduction in these plastics would significantly reduce the effective resistance by increasing the width of the conduction path (Δ) if it were not controlled by the conduction path in the explosive.

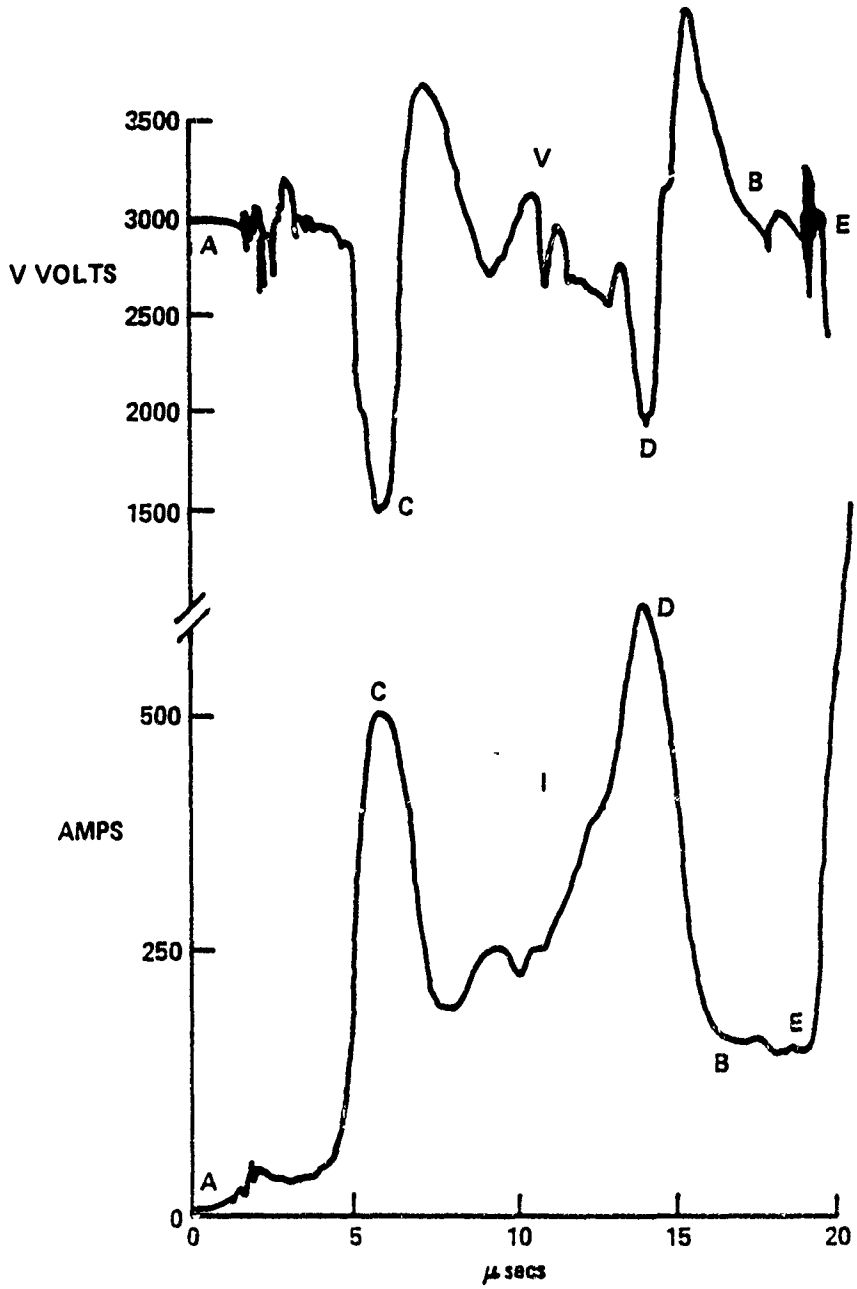

FIGURE 6-4. VOLTAGE AND CURRENT RECORDS LEXAN, E 395 B

CHAPTER 7

PULSED POWER EQUIPMENT, DESIGN, AND DEVELOPMENT

ENERGY STORAGE TECHNIQUES

Since the inception of the Energy Coupling program at White Oak, a substantial effort has been devoted to the development of the Pulse Power facility. Original calculations of the currents and voltages necessary to effect a significant enhancement of explosive performance by Joule heating overestimated the magnitude of the voltages required.[10] It was originally felt that voltages in excess of 100kV would be required; these estimates were based on conductivity data obtained from the literature. The work presented in Chapter 2 has demonstrated that significant enhancements can be obtained with lower voltages, typically 20-40kV, provided that the voltages are applied across short distances in the explosive, typically a few millimeters.

The transfer of large currents, 100kA to 1MA, to the detonation zone of an explosive is particularly difficult; typically energies of 0.1 to 1MJ must be transferred in less than 10μsecs. If voltages of 100kV or greater were required then storage of the electrical energy in an inductor would appear to be a viable proposition. A capacitive storage system may have been too slow to transfer energy due to the difficulties of eliminating stray inductances in the electrical circuit; however, a storage inductor would not suffer from these problems. However, the extraordinary problems associated with opening switches in such circuits were not foreseen. Consequently a significant effort was expended in perfecting current transfer techniques using the intermediate storage inductor. The basic method of using a storage inductor has been reported previously.[11] Significant progress has been made both in the experiment and the instrumentation since that report was written. Present day methods differ substantially from those reported.

The basic circuit is shown in Figure 7-1. At time t=0 the closing switch, CS, is closed by firing three exploding bridgewire detonators which rupture a polyethylene insulator. Current I then flows from the capacitor C through the loop comprised of the explosively activated circuit breaker, EACB and fuse F, the storage inductor L_s and the leakage inductance L_c. The circuit breaker is based on an NRL design.[11] The current rises sinusoidally to a peak of 140kA in a time of approximately $\frac{\pi}{2}\sqrt{LC}$ or 400μsecs (here $L = L_s + L_c$). At this time, the circuit breaker opens and commences to arc. This arcing is resistive so that current is diverted into the lower resistance coaxial fuse F. The fuse is coaxial to render it insensitive to external magnetic fields which would otherwise cause premature rupture of the fuse (this coaxial design is a recent NSWC innovation), further details can be found in Appendix B. The fuse is designed to conduct just long enough for the arcs within the EACB to cool; then

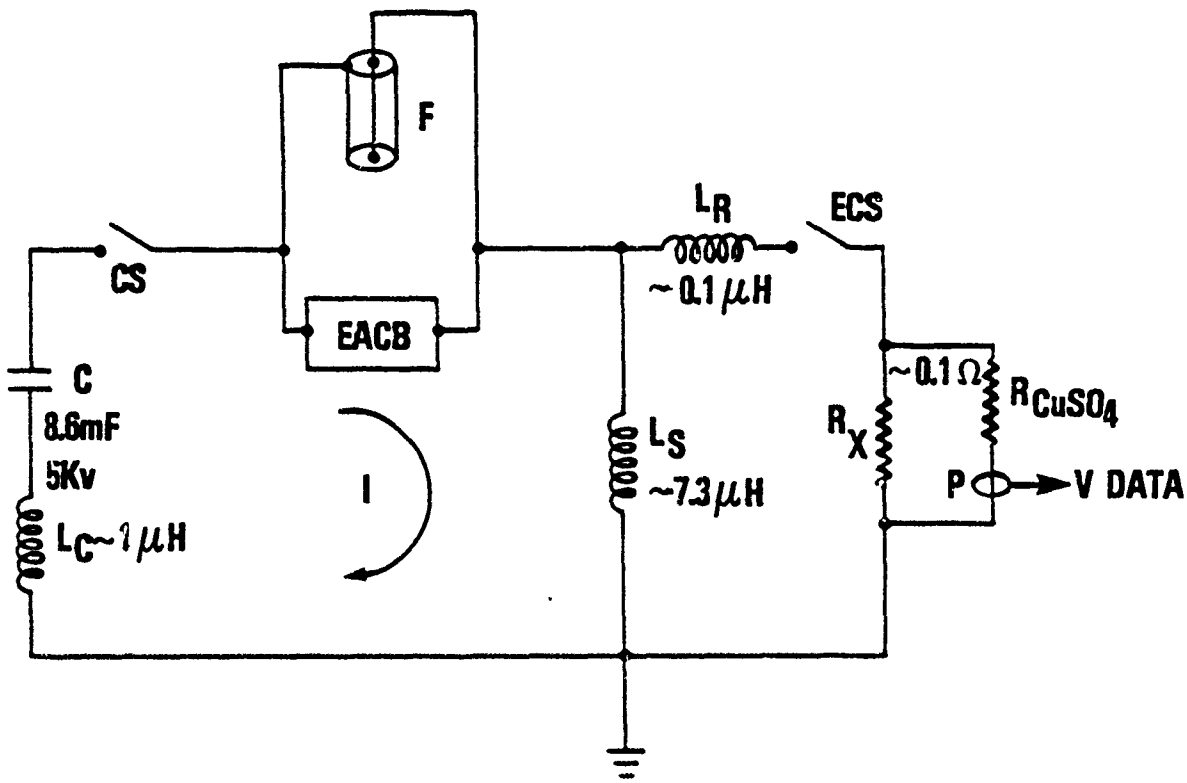

FIGURE 7-1. INTERMEDIATE STORAGE INDUCTOR CIRCUIT, SCHEMATIC

the fuse varporizes and explodes; current in the storage inductor is then rapidly turned off. The voltage across the storage inductor then rises to L di/dt . Current is then transferred to the explosive load Rx by the closing switch ECS and the leakage inductance L_R. The closing switch is usually effected by the explosive itself which acts as a good insulator until the detonation wave enters the electrodes, then the current rapidly flows through the detonation zone. Currents in the circuit are measured with Rogowski coils and voltages with copper sulphate resistors R_{CuSO_4} and current transformers P, (Appendix A.)

Significant problems with this storage inductor circuit have been encountered:

(a) The EACB takes approximately 40μs to commence arcing after initiation of the explosive Detacord within it. It then takes a further 40μs for the arcs to cool before it can turn off. The coaxial fuse automatically conducts as soon as the arcs commence. However, the complete process from closing the switch CS to the fuse exploding takes 414 ± 10μsecs; the variation is caused by a combination of small changes in circuit inductance, resistance, switch response, etc. The variation is unpredictable and too large for an explosive experiment because the explosive is consumed by the detonation wave at a velocity of 8.8mm/μs, so that an Energy Coupling experiment typically lasts for 10μsecs.

The explosive must be detonated before the fuse explodes so that the entry of a stable detonation wave at the beginning of electrodes coincides with the time of fuse explosion. If the fuse breaks too soon, the open circuit voltage across the undetonated explosive will lead to dielectric breakdown. With an uncertainty in this time of ±10μsecs, it is virtually impossible to obtain perfect coincidence. Various techniques have been employed to predict the fuse explosion time but none of them have been successful, the large, changing magnetic fields within the circuit (circa 10 Tesla) have caused too much noise to allow subtle changes in the circuit to be monitored reliably.

(b) The rapidly changing magnetic field in the storage inductor makes measurement of currents and voltages within the circuit extremely difficult, where magnetic fields exceed 10 Tesla; see Appendix A.

(c) The energy required to vaporize the copper fuse is extremely large. The time from start of conduction to fuse explosion is diameter dependent. To conduct 140 kA for 50μsecs, and thus cool the arcing EACB, the fuse cross-sectional area must be 2.35 mm^2. Moreover, to behave as an opening switch the fuse must withstand the voltage across the storage inductor when the fuse explodes. The voltage above which the fuse will restrike, and therefore fail, is the restrike voltage; this voltage is length dependent and typically the fuse can withstand 0.1 kV/mm to 0.2 kV/mm. In short, to conduct 140 kA for 50μs, then withstand 40 kV, the fuse must have a volume of 940 mm^3 for a 400 mm length of wire. The energy required to vaporize the copper is 55.4J/mm^3 or 52 KJ.[12] The capacitor stores 100 kJ; so a massive fraction of the stored energy is required to vaporize the fuse alone and never reaches the explosive (if the voltage was 77 kV then all the energy would be consumed by the fuse). This problem can be reduced by employing two fuses in parallel. The first is of 2.35 mm^2 area but relatively short. When it breaks, the current is transferred to

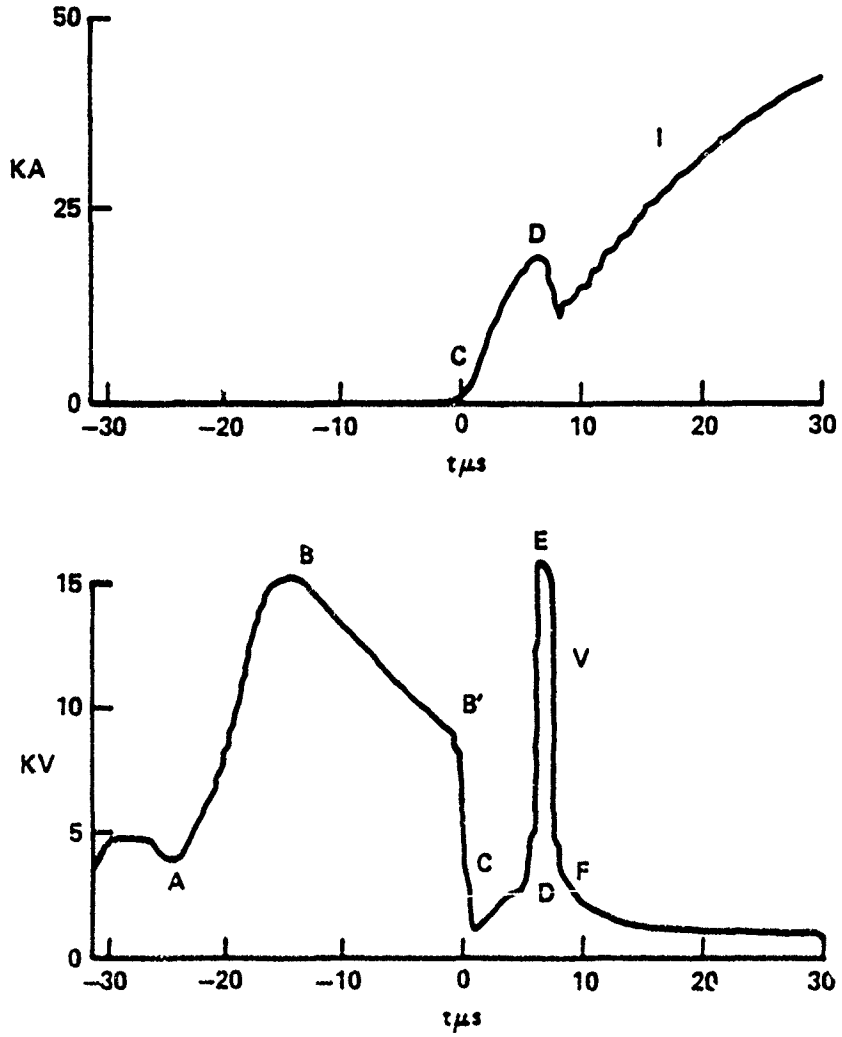

FIGURE 7-2. VOLTAGE AND CURRENT DATA, EC 17

the second fuse which is long and thin. This fuse need only conduct for a few microseconds before the first fuse is cool enough to withstand electric fields considerably in excess of 0.1 kV/mm. The second fuse then explodes and must withstand 0.1 kV/mm, but it is long enough to avoid restrike. By using two fuses, less copper mass is therefore required. Nevertheless, a lot of energy is lost to the fuses and the system is still inefficient.

(d) The fuse restrikes at the voltage determined by its length. It then shares current with the explosive load and further diminishes the efficiency of the circuit. The resistance of the fuse on restrike is typically 1/3Ω and conducts up to 50 kA.

RESULTS WITH INTERMEDIATE STORAGE INDUCTOR

As reported in Chapter 2, the circuit was used to successfully transfer current to detonating PBX-9404. The problems described above were minimized as follows:

(a) The detonation of the PBX-9404 was delayed to ensure that the detonation wave entered the electrodes after the single fuse had exploded. The mean time to rupture of the fuse is known to be 414μs with an estimated standard error of the mean of 3.3μs. We were therefore 99.9% confident the fuse had exploded if the detonation wave entered the electrodes at 414μs plus three standard errors, i.e. at 424μsecs, assuming a normal variate. It was also most likely that the current would decay for 10μsec (a maximum of 20μsecs) at a rate

of $\frac{di}{dt} = \frac{V_{max}}{L_s}$. If V_{max} = 40 kV and L_s = 7.3μH then the current would decay

from 140 kA to 85 kA. Moreover, the explosive was likely to have to withstand 40 kV for an average of 10μsecs, a maximum of 20μsecs. If the fuse restrike voltage were higher than 0.1 kV/mm, then the explosive would break down prior to detonation.

(b) Errors in voltage and current measurement, due to the large magnetic fields, were minimized as described in Appendix A and Chapter 2.

(c) Energy lost to the fuse was minimized by reducing the fuse length to a minimum, in this case 160 mm so that restrike would occur between 16 and 32 kV.

(d) Unfortunately, by using a short fuse the resistance on restrike would be reduced below 1/3Ω, and more current would be lost to the fuse.

The results of the experiment are reproduced here as Figure 7-2. At A the fuse vaporized, the voltage across it reached its peak at B, 16kV, over a time of 14μsecs; the detonation was therefore 14μsecs late. Conduction in the fuse after restrike discharged the storage inductor from B to B'. At the time of detonation wave entry into the electrodes at C, the voltage had fallen to 10 kV, only twice that of the capacitor bank. The current flowed in the explosive between C and D, and inductive losses in the circuit prevented a rapid rise of current; it rose from 0 to 19.3 kA in 6μsecs. After D the detonation wave destroyed the insulation of the stripline which broke down at E and thereafter

presented a low resistance.

CONCLUSIONS

The experiment represents a successful operation of the inductive storage circuit. However, of the original 100 kJ in the capacitor bank less than 10 kJ was transferred to the load. This clearly demonstrates the inefficiency of the circuit, i.e. less than 10%. If the voltage required is never to exceed 40 kV, then it is very much easier to use a conventional capacitive storage system.

A 40 kV, 100 kJ capacitor has been installed at the White Oak facility, and the storage inductor system will no longer be used. The 40 kV capacitor storage system is comprised of a 125 F capacitor C, stripline connectors, a closing switch S and the explosive load Rx; see Figure 7-3.

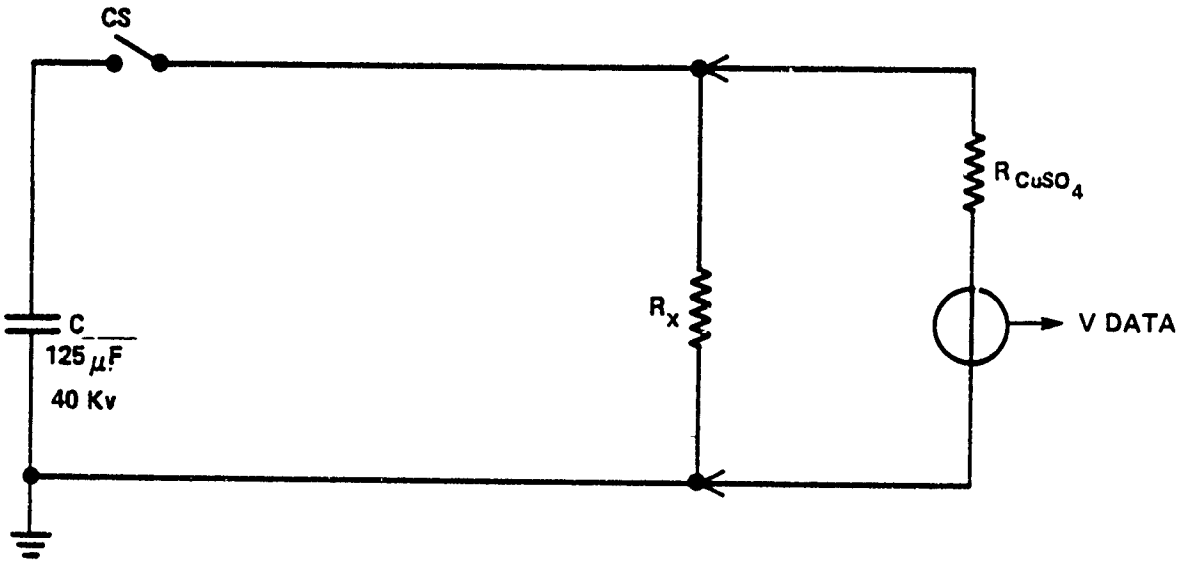

FIGURE 7-3. NEW 40 Kv CAPACITOR SYSTEM

CHAPTER 8

SHOCKED AIR RESISTANCE EFFECTS

The explosive cylinder in Figure 2-1 had inadvertently been manufactured with a slight taper of 1μ{ diameter per mm length although the brass tube was perfectly cylindrical. The largest end of the taper was closest to the detonator, so that an air gap between the tube and explosive increased from 0 at the detonator end to 37μm along the length of the explosive. The results show that the resistance increased with length commensurate with this increase in air gap. The resistance of the explosive, obtained from other experiments, is approximately 0.14Ω without the air gap. The slope of Figure 8-1 started at 0.16Ω and then increased to 0.690Ω. This non-linearity is not believed to be due to instabilities in the detonation wave structure of PBX-9404 or an excessively wide conduction zone width. The former should occur in a much shorter time while the latter would tend to cause the resistance to decrease with time. Consequently the air resistance of the 75μm air gap (d) was 0.53Ω, (R_{air}). If a planar conduction front is assumed and no jetting into the void occurred then the conductivity of the air, σ_{air}, can be estimated from

$$R_{air} = \frac{d}{2\pi r \sigma_{air} \Delta},$$

where r is the radius and Δ the conduction zone width. Hence $\sigma_{air}\Delta = 2\times10^{-3}$ mhos. It must be made clear that the gap between explosive and tube may also be filled with product gases and ejecta immediately adjacent to the detonation zone. Hence the $\sigma_{air}\Delta$ data must be used with caution as they may not represent pure air. If Δ = 0.1 mm for PBX-9404 then σ_{air} ~ 20 mhos/m. Clearly several crude assumptions have been made here; nevertheless, these data are consistent with air resistance effects we have observed in other experiments and in fair agreement with data extrapolated from published work.[13]

It is both unsafe and difficult to insert a perfectly cylindrical charge into a tube with less than a 10μm clearance on the radius. Consequently, the apparent resistance of a perfectly cylindrical charge with a 10μm clearance would always include approximately 0.06Ω of air resistance, based on $\sigma_{air}\Delta = 2 \times 10^{-3}$ mhos.

In order to prove that air resistance was responsible for these resistance measurement anomalies, and to eliminate the problem, matched tapered outer electrodes were used in subsequent experiments (see Figure 8-2). The results from these experiments clearly demonstrated that the resistance increase was caused by air, as discussed in Chapter 2. The results are reproduced in Figure 8-3 for comparison with Figure 8-1, a good linear voltage-current plot is shown.

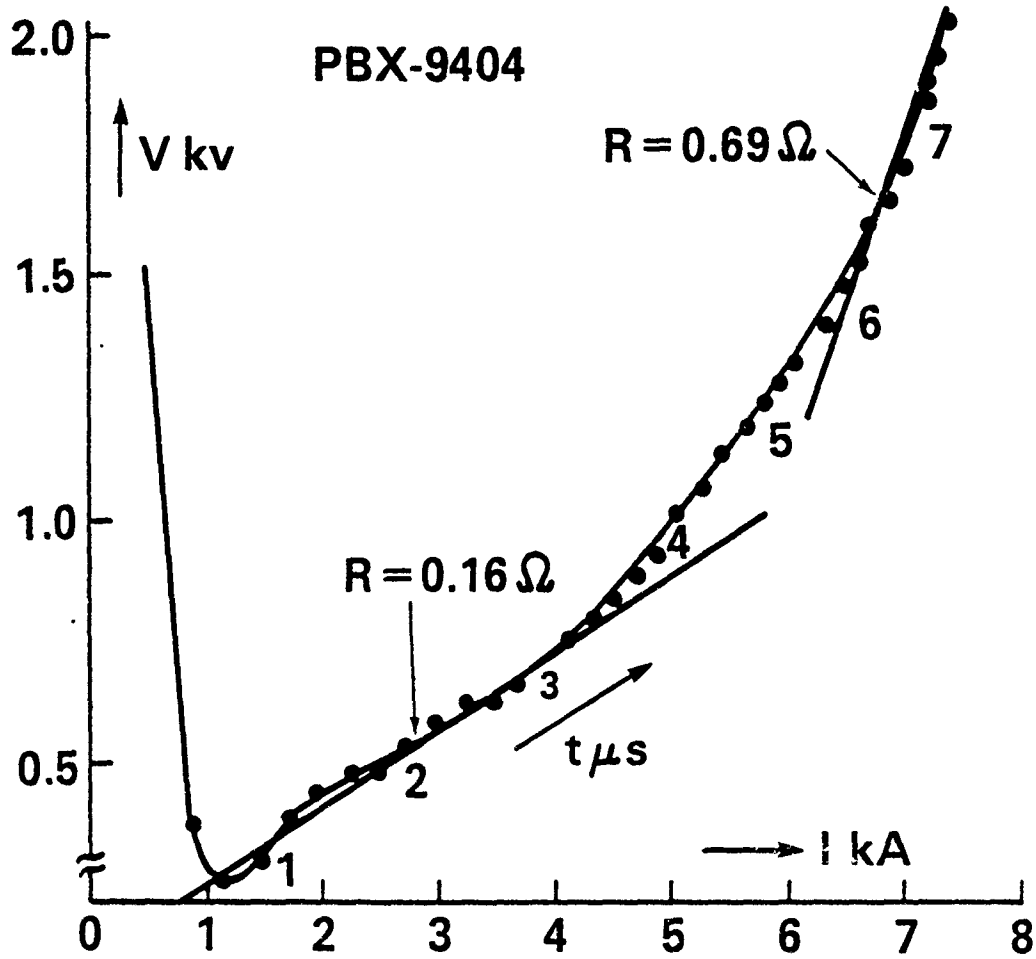

FIGURE 8-1. EFFECTS OF AIR GAP

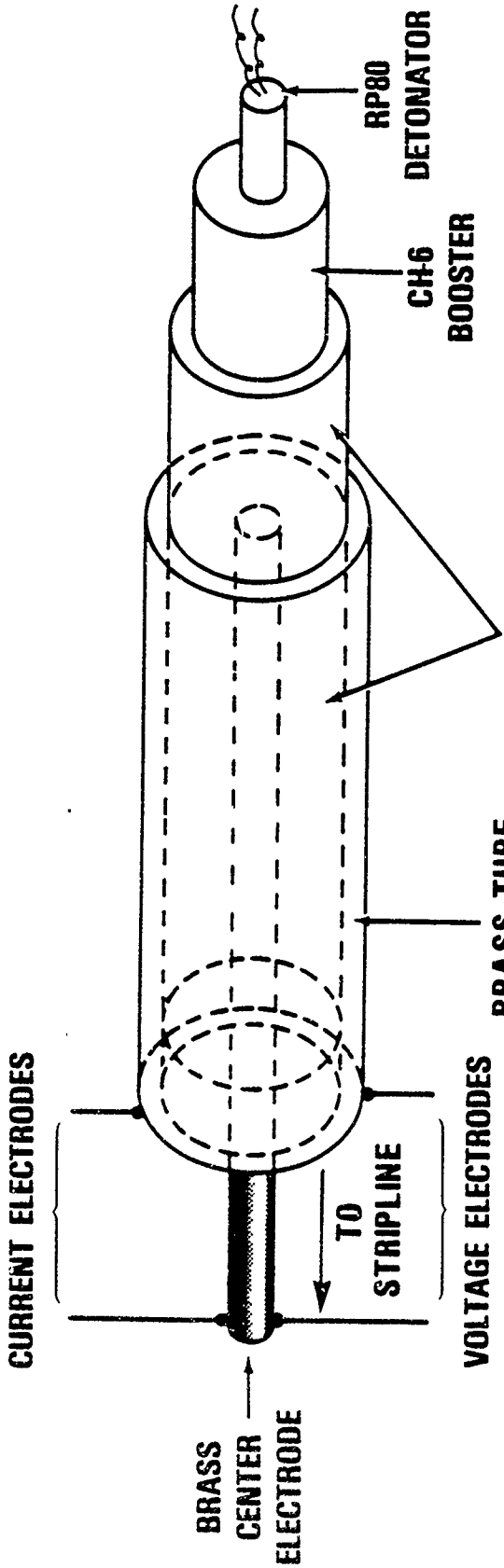

FIGURE 8-2. COAXIAL CONDUCTIVITY MEASUREMENT

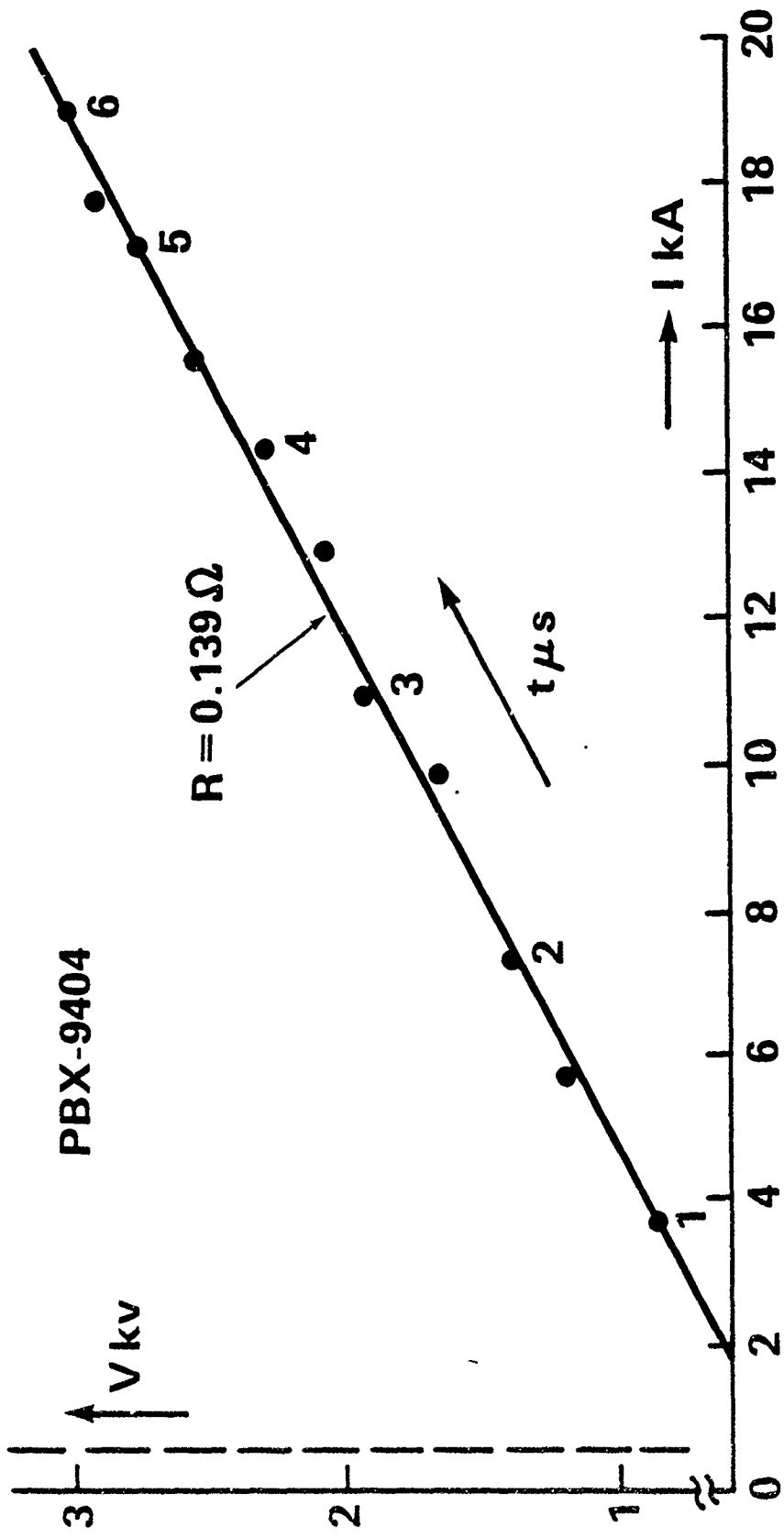

FIGURE 8-3. PBX-9404 DATA WITHOUT AIR EFFECTS

CHAPTER 9

SUMMARY

ELECTRICAL CONDUCTIVITY

In this report the various measurements of electrical conductivity in detonating HE's at very high current densities (circa 10^9 to 10^{11} A/m^2) have been described. These measurements were made extraordinarily difficult by the combination of large rapidly changing electrical currents (and voltages) with the already hostile environment of a detonating explosive. The difficulties imposed by these conditions were described as well as the techniques that have been developed to surmount them.

Conductivities have been measured for a number of explosives, although these studies have concentrated on just two: PBX-9404 and PBX-9501. Their products of conductivity and conduction zone width were in the range of 1-2 mhos.

ANOMALIES

Anomalies due to conduction within shocked gases and plastics observed. The measurement of the electrical conductivities of [illegible] plastics and air are therefore of great importance to the program.

ENHANCEMENTS

Measurable performance enhancements of PBX-9501 have been obtained which demonstrate that the technique is viable. Moreover these measurements are in good agreement with calculations.

FUTURE REPORTS

The application of the physics associated with EMEC phenomena will be described in a future report. This will provide methods of predicting performance, the development of equations of state for the enhanced explosives and the modifications necessary for computer models to account for electromagnetic effects. A number of potential applications will also be reviewed together with their electrical power sources.

OUTLOOK

The future for EMEC looks bright; no fundamental difficulties can be identified that would mitigate against the successful application of the technique. The physics of the enhanced detonation phenomena are fascinating; irrespective of the success of the program, our understanding of detonation

fundamental topics.

Plasma Physics is being applied to detonating explosives for the first time by Griem and Daniels at the University of Maryland. By estimating the mobilities, ionization potentials and number densities of likely product species, it should be possible to calculate the conductivities of the explosives. Preliminary results are very interesting; they suggest the probable dominance of hydrogen minus ions as electrical carriers if a mixture of monatomic product species is assumed. The final results will be compared with experiments and used to test reaction pathway calculations.

Solid State Physics is to be used to calculate the conductivity of compressed, organic explosive crystals; this is another new avenue of research. Preliminary calculations, by Crawford of Oak Ridge National Labs, of the modified band gap structure of materials such as TNT are particularly interesting. The gap can be sufficiently modified by the application of high pressures, commensurate with the detonation process, that electrical conductivities comparable to those actually observed may be obtained.

Spatial Distribution of Conductivity. The distribution for detonating explosives is currently being measured. The reaction zone may be as narrow as 0.1 mm so that these difficult measurements must provide detailed data within the nanosecond time scale. This work is of fundamental importance. It provides an entirely new diagnostic tool for probing the detonation zone, provides vital data to test the theoretical research described above, and provides information that is essential for the accurate modelling of the enhanced detonation process.

Further work on dielectric breakdown is planned in which the effects of the time duration of the applied fields will be studied.

Mathematical Modelling. Other original research includes mathematical modelling of the enhanced detonation process, where a two rate energy deposition mechanism is considered. This situation applies equally well to both insensitive (non-ideal) explosives and electromagnetically enhanced explosives.

Shock Wave Stability. The stability of these two rate deposition mechanisms is also being modelled theoretically for the first time.

REFERENCES

1. Lee, R. J., Static Dielectric Breakdown Studies of High Explosives, NSWC TR 85-380, in preparation.

2. Brish, A. A., Tarasov, M. S., and Tsukerman, V. A., "Electrical Conductivity of the Explosion Products of Condensed Explosives," Soviet Physics, JETP, Vol. 37(10), No. 6, Jun 1960, p. 1095.

3. Hayes, B., "On Electrical Conductivity in Detonation Products," Fourth Symposium (International) on Detonation, Proceedings, Office of Naval Research, Department of Navy, Washington, DC, Oct 1965, p. 595.

4. Ershov, A. P., Zubkow, P. I., and Lukjantshikov, L. A., "Measurement of the Electrical Conductivity Profile in the Detonation Front of Solid Explosives," Combusion, Explosion, and Shockwaves, Vol. 10(6), Nov-Dec 1974, p. 776.

5. Demske, D. L., Forbes, J. W., and Tasker, D. G., "High Current Electrical Resistance of PBX-9404 and Dielectric Breakdown Measurements of Naval High Explosives," Shock Waves in Condensed Matter, Elsevier Science Publ., 1983, p. 551.

6. Dobratz, B. M., "Properties of Chemical Explosives and Explosive Simulants," LLNL Explosives Handbook, Lawrence Livermore National Laboratories, UCRL-52997, 16 Mar 1981.

7. Spaulding, R. L., Jr., "Precursors in Detonations in Porous Explosives," Seventh Symposium (International) on Detonation, Annapolis, Maryland, 16-19 Jun 1981, p. 877.

8. Hayes, B., and Tarver C., "Interpretation of Detonation Parameters from Experimental Particle Velocity Records," Seventh Symposium (International) on Detonation, ibid., p. 1029.

9. Short, J. M., Adolph, H. G., and Kamlet, M. J., "Simplified Methods for Predicting Explosive Performance Parameters Including Ermenko's Relative Detonation Impulses," Seventh Symposium (Internation) on Detonation, ibid., p. 952.

10. Toton, E. T., High Explosive Detonation and Electromagnetic Interation, NSWC TR 79-205, 30 Mar 1979.

11. Demske, D. L., Experimental Aspects of Coupling Electrical Energy into a Dense Detonation Wave: Part 1, NSWC TR 79-143, 17 May 1982.

REFERENCES (Cont'd)

12. Webb, F. H., Hilton, H. H., Levine, P. H., and Tollestrop, A. V., "The Electrical and Optical Properties of Rapidly Exploded Wires," Exploding Wires, Chace, W. G. Moore, H. K., eds. (New York: Plenum Press, 1962), Vol. 2(37).

13. Punkevich, B. S., and Stepanov, B. M., "Electrical Conductivity of Air Behind the Shock Front with Explosion of Condensed Explosives," Fizika Goreniya:Vzryva, Mar-Apr 1982, Vol. 16(2), p. 109.

14. Measurement of Electrical Quantities in Pulsed Power Systems, Proceedings of Workshop, National Bureau of Standards, Boulder, Colorado, 2-4 Mar 1981.

15. McClenahan, C. R., Current Transformer High Voltage Probes, Sandia Laboratories, Albuquerque, New Mexico, 87185, 1978.

16. Braunsberger, U., Salge, J., and Schwarz, U., "Circuit Breaker for Power Amplification in Poloidal Field Circuits," Proceedings of the Eighth Symposium on Fuse Technology, Noordwijkerhout, Netherlands, Jun 1974.

17. Grover, F. W., Inductance Calculations, Chapter 17, North Carolina: Instrument Society of America, 1973.

APPENDIX A

VOLTAGE MEASUREMENTS

The measurement of high voltages in pulse power experiments is notoriously difficult; specialist conferences have been dedicated to it.[14] The measurement of high voltages in an explosives environment is therefore even more challenging. Until the identification of the source of errors in voltage measurement, discussed below, reliable voltage data have proven to be exceedingly difficult to obtain in Energy Coupling experiments.

A.1 The Errors in Voltage Measurements Due to Rapidly Changing Electric Currents

These errors can be large and are often comparable to the true voltage data required. The errors can be traced to the peculiar nature of Energy Coupling experiments in which very large electric currents, typically 10^5 Amps, are rapidly switched on or off by the conducting explosive. These problems are particularly acute when an intermediate storage inductor is used (see Chapter 7). Various techniques have been developed which have reduced these errors to the point where they are negligible.

Theory

In a typical voltage measurement circuit, little attention is paid to the physical layout of connecting leads. Voltage measurement circuits, or voltage probes, almost by definition, measure voltage with a negligible flow of current in the measurement circuit. As little or no current flows in the measurement circuit, there is usually no need to consider the resistance or inductance of the connections. These lead impedances are swamped by the resistance of the probe itself. However, consider a typical voltage measurement in the Energy Coupling experiment, Figure A-1. A large current, i_1, typically 100kA, flows through the small resistance r, the resistance of the conducting explosive that is to be measured, say r=0.1Ω. The voltage ΔV is measured by the probe V_2 which conducts a comparatively small current i_2, perhaps 10A.

Now, if the stray circuit inductances are included, the equivalent circuit is that of Figure A-2. L_1 is the inductance of the leads providing large currents to the explosive load. In earlier Energy Coupling experiments, this could be between 0.1 and 1μH; here we will use 1μH as the worst case. Similarly, the voltage probe leads would be simple flying lead connections and would have an inductance, L_2, of several μH, say 1μH. It is entirely possible that the mutual inductance between these circuits could be up to 100nH. It is this mutual inductance that causes the large errors.

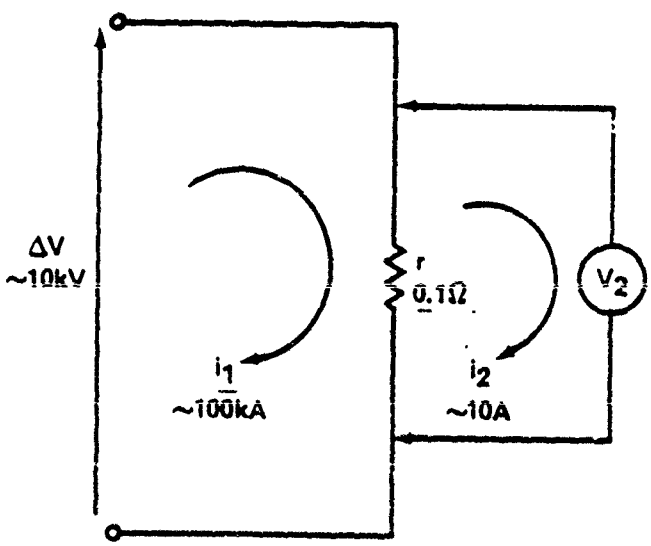

FIGURE A-1. VOLTAGE PROBE CIRCUIT

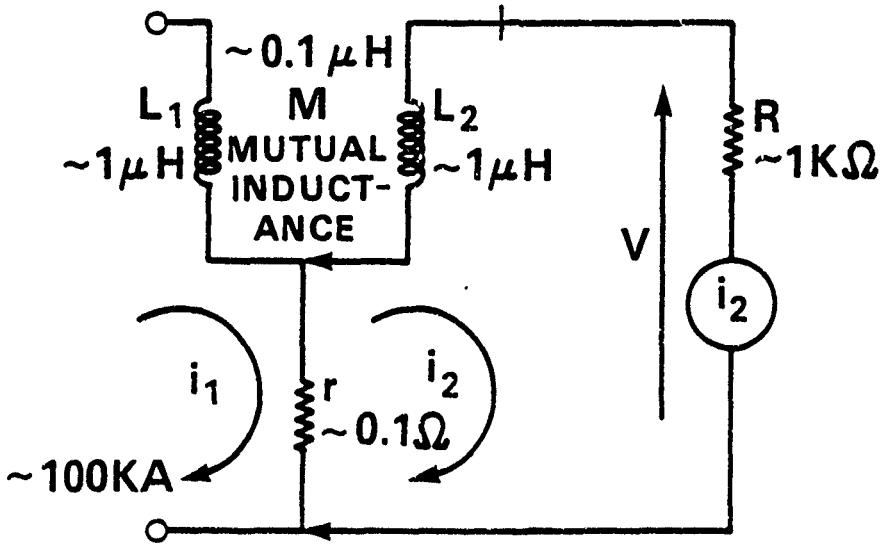

FIGURE A-2. VOLTAGE PROBE EQUIVALENT CIRCUIT

The voltage to be measured, ΔV, is

$\Delta V = i_1 r$ whereas the voltage detected is V_2,

$V_2 = i_2 R$ where R is the resistance of the voltage probe,

we will show that $\Delta V \neq V_2$. From Kirchoff's laws

$$i_2(r+R) + L\frac{di_2}{dt} - M\frac{di_1}{dt} - i_1 r = 0$$

Now $R >> r$, $i_1 >> i_2$ and therefore $L_2 \frac{di_2}{dt} << M\, di_1/dt$.

Hence $\Delta V = i_1 r = i_2 R - M\, di_1/dt$, or the detected voltage V_2 is

$$V_2 = \Delta V + M\, di_1/dt$$

$M\, di_1/dt$ is the error signal. In an Energy Coupling experiment, $di_1/dt \sim 10^{11}$ A/S, then $M\, di_1/dt$ = 10kV and $V_2 = \Delta V + M\, di_1/dt$ = 20kV.

Clearly, errors comparable with the true voltage are entirely possible. Although such large errors were rare, significant errors were common. Notice that these errors are independent of the resistance R of the probe; they are common to all probes of all types (resistive, capacitive, etc.) and exist wherever there are large di/dt's in an experiment.

There is no way to completely eliminate the $M\, di_1/dt$ signal because M and di_1/dt are not constant from experiment to experiment. If they were constant, then a differential amplifier could be used to subtract this effect. However, the error can be reduced to negligible proportions if M, and of course di_1/dt, are reduced. The mutual inductance M is dependent on the two inductances L_1 and L_2, $M = K\sqrt{L_1 L_2}$ where K is the coupling constant of the experiment and is between 0 and 1 in magnitude. In a typical circuit it would be approximately 0.1.

Solution

The pulse power circuits are now built using stripline techniques; in this way stray inductances can be drastically reduced. Stripline techniques are also required to minimize circuit risetimes. Stray inductances have thus been reduced by several orders of magnitude from ~1μH to ~10nH; moreover, the voltage probe connections are now made using a combined stripline and coaxial connector so that K, the coupling coefficient, has been reduced by at least 10. Consequently, $M\, di_1/dt$ errors have been reduced to approximately 0.1% of the true signal; the errors are thus considered negligible.

A.2 Copper Sulphate Voltage Probes

Another source of error in voltage measurement is the reactive nature of large high voltage resistors. Stray inductances and capacitances in these resistors change the impedance of the probes at high frequencies. Many techniques have been used to reduce these errors, including complex impedance trimming networks typified by those used in the Tektronix P6015 probe. These devices are expensive, therefore not expendable, shock sensitive and extremely difficult to use in a differential fashion (so as to eliminate ground loops). Also, the P6015 cannot be used above 40kV. High voltage probes are usually designed to minimize loading of high impedance circuits, and the P6015 has a resistance of 100 MΩ; yet in an Energy Coupling application even a 100Ω resistance would present a negligible load in comparison to the explosive resistance (0.1Ω). If a smaller probe resistor is used, then stray inductances and capacitances will have negligible effects and the probe is simply rendered frequency independent, which is the required goal. It was suggested by J. Goforth of LANL that small, high voltage resistors can be made simply and cheaply with saturated solutions of copper sulphate; these have a resistivity ρ = 25 Ω cm. They have excellent high voltage stability but must be calibrated immediately prior to their use to eliminate errors due to thermal drift and aging. These solutions can withstand very high voltages and large, short duration powers without change of resistivity. They can be used routinely in explosives experiments without concern for their loss; they are expendable. The resistors are made by filling Tygon plastic tubes with the saturated solution and inserting stainless steel electrodes in the ends as plugs. The resistance can be controlled by changing the tubing length and diameter. A tube of 6.35mm internal diameter and 127mm length has a resistance of approximately 1KΩ. The exact resistance is measured immediately prior to use of the voltage probe using a high frequency (10kHz to 1MHz) precision AC bridge, Hewlett Packard 4227A. To prevent ground loops, between the measurement circuit and the high current circuit, current in the copper sulphate resistor is measured using a Pearson current transformer.[15] The plastic tubing is passed through the center of the transformer. From the measured resistance of the copper sulphate and the known sensitivity of the current transformer the sensitivity of the probe can be calculated. Typically, this sensitivity agrees to within 1% with calibration against a known voltage.

A.3 Capacitive Effects

The voltage probe circuit is shown in Figure A-3. Current in the copper sulphate resistor R is monitored with the current transformer C.T. The reactance of the current transformer primary is negligible, so that V = iR. The signal detected in the secondary is

$$v = Ki.$$

Stray capacitance, C_s, will exist between primary and secondary circuits, both within and without the transformer. Typical values are K = 0.05 A/V, V = 1 kV,

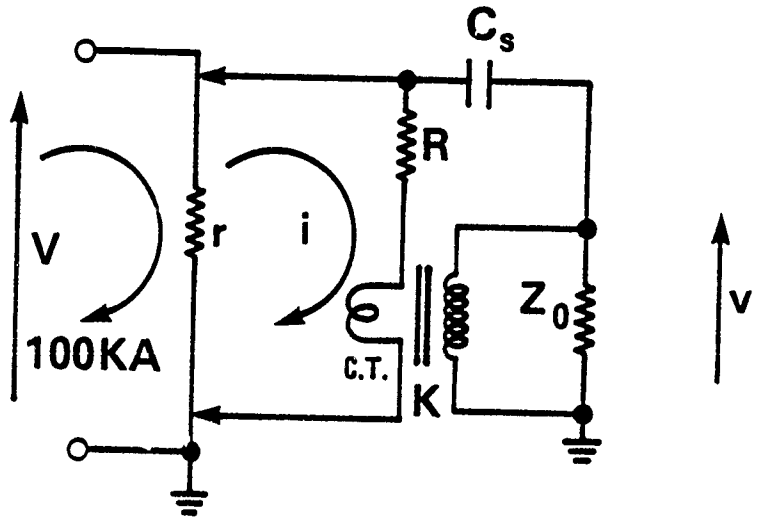

FIGURE A-3. VOLTAGE PROBE CIRCUIT

$dV/dt = 10^9$ V/s, R = 500 Ω, C_s = 4pF and Z_0 = 25 Ω. So the error from the capacitive signal is

$$C_s(dv/dt)Z_0 = 100 \text{ mV}$$

which can be comparable to the true signal, i.e.

$$Ki = K(V/R) = 100 \text{ mV}.$$

Clearly, great care must be taken to minimize these errors by minimizing stray capacitances, reducing R and increasing K. If C_s = 1pF, K = 0.5 A/V and R = 100 Ω, then the effect is reduced to 1/2%.

A.4 Other Improvements to Instrumentation

Other sources of noise in the Energy Coupling diagnostics have been identified. A careful analysis of noise in Rogowski coil detectors has led to the design of a new distributed integrator technique, Appendix C; this has virtually eliminated noise due to stray magnetic fields external to the current generated magnetic field of interest. Grounding of instrumentation racks with wide copper ground planes and grounding modifications to digital oscilloscopes have eliminated signal errors previously encountered.

Conclusions

The combination of the use of copper sulphate voltage probes and stripline methods represents a major breakthrough in Energy Coupling experimentation that cannot be overstated. Accurate voltage measurements are now routinely obtained. Further improvements in instrumentation have virtually eliminated all remaining sources of noise. Accurate, reliable current and voltage data are now obtained.

APPENDIX B

COAXIAL FUSE, THEORY, AND DESIGN

Theory

The explosively activated circuit breaker (EACB), described in Chapter 7, was employed to interrupt a current of 140kA flowing in the storage inductor of the experiment. The magnetic energy trapped within the inductor could then be diverted to the explosive load. The EACB had an initial circuit resistance of approximately 60μΩ; when the device was initiated then the cylindrical aluminum conductor was ruptured by explosively driven paraffin wax, and the resistance rose to 40mΩ; the voltage thus rose to 5.6kV (i.e. 140kA x 40mΩ). The subsequent reduction of the current generated a voltage L dI/dt across the storage inductor (6 kucV). At the time of rupture, the voltage across the capacitor was close to zero, then the EACB and the circuit inductances were effectively in parallel and the voltage across both was 5.6kV. The small openings in the ruptured aluminum thus had a large voltage across them, and arcs were generated in the hot paraffin wax. The linear copper fuse LF was designed to divert current from the EACB and thus allow the wax to cool; then it can withstand the applied voltage; see Figure B-1. From experience it was known that the EACB could withstand 100kV if it were allowed to cool for at least 40μs; 50μs was selected for the fuse to err on the safe side. Consequently, the fuse was designed to conduct 140kA for 50μs, then vaporize; the fuse thus became the opening switch. The design criteria for the cooper fuse are well known; the following formula (due to Braunsberger[16]) was used to calculate the diameter of copper wire required,

$$I = 5 \times 10^5 \; a \; t_f^{0.54} \qquad \text{(B-1)}$$

where I is in Amps, a the cross-section in mm^2 and t_f the time to fuse vaporization in μsec.[16] Rearranging we obtain

$$\int_0^{t_f} \left(\frac{I}{a}\right)^{\frac{-1}{0.54}} dt = 3.58 \times 10^{10} \; . \qquad \text{(B-2)}$$

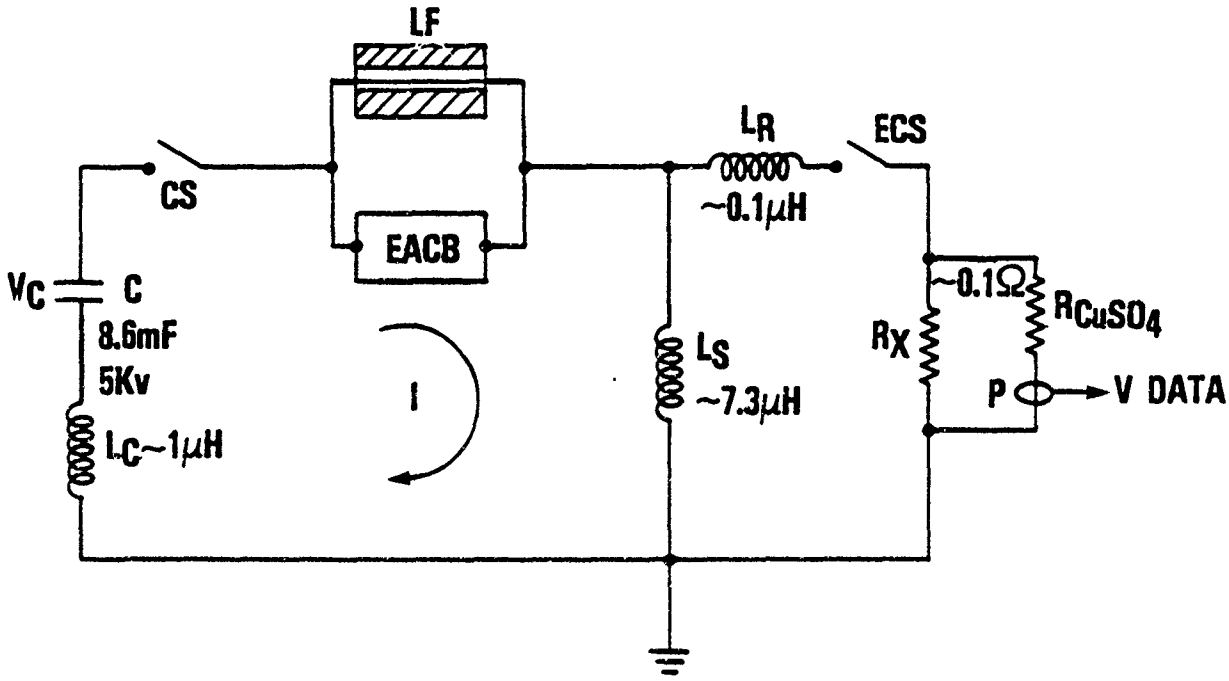

FIGURE B-1. INTERMEDIATE STORAGE INDUCTOR CIRCUIT, SCHEMATIC

The expression of Eq. B-2 is a best fit to data that was obtained experimentally; it is a convenient approximation to an expression of the form

$$\int_0^{t_f} I^2(t)R(t)\,dt = alK \equiv 5.54 \times 10^{10}\ J/m^3 .$$

where R(t) is the fuse wire resistance which increases by perhaps two orders of magnitude as the wire heats up, l is the wire length, and K is a constant which accounts for the heat required to raise the temperature of the copper to vaporization. The heat required to vaporize copper, from the solid state at room temperature, is 5.5×10^{10} J/m^3. By changing the exponent from 2 to (1/0.54), the fit of (B-2) to the experimental data is good enough for engineering purposes. From Eq. B-1, a copper wire with a cross section of 2.3 mm^2 would correctly commutate current in the EACB for 50μs; a wire of 1.74 mm diameter was used. The linear fuse comprised of a 1.74 mm diameter wire up to 400 mm long, soldered between two 25.4 mm diameter hemi-spherical brass[1] electrodes. These were confined in a 100mm diameter polylethylene cylinder, and the cavity surrounding the wire was filled with distilled water, see Figure B-2.

Results

In no experiment did the linear fuse correctly operate; a typical experiment is shown in Figure B-3 in which both the EACB and fuse currents are plotted. For the 300μs after the switch CS was closed, the EACB and fuse currents rose sinusoidally with the EACB carrying most of the current. At that time the EACB started to open mechanically, and arcing commenced. Consequently the current fell in the EACB and rose in the fuse so that the total current flowing through the storage inductor, L_s, remained approximately constant. The EACB current dropped almost to zero which started to cool whilst the fuse current reached a plateau of approximately 140kA. The fuse current should have stayed at approximately 140kA for 50μs. Yet after less than 10μs, the fuse current started to fall and, consequently, the still hot EACB began to conduct again. The EACB was not turned off by the fuse for long enough to stay off, and no useful voltage could be generated to transfer to the explosive load.

Energy Considerations

Clearly, the current flow in the fuse was not a square pulse, that is the current did not start conducting 140kA instantaneously, but started by rising slowly to approximately 20kA over 300μs. It is therefore necessary to determine if the subsequent premature heating of the wire could account for the short lifetime of the fuse current at 140kA. If we return to Eq. B-3 then we can write

$$\int_0^{t_f} I(t)^{-1/0.54}\,dt = 3.58 \times 10^{10}\ a^{1/0.54} .$$

This integral was calculated numerically for the record of Figure B-3, after corrections had been made for the Rogowski coil integrator time constants as in Appendix C. [The currents are accurate to within 1%]. The results are shown in Figure B-4.

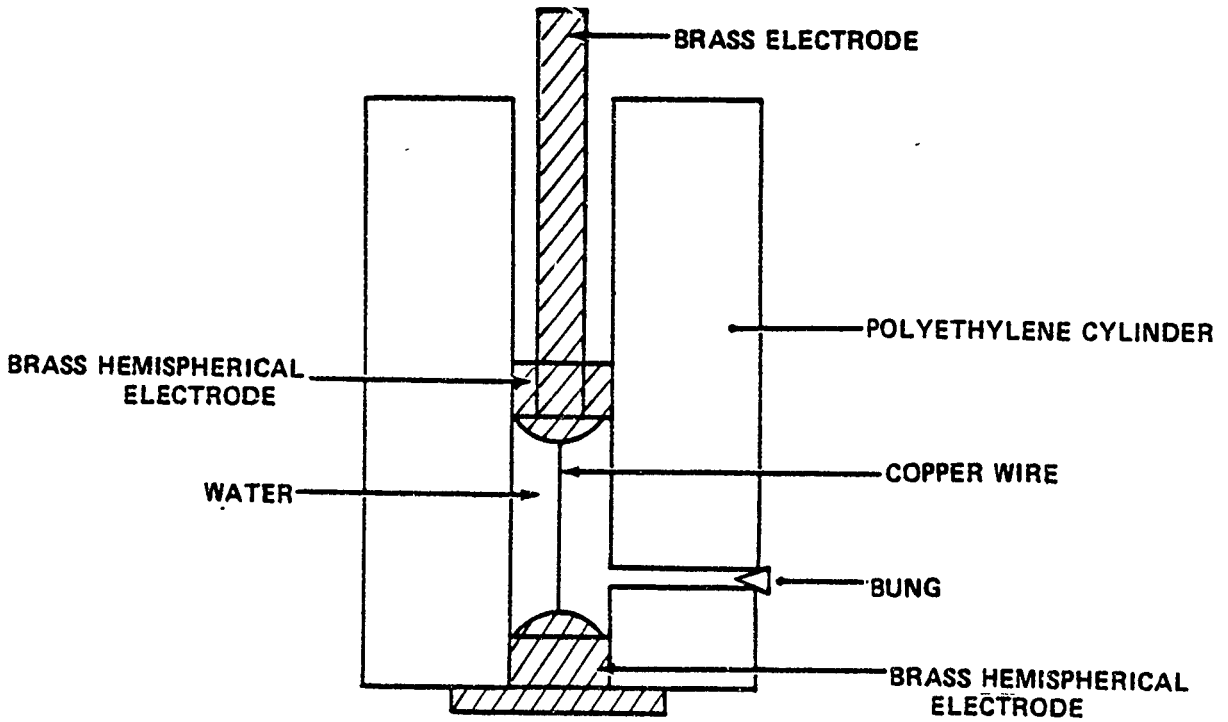

FIGURE B-2. CROSS SECTION OF LINEAR FUZE ASSEMBLY

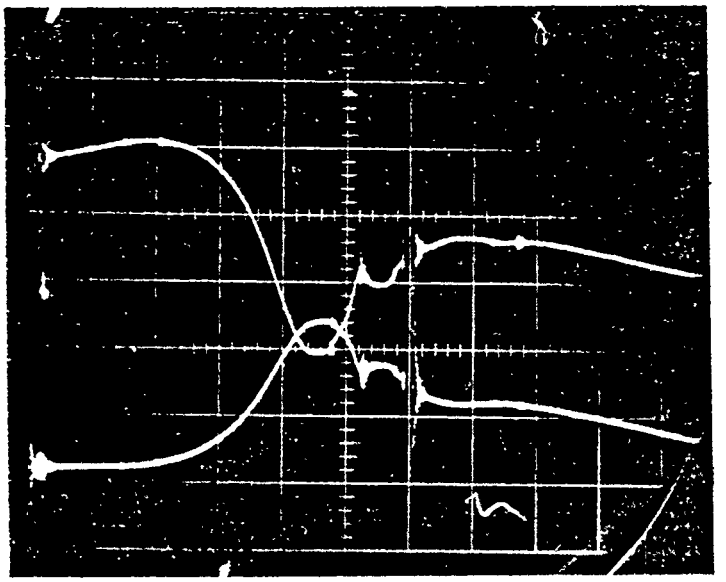

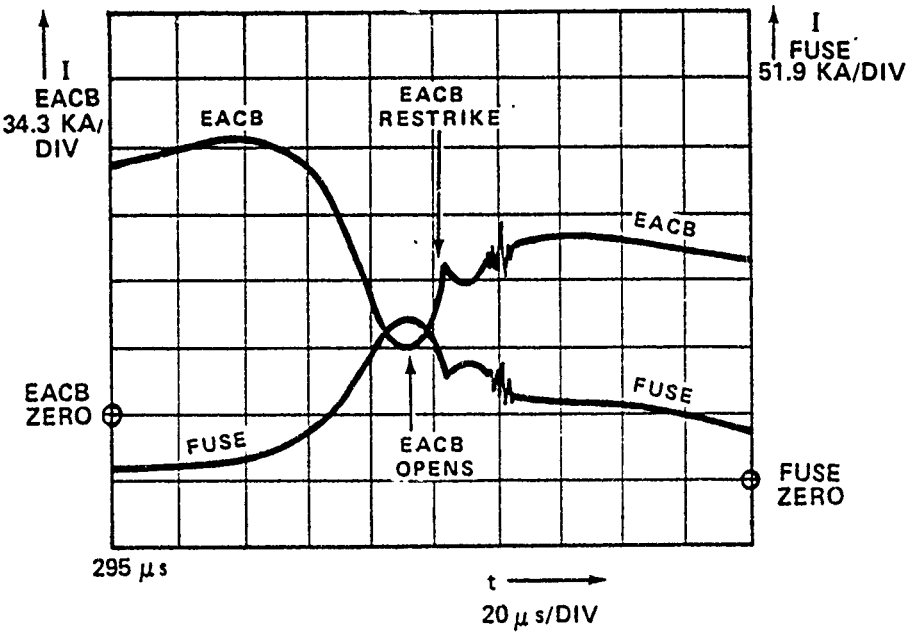

(CURRENTS NOT CORRECTED FOR INTERGRATOR EFFECTS)

FIGURE B-3. EACB AND LINEAR FUSE RESPONSE

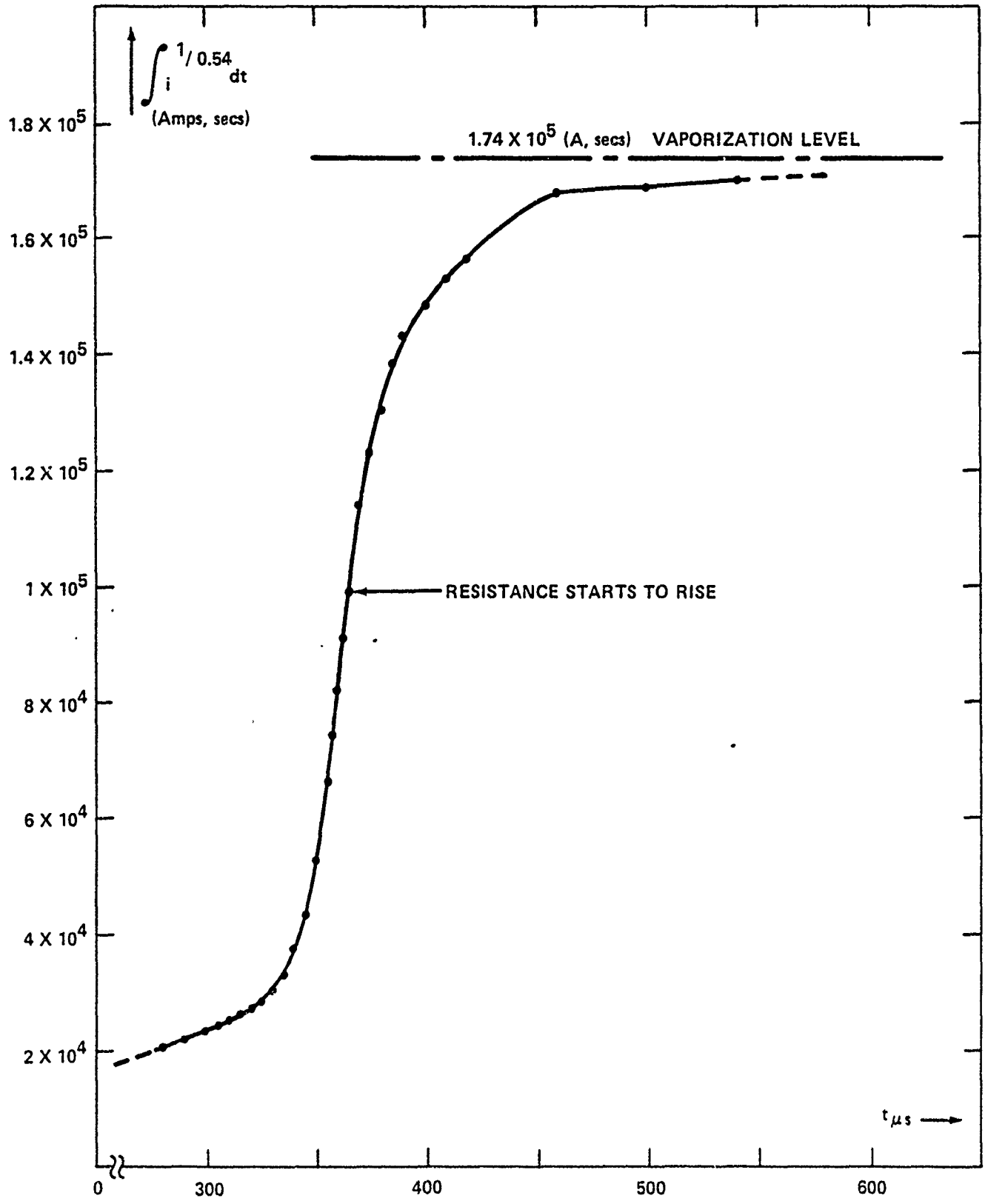

FIGURE B-4. CURRENT - TIME INTEGRAL

From the above equation, the integral should have equalled 1.74×10^5 (in units of A,secs) for a wire of 2.35 mm^2 cross section to vaporize. It can be seen that the resistance of the wire started to rise at the end of the plateau when the integral was only 9.9×10^4 (A,secs), a little over half the necessary value. From this we must infer that the fuse did not vaporize. Moreover, current continued to flow long after the end of the plateau, but note that the integral never reached that required for vaporization.

Magnetic Effects

The results above necessitated a re-evaluation of the fuse operation. Some of the many possibilities considered were various instrument errors, shock loading from the EACB action and magnetic effects. The instrument errors were systematically discounted. Shock loading could not account for the problem; the timing was wrong and the insertion of shock attenuators had no effect. Consequently, the magnetic loading was considered as follows.

Magnetic loading could be due to $\vec{J}x\vec{B}$ forces imposed on the fuse wire by the storage inductor field. This was discounted because the error was very reproducible and independent of the separation of the fuse from the storage inductor. The other possibility was a magnetic interaction between the currents flowing in the EACB and fuse.

The EACB and fuse had been placed as close as possible together to minimize inductance; this was necessary to ensure a fast commutation of currents. The arrangement is shown in Figure B-5.

The force per unit length, dF, of wire can be calculated using the definition for the Ampere,

$$dF = \frac{\mu\mu_o I_1 I_2}{4\pi r^3} \quad \vec{d\ell}_1 \times (\vec{d\ell}_2 \times r) \quad , \qquad \text{(B-3)}$$

where $d\ell_1$ and $d\ell_2$ represent elements of each of the two conductors that are interacting.

Two simplications are used. First, the current flowing over the surface of the EACB can be represented by an identical current along its axis. Secondly, the two conductors are separated by air. For two parallel inductors the force on them becomes

$$dF = \frac{\mu_o I_1 I_2 \ell}{2\pi r} \quad ,$$

and the force is attractive since I_1 and I_2 are in the same direction. Now, when the EACB is turning off we can have the situation where $I_1 = I_2 = 70$ kA, and the force is a maximum. Then the force on the total fuse is F = 980N for a wire of length l = 15 cms and a separation r = 15 cms. This is a very large force that will try to stretch the wire towards the EACB in a catenary. The wire is thus put into tension.

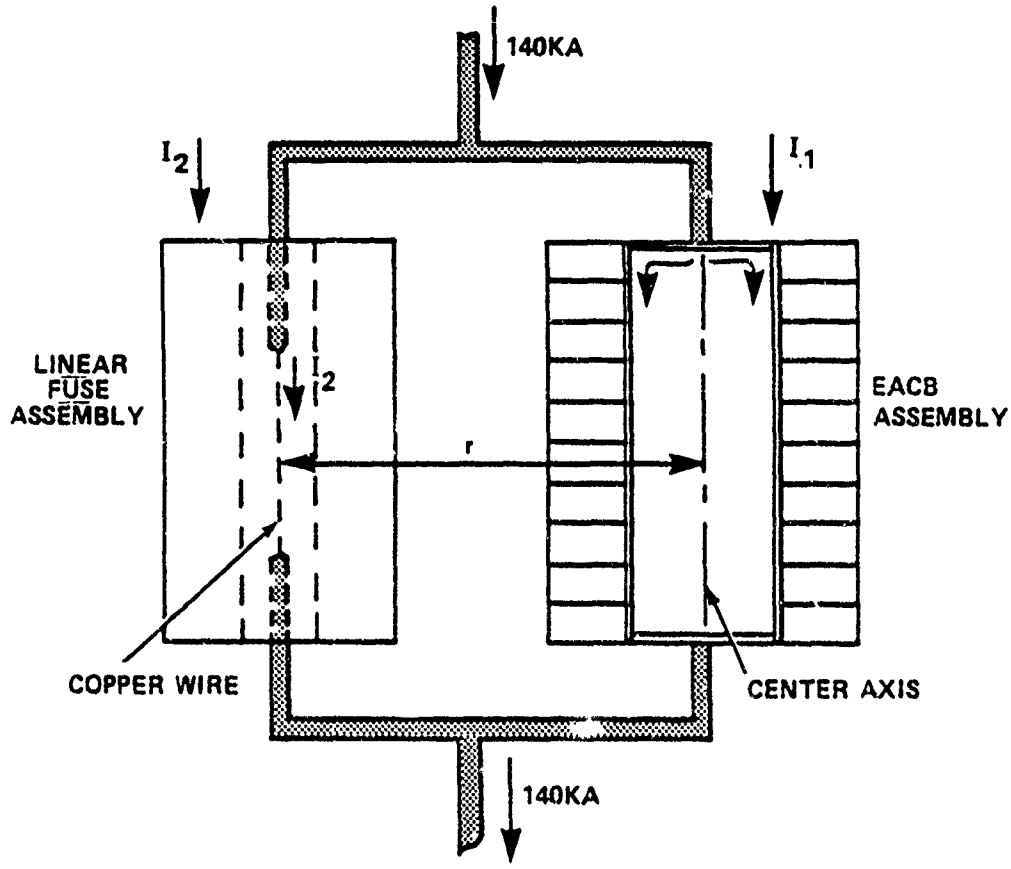

FIGURE B-5. EACB/FUSE INTERACTION

An exact analysis of the mechanics of the wire, although desirable, may not be possible and is certainly beyond the scope of this appendix. As the wire heats, it thermally softens, stretches, becomes more resistive in the thinner areas and may impact the polyethylene wall if it has enough time to get there. Moreover, the vector forces described by Eq. B-3 will be modified by the angle the stretched wire subtends to the normal. However, it is easy to demonstrate that the forces are large enough to produce mechanical failure.

If you consider the wire of diameter d to behave as a classical solid round beam, supported at both ends, under a uniform load F, over the whole length ℓ, then the stress T in the extreme fibers or filaments of the wire will be

$$T = \frac{4F\ell}{\pi d^3} .$$

This tensile stress equates to -35.5 GPa, whereas the tensile strength of rolled copper, at room temperature, is no larger than -0.4 GPa. Although the treatment is not rigorous, the message is clear; the wire will readily stretch under the action of the magnetic forces. The stretching will continue until the fuse fails by a combined mechanical breakage and electrical vaporization process; consequently the fuse will not last the necessary 40μs, and it will fail prematurely.

NSWC Coaxial Fuse Design

To completely eliminate the magnetic loading of the wire, a unique coaxial fuse was designed. This is shown in Figure B-6. The copper fuse is soldered between two hemispherically ended brass conductors of 0.500 in. diameter. The bottom electrode is screwed into the base of a flat bottomed solid brass tube, 14.00 in high, 3.00 in. outside diameter, 2.50 in. inside diameter. The electrodes are enclosed by a polyethylene tubular insulator, 2.50 in. outside diameter, 0.50 inside diameter, and the cavity surrounding the wire is filled with distilled water.

The magnetic field generated by the current I in the wire does not extend beyond the outside of the brass cylinder. Everywhere outside the cylinder the magnetic fields generated by the wire and cylinder exactly cancel each other. Consequently, no forces are applied to the EACB or the fuse.

Coaxial Fuse Performance, Results

The results obtained with the coaxial fuse, in an otherwise identical experiment to the one above, are shown in Figure B-7.

The fuse current remained approximately constant for at least 40μs, and during that time the EACB did not conduct. When the fuse burst, current was successfully transferred to the load, and the EACB did not turn on again.

Conclusions

It was postulated that the premature failure of the linear fuse design was due to magnetic loading. The NSWC coaxial design successfully eliminated the problem, thereby proving that the theory was correct.

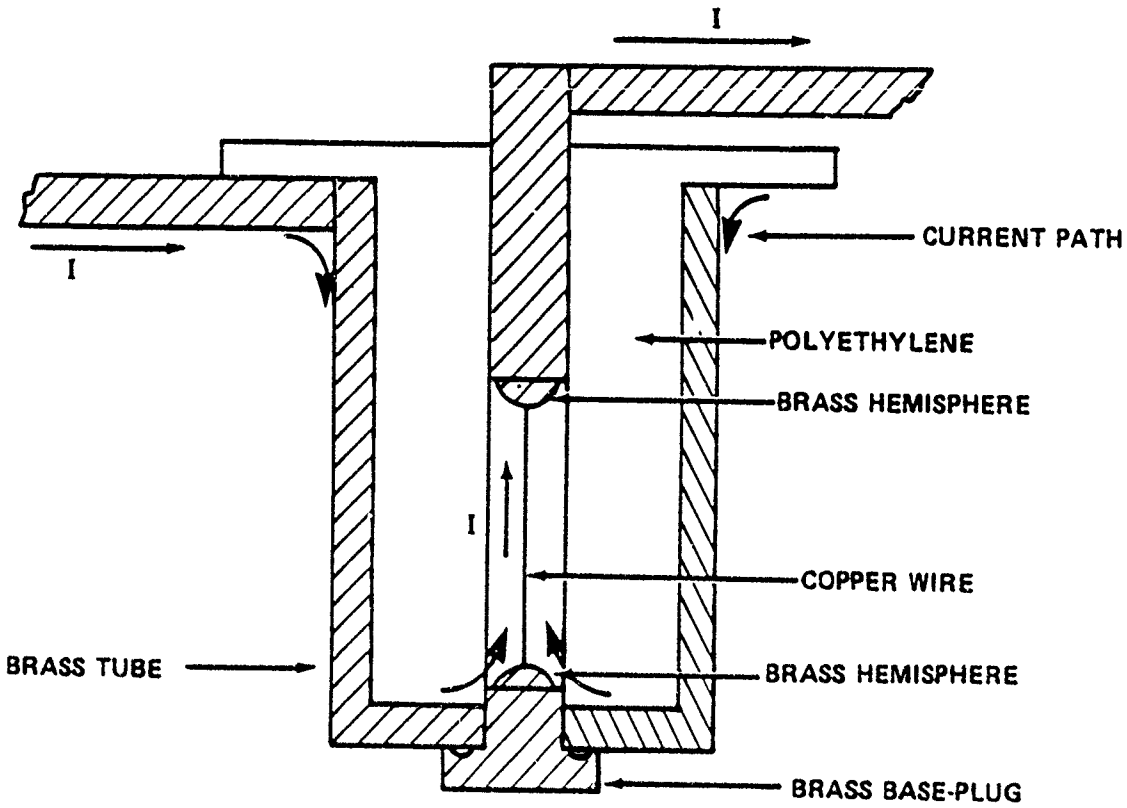

FIGURE B-6. NSWC COAXIAL FUSE ASSEMBLY

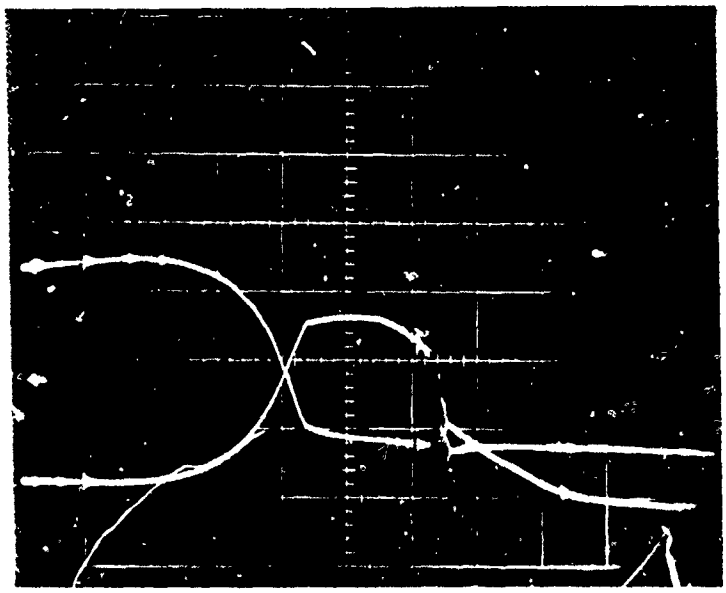

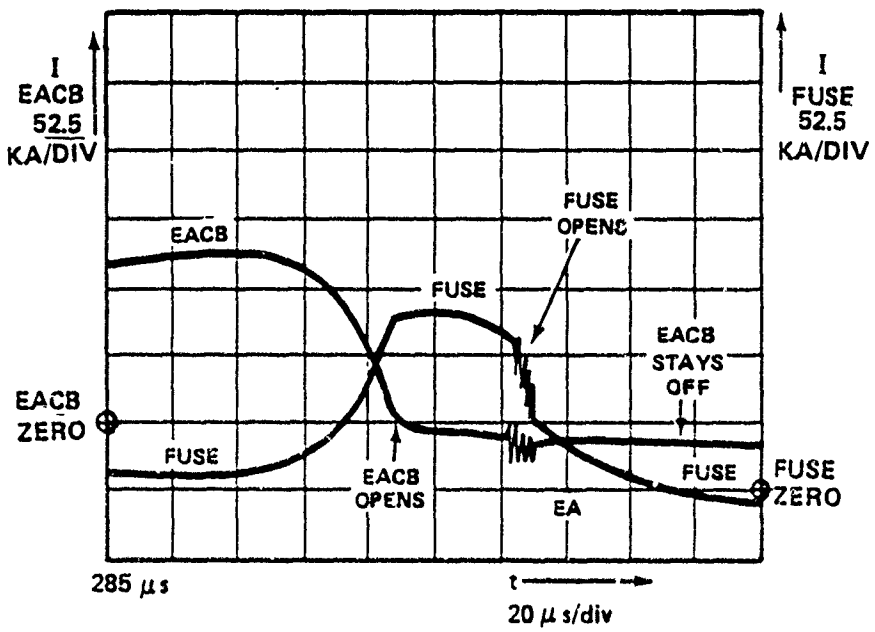

(CURRENTS NOT CORRECTED FOR INTERGRATOR EFFECTS)

FIGURE 8-7. COAXIAL FUSE RESPONSE

APPENDIX C

ROGOWSKI COIL CURRENT MONITORS, ERROR ANALYSIS AND IMPROVEMENTS

The Rogowski coil is a device for the measurement of electric current that lends itself to pulsed power applications, as will be seen. It is based on a toroidal coil configuration; a typical device is shown in Figure C-1. The current to be measured, I, flows through the conductor at the center of the coil.

Theory

A brief theoretical analysis will be helpful in order to understand the sources of error. From Ampere's circuital law we can describe the magnetic field induced by the current in the region outside the wire as

$$\int \vec{B} \cdot \vec{dl} = \mu_0 \int_S \vec{J} \cdot \vec{da} = \mu_0 I ,$$

where J is the current density and da the cross section of the coil. The surface integral in this case can be replaced by I, the current in the wire. μ_0 is the permittivity of the free space surrounding the wire. The left hand side describes the line integral of the magnetic field B along a closed path. For a long wire the equation reduces to its scalar form since B is azimuthal,

$$B = \frac{\mu_0 I}{2\pi r} ,$$

where r is the radius from the center of the wire. Now in a Rogowski coil the field B normally intersects the plane of a toroidal coil of n turns per unit length and cross section πa^2. In so doing, this coil reacts to the applied B field in such a way as to oppose a change of field (Lenz's law). By Faraday's induction law we can calculate the magnitude of the electic field E induced in the coil, so as to oppose a change of B, and the subsequent electromotive force (e.m.f.) ε generated across the output terminals

$$\int \vec{E} \cdot \vec{d\ell}' = - \frac{d}{dt} \int_S \vec{B} \cdot \vec{da} .$$

Here $d\ell'$ describes a line integral around the loops of the coil, and the right hand side represents the integral of the B field crossing the surface of cross-section of the coil. For simplicity, B is assumed to be normal to the

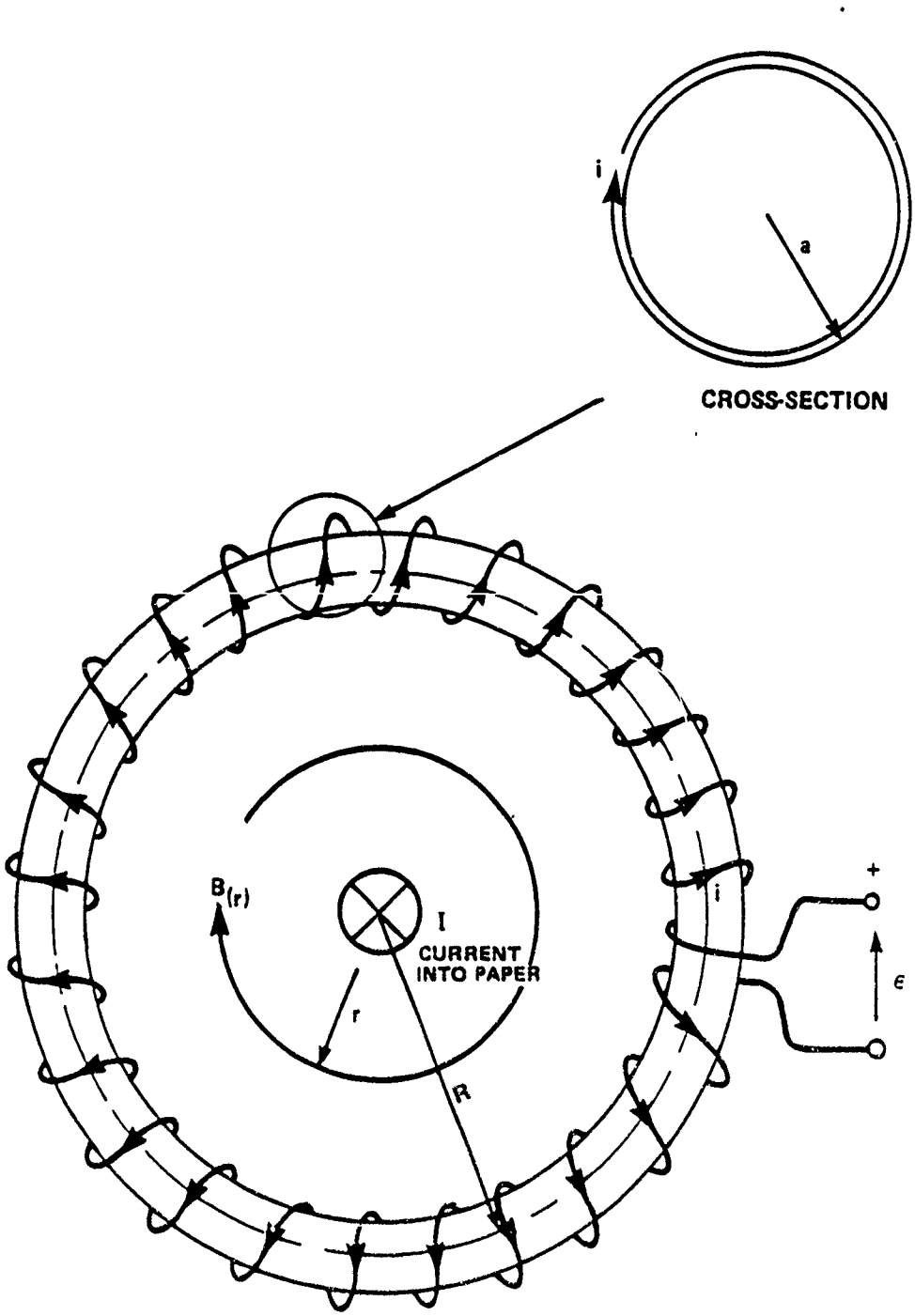

FIGURE C-1. TOROIDOIL COIL

cross section everywhere and constant over the complete surface of the coil. Then

$$\oint \vec{E} \cdot d\vec{\ell}' = -\frac{d}{dt}(B\,\pi a^2)$$

$$= -\frac{\mu_o}{2\pi R}\,\pi a^2 \frac{dI}{dt} \quad \text{for each turn}$$

from above. Here D is the major diameter, R the major radius of the coil, and we have assumed that R>>a so that B is constant across the whole cross section of the coil. Finally, we know that the detected e.m.f. ε is the product of the circumference of the wire and the electric field,

$$\varepsilon = 2\pi a E n.$$

Thus,

$$\varepsilon = -\frac{\mu_o n a^2}{2R}\frac{dI}{dt} \quad . \tag{C-1}$$

The measured e.m.f. is in effect that due to the mutual inductance M between the center wire and the surrounding coil where

$$M = \frac{\mu_o n a^2}{2R} = \frac{\mu_o n a^2}{D} \tag{C-2}$$

$$\varepsilon = -M\frac{dI}{dt} \quad . \tag{C-3}$$

The negative sign is usually omitted for simplicity.

Consequently, by the measurement of ε and a knowledge of M, we can measure the magnitude of dI/dt. This measurement is non-intrusive. However, toroidal probes are relatively insensitive, typically M 1nH, so that if we monitor a current of 1 Ampere (A) flowing at a frequency of 1 MHz we detect a signal of a mere 6 mV. Consequently, they are best suited to pulsed power applications, where $dI/dt = 10^9$ A/sec or higher. Moreover, the signal ε must be integrated with respect to time to obtain the true current.

Rejection of External Fields, the Rogowski Coil

The toroidal coil of Figure C-1 is sensitive, not only to fields generated internally by the current I, but to external fields also. Consider Faraday's law again,

$$\oint \vec{E} \cdot d\vec{l}' = \frac{-d}{dt}\int_S \vec{B} \cdot d\vec{a} \quad .$$

If we consider the coil of Figure C-1, then it can be seen that a B field entering the loop normal to its plane, i.e. into the paper, will introduce an additional signal ε'. If the field is uniform and R>>a then this will produce a signal,

$$\oint \vec{E} \cdot \vec{dl}' = - \frac{dB}{dt} \times \pi R^2 = \varepsilon' ,$$

for a single loop. To correct for this error a return loop is used; Figure C-2. In this device the signal ε' is ingeniously negated by doubling back one conductor around the loop along its axis. This only works perfectly if the length of the path doubled back is exactly equal to the perimeter of the effective loop detecting ε'. Then the Rogowski coil is only sensitive to B fields generated by currents that are enclosed by the loop.

Integration and Associated Errors

The detected signal, albeit free from error, is proportional to the time derivate of the measured current I, Eq. C-3,

$$\varepsilon = - M \frac{dI}{dt} .$$

To obtain the true current I, the signal is usually integrated with an RC filter; Figure C-3, which gives an approximation to the true integral. However, the exact signal V detected at the output of the integrator is obtained as follows. Consider the charge q flowing in the circuit as

$$V_{in} = R \frac{dq}{dt} + \frac{q}{c} .$$

Then the output voltage v is q/c, thus

$$V_{in} = CR \frac{dv}{dt} + v ,$$

If the integrator input impedance is very much greater than the source impedance of the coil, then the voltage drop across the inductance of the Rogowski coil, $L\, d^2q/dt^2$, can be neglected. (The case where the inductance voltage cannot be neglected is treated later).

Thus, $V_{in} = \varepsilon$ and

$$M \frac{dI}{dt} = CR \frac{dv}{dt} + v ,$$

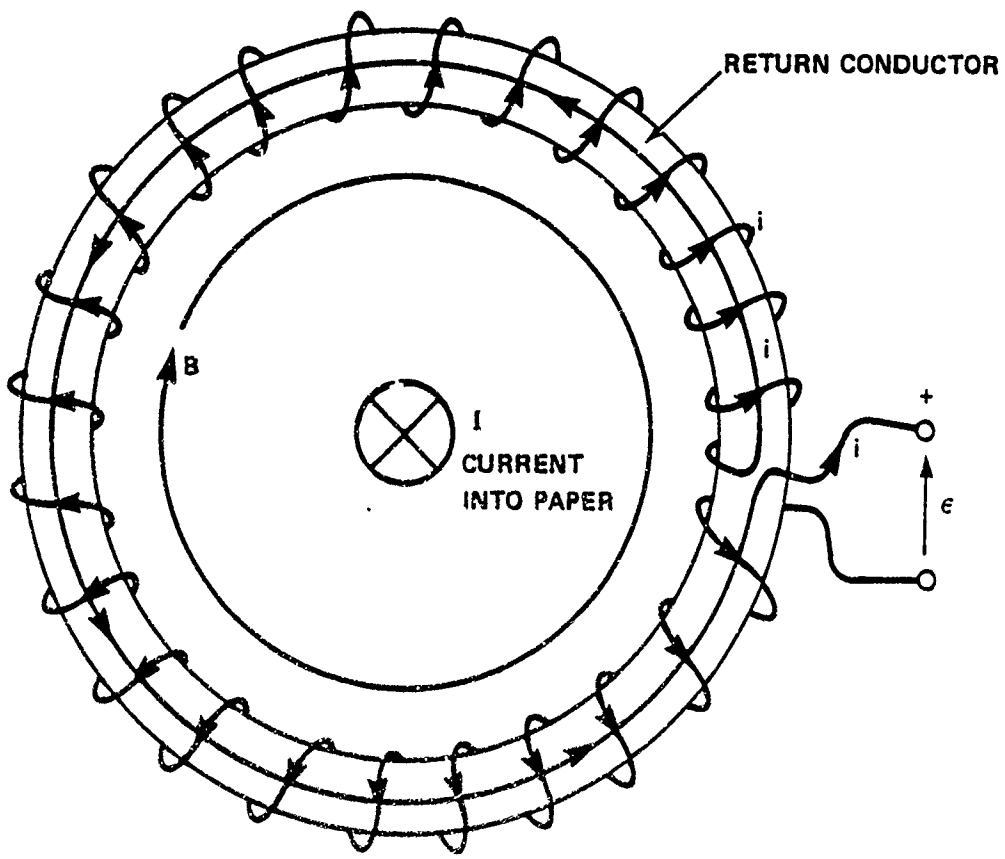

FIGURE C-2. ROGOWSKI COIL

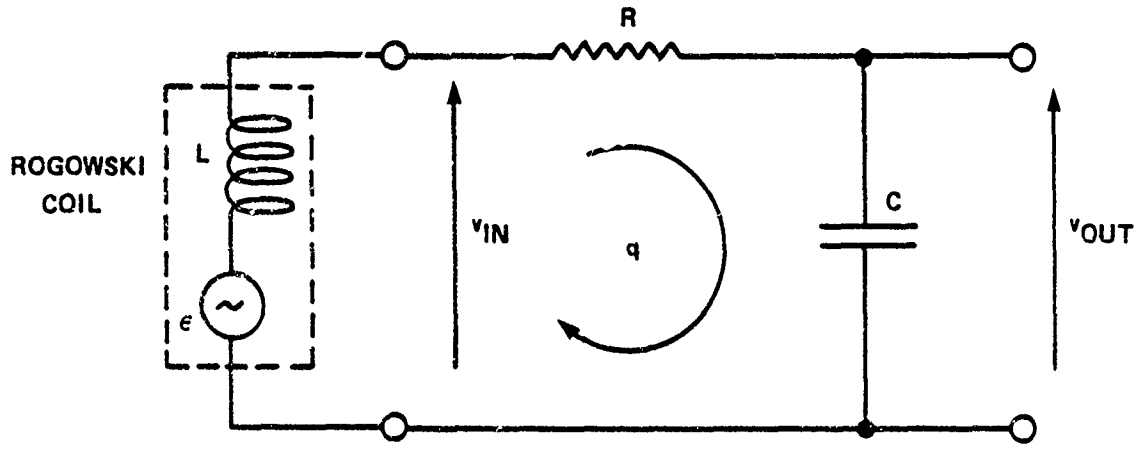

FIGURE C-3. ROGOWSKI COIL INTERGRATOR

where the sign has been dropped for convenience. By integration

$$I = \frac{CR}{M} v + \frac{1}{M} \int v \, dt$$

or

$$\frac{M}{CR} I = v(1 + \frac{1}{CR} \frac{1}{v} \int v \, dt).$$

The detected signal thus includes the rightmost error term, due to the voltage developed on the capacitor. The error is thus due to the very signal that is required and cannot be eliminated. The error is minimized by making $\varepsilon >> v$. Consequently, the larger the time constant CR is made, the smaller the error will be and the smaller the signal v. This error accumulates with time, so that for short duration signals, short with respect to CR, the error may be small. However it is possible to accurately correct for the error numerically.

Integrator Error Corrections

The integral $\int v \, dt$ can be accurately calculated using one of a variety of techniques. The oscilloscope record can be digitized by conventional trace reading techniques. If the low frequency bandwidth of a digital oscilloscope (circa 5 MHz) is not a limitation, then such equipment is the obvious choice. The records shown in this report were recorded on Nicolet digital oscilloscopes. Integration and correction were then performed using a simple programmable calculator, e.g., Texas Instruments TI59 or Hewlett Packard HP41CX. Simpson's rule has been used to numerically integrate the records; it gives accurate results very efficiency, i.e., with the minimum of computation.

The correction relies on an accurate knowledge of the time constant CR. The integration capacitor and resistor are both high stability precision components. Immediately prior to their use, the time constant is obtained by the accurate measurement of the risetime of an integrated square wave, so that temperature and time drifts are minimized. Using the same digital oscilloscopes, errors of 0.1% are thus achieved in the measurement of CR. Consequently, the error correction for the integral is very accurate and an accurate measurement of current is obtained.

Resonance and High Frequency Effects

Equivalent circuits of the Rogowski coil are shown in Figure C-4. The current to be measured, I, induces a voltage $M \frac{dI}{dt}$ in the coil which has a resistance r and inductance L. The resistance r is frequency dependent because of the skin effects, but this effect can be ignored for our purposes. A stray capacitance is represented by C_L. The integrator is shown as R and C whilst the oscilloscope is O.

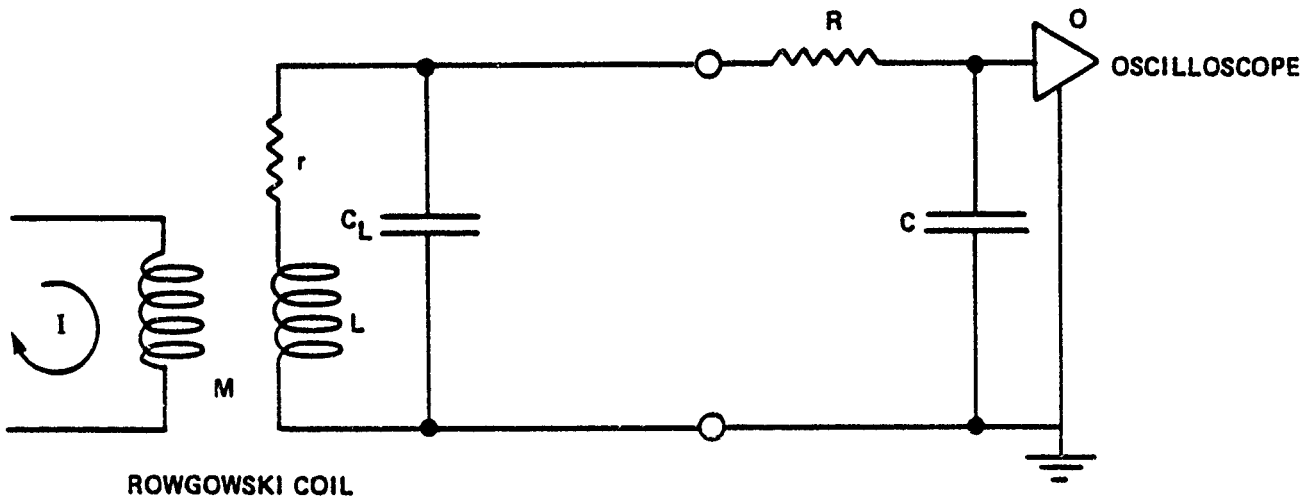

FIGURE C-4(A). ROWGOWSKI COIL MEASUREMENT CIRCUIT

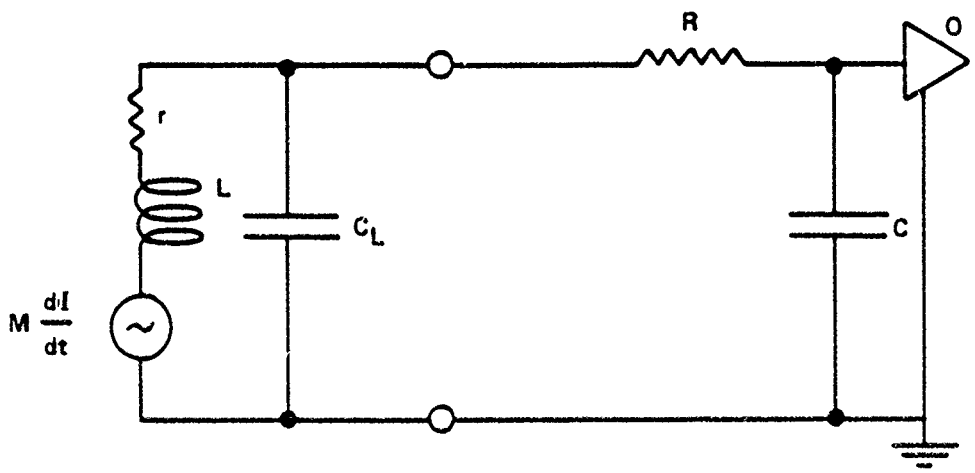

FIGURE C-4(B). EQUIVALENT CIRCUIT

Parameters for the design typically used, and described later, are:

Table C-1. NSWC Rogowski Coil Parameters

I 100 kA	a = 1.714 mm
L = 6.96 μH	D = 49.34 mm
M = 22.8 nH	n = 305
C_L 3 pF	r = 1Ω
	R = 10kΩ
Sensitivity k = 4.86 μ V/A	C = 0.47 μF

Self-integration

Now, when $L \times \frac{1}{i}\frac{di}{dt} >> R$ or $\omega L >> R$ it can be shown that the coil becomes self-integrating. Ignoring the capacitances, and noting that R>>r, we have

$$M \frac{dI}{dt} = L \frac{di}{dt} + i(R+r).$$

Clearly, if the $L\, d_i/d_t$ is larger than the second term,

$$M \frac{dI}{dt} \approx L \frac{di}{dt}$$

and

$$i \approx \frac{M}{L} I \approx \frac{1}{n} I.$$

In other words the coil behaves like a simple current transformer.

Then the RC integrator is superfluous, the signal starts to roll off at -6dB/octave for frequencies above $\omega = R/L$ or above 220 MHz. With this particular design the self-integrating frequency is very high. If R was reduced to 100Ω, then the self-integrating frequency would be 2MHz and a serious limitation. Clearly, this self-integration can be put to good effect if a very high frequency sensor is required; then the RC integrator is dispensed with and a suitable value of R chosen such that the coil is used at frequencies above R/L. However, in practice, lower frequencies are usually of interest and the self-integration technique is not employed. Stray capacitive effects also tend to mitigate against the use of the probe at high frequencies because of resonance. Self-integration is used as a method of band-limiting to prevent resonance, as discussed later.

Self-resonance and Cable Matching

From Figure C-4 it can be seen that the loop, L, r, C_L can resonate. With

the data given above, this circuit would be strongly resonant (Q=1523 at 35 MHz), and the gauge cannot be used at frequencies much beyond 20 MHz. This is not a serious limitation, although if the Rogowski coil were used in the self-integrating mode, then such resonances are intolerable. However, no cables are shown in Figure C-4, although in reality the oscilloscope would be situated several meters from the gauge.

In Figure C-5 cables have been included. The circuit here is only suitable for frequencies where cable impedance mismatching can be neglected. If the cable lengths l_1 or l_2 are such that their reflection times $2l_1/c$ or $2l_2/c$ (c is the wave velocity) are comparable with the time duration of interest, then this circuit cannot be used. However, for all the data presented in this report the maximum frequency is limited by the digital oscilloscopes to 7 MHz; the corresponding minimum risetime is therefore 50 nsecs and the equivalent length of 50Ω cable is 5m. The frequency response of the circuit can be improved by the inclusion of resistors R_1, R_2 and R_3.

Resistor R_3, a 50Ω resistor, is included to match to the impedance of the cable Z_0. Signals measured across the capacitor are halved at the cable input and doubled at the open circuit oscilloscope termination by wave reflection. The subsequent return reflection is matched at the source end. Consequently, the signal is unattenuated, devoid of reflection effects and delayed by l_2/c. It is assumed that cable losses can be ignored, which is correct in our case. Similarly R_2 matches the cable length l_1 to the RC integrator. Resistor R_1 is necessary to damp resonances in the Rogowski coil and may also match to the cable impedance Z_0, although this is not esential if R_2 is present. Usually, it is not necessary to use both R_1 and R_2.

To avoid resonance problems, R_1 can provide sufficient circuit damping, so that the Q of the LC circuit is less than or equal to 1/2. Without R_1 or R_2 the capacitive load of cable l_1 can lead to an undesirable low frequency resonance. Typically, the cable provides a load of 100 pF/m, so that the resonant frequency could be 6 MHz for a 1m cable. Note that a 1m cable has a pulse reflection time of only 10nsecs, thus the cable "rings-up" and behaves like a capacitor. R_1 or R_2 are thus employed to prevent the resonance. They in turn provide band limiting by forcing self-integration of the coil as described earlier. For critical damping R_1 = 132Ω. Then the signal is attenuated by -3dB at 6MHz and no resonance is possible; a value close to this is usually selected. A circuit that optimizes performance up to 5MHz is shown in Figure C-6. The right hand cable is matched for any length by the 50Ω resistor. Note that the integrator components R and C have been separated. This is done for two reasons. First, the separation facilitates cable matching by allowing the placement of the 50Ω at the load end of the cable. Secondly, it allows for improved magnetic field rejection as described below. Note that to obtain the exact integrator time constant, the cable capacitance between the 10kΩ and 50Ω resistors must be added to the 0.47μF, and similarly 10.050 kΩ must be used when the 50Ω is included; as before, the time constant is usually measured immediately prior the experiment.

External Magnetic Field Pick-up

As has been described above, the Rogowski coil has been designed to reject

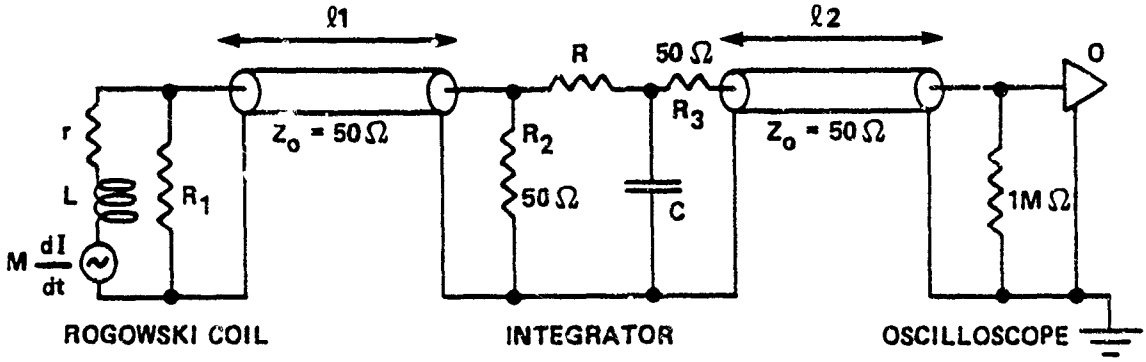

FIGURE C-5. COAXIAL CABLE CONNECTIONS

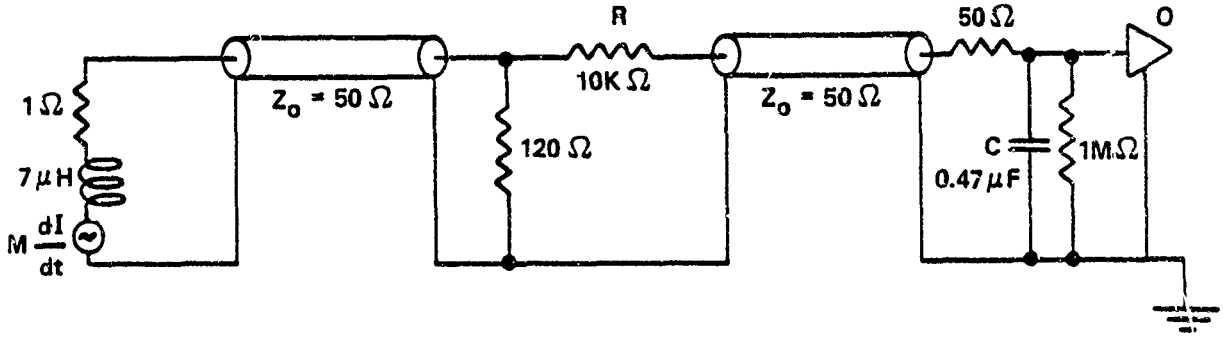

FIGURE C-6. OPTIMIZED COMPLETE CIRCUIT

external magnetic fields. However, great care must be taken to ensure equal effective lengths of toroid and return loop; the NSWC design described below is carefully manufactured to this end. However, the coaxial cables that are attached to the coil and the integrator must also be able to reject external fields at high frequencies. Regular coaxial cables such as RG58 do not have a perfect outer conductor. The outer braid has typically 90% coverage, which means that the cable's high frequency field rejection may be only -50dB. Consequently, in the large, rapidly changing fields of the pulsed power experiment of Chapter 7, circa 10 Tesla at frequencies of 30kHz, significant errors can be obtained. However, double braided coaxial cable such as RG223 has a rejection of circa -100dB, and this reduces such errors to negligible levels. RG223 is used as standard in the NSWC design.

Care must also be taken with the magnetic screening of the integrator circuit. We have found by experiment that die-cast circuit boxes do not provide adequate magnetic screening, e.g., ITT Pomona boxes. The most successful screening has been obtained with the integrator resistor, R, separated from the capacitor C. The resistor was soldered between the center pins of two BNC connectors and the ground consisted of a solid copper tube, 6.35 mm internal diameter and 25mm long, that was crimped in place. The tube thus formed a perfect coaxial high frequency magnetic shield. The precision capacitor was placed at the oscilloscope end of the cable, Figure C-6. This removed the capacitor from the hostile magnetic environment and also protected it from accidental damage in the explosive experiment.

NSWC Rogowski Coil Design and Calibration

The coil comprises of approximately 300 turns of #30 AWG insulated wire, wound on center of a RG58 coaxial cable which is insulated with its own polyethylene sheath. The center conductor serves as the return loop for the coil. The coil is tightly wound around the RG58, center so that the insulation of adjacent turns touches. Great care is taken to wind the coil as close to the end of the center core as possible to match the lengths of core and coil. A 1m length of RG223 cable is soldered to the end. A thin disc (0.4mm) of polyethylene insulation is inserted between the two ends of the toroid which are then held closely together and in line by a heat shrinkable PTFE (Teflon) sleeve.

The inductance of the coil can be calculated by use of the long solenoid (current sheet) formula, provided that the ratio of radii is large,

$$\frac{R}{a} >> 1. \quad \text{Then}$$

$$L = \frac{\mu_o n^2 a^2}{2R} = \frac{\mu_o n^2 a^2}{D} .$$

Now from Eq. C-2 we know that

$$M = \frac{\mu_o n a^2}{D}$$

so

$$L = nM .$$

Clearly, L can be found by measurement or calculation, and thus M is obtained if n is known. This is only approximate because even a close wound toroid does not behave as a perfect current sheet; there are some small flux losses although the correction is usually small. For example, the coil design described here has the following data:

TABLE C-2. INDUCTANCE CALCULATION DATA

a = 1.714mm	L = 6.960 μH (calculated)
D = 49.34mm	P (outer diameter of #30 wire) 0.482mm
n = 305	δ (core diameter of #30 wire) 0.254mm
M = 22.8 nH (calculated)	

Note that "a" represents the radius of the center core of the RG58 plus the radius of the coil wire; it is thus the mean radius that serves as the magnetically sensitive cross section of the coil. The error in L due to leakage can be calculated using the following formula due to Grover[17],

$$\Delta L = \mu_o \, an \, (G+H),$$

where G is a function of the ratio of wire diameter δ, to winding pitch P, G(δ/P) = 0.0838. Similarly H is a function of n, H(n) = 0.3336 from tables.[17] Thus,

$$\Delta L = 274 \text{ nH}$$

and

$$L = 6.960 - 0.274 \text{ μH} = 6.69 \text{ μH}.$$

Thus the flux leakage represents a 4% error. Consequently the measurement of L and n allows a calculation of M with an error of 4%.

The coils are usually calibrated against a Pearson 1423 current transformer which is accurate to within 1%. The 40kV capacitor bank, described in Chapter

7, is charged to approximately 5kV, then discharged, via the closing switch, into a resistor or a 7.3 μH inductor. The resultant current flow is simultaneously monitored by the Pearson gauge and the coils under calibration on digital oscilloscopes. The Rogowski coil data are corrected for the time constants of their integrators as described above. The results are plotted graphically against the Pearson record, and straight line least square fits are used to produce the desired calibrations.

DISTRIBUTION

	Copies
Commander Naval Air Systems Command Attn: AIR-350	1
AIR-440 (G. Heiche)	
AIR-54131	1
AIR-54131 (R. Jaramillo)	1
AIR-00D4 (Library)	1
Department of the Navy Washington, DC 20361	
Commander Naval Sea Systems Command Attn: PMS-400M	1
SEA-06H3	1
SEA-09B312	1
SEA-06R	1
SEA-62E	1
SEA-63R (F. Romano)	1
SEA-62D32 (G. Edwards)	1
SEA-62YB	1
SEA-62Y13C	1
SEA-62Z	1
SEA-62Z31E	1
SEA-06642	1
Department of the Navy Washington, DC 20362	
Chief of Naval Research ATTN: ONR-1132P (R. Miller)	1
ONR-12D	1
ONR-1112 (R. Junker)	1
ONR-01232L (Technical Library)	1
Department of the Navy Arlington, VA 22217	
Defense Technical Information Center Cameron Station Alexandria, VA 22314	12

	Copies
Commander Naval Weapons Center Attn: Technical Library	1
Code 3835 (R. G. Sewell)	1
Code 3205 (J. Bryant)	1
Code 3262 (G. Greene)	1
Code 3265 (T. Joyner)	1
Code 385	1
Code (E. Royce)	1
Code (D. Mallory)	1
China Lake, CA 93555	
Director Naval Research Laboratory Attn: J. Aviles	1
J. Ford (B. 704T)	1
A. Stolovy	1
I. Vitkovitsky (B. 71)	1
Technical Information Section	2
Washington, DC 20375	
Director Defense Advanced Research Projects Agency Attn: H. D. Fair	1
P. Kemmey	1
J. Entzminger	1
Library	1
Washington, DC 20301	
Commanding Officer Naval Weapons Station Attn: R & D Division	1
L. Rothstein	1
Yorktown, VA 23691	
Air Force Office of Scientific Research Attn: Col. R. Detweiler	1
Col. H. Bryan	1
T. Walsh	1
Library	1
Bolling Air Force Base Washington, DC 20332	

	Copies
Superintendent Naval Postgraduate School Attn: Library Monterey, CA 93940	1
Commanding Officer Harry Diamond Laboratories Attn: Library R. K. Warner R. Garver W. Gray W. Petty 2800 Powder Mill Road Adelphi, MD 20783	1 1 1 1 1
Commander Naval Intelligence Support Center Attn: NISC-30 4301 Suitland Road Washington, DC 20390	1
Chief of Naval Research Office of Naval Technology Attn: ONT-213 (D. Siegel) ONT-21 (E. Zimet) ONT-23 (A. Faulstich) Washington, DC 20362	1 1 1
Commanding Officer Naval Ordnance Station Attn: Research and Development Department Technical Library Indian Head, MD 20640	1 1
Commanding Officer Ballistics Research Laboratory USARRADCOM Attn: Technical Library R. Frey F. Grace P. Howe R. Jamieson H. Reeves J. Starkenberg W. Walters Aberdeen Proving Ground Aberdeen, MD 21005	1 1 1 1 1 1 1 1

	Copies
Air Force Armament Test Laboratory Attn: DLYV (A. Rutland) DLDE (T. Floyd) DLJW (R. McGuire) Eglin Air Force Base, FL 32542	1 1 1
Director Army Material Systems Analysis Agency Attn: DRXSY-D DRXSY-J (J. McCarthy) Aberdeen Proving Ground, MD 21005	1 1
Commander Air Force Armament Development and Test Center Attn: Lt. Col. Scott Eglin Air Force Base, FL 32542	1
Commanding Officer Aberdeen Research and Development Center Attn: Technical Library Aberdeen, MD 21005	1
Commanding Officer U. S. Army Armament Research and Development Center Attn: F. Owens N. Slagg R. Walker Technical Library Dover, NJ 07801	1 1 1 1
Lawrence Livermore National Laboratory Attn: L. Green M. Finger B. Hayes H. Kruger N. Keeler E. Lee R. McGuire P. Urtiew W. Von Holle F. Rhee, Code L-299 Livermore, CA 94550	1 1 1 1 1 1 1 1 1 1

	Copies
Director Los Alamos National Laboratory	
Attn: G. Andrews (M-9)	1
M. Butner	1
W. Davis (M-9)	1
C. Max Fowler (M-6)	1
T. Frank	1
D. Erickson (M-6)	1
M. Ginsberg (M-8)	1
J. Goforth (M-6)	1
T. McDonald	1
R. Rabie (M-9)	1
R. Rogers	1
J. Shaner (M-6)	1
G. Wackerly	1
Technical Library	1
Los Alamos, NM 87544	
Director Johns-Hopkins Applied Physics Laboratory	
Attn: S. Koslov	1
Technical Library	1
Johns-Hopkins Road Laurel, MD 20707	
University of Maryland	
Attn: Plasma Physics Dept.	1
H. Griem	1
Technical Library	1
College Park, MD 20740	
SRI International 333 Ravenswood	
Attn: M. Cowperthwaite	1
Menlo Park, CA 94025	
Texas Technical University	
Attn: M. Kristiansen	1
Department of Electrical Engineering Lubbock, Texas 79409	
AAI Corporation	
Attn: E. P. Connell	1
P. O. Box 6767 Baltimore, MD 21204	

	Copies
ARTEC Associates, Inc.	
Attn: R. Barry Ashby	
S. P. Gill	
26046 Landing Road Haywood, CA 94545	
F. J. Seiler Research Laboratory	
Attn: Col. B. Loving	
U. S. Air Force Academy Colorado Springs, CO 80840	
Battelle Research Institute	
Attn: J. Backofen	1
Columbus Laboratories 505 King Avenue Columbus, OH 43201	
Scientific Research Associates, Incorporated	
Attn: B. Weinberg	1
P. O. Box 498 Glastenbury, CT 06033	
Science Applications	
Attn: W. Chadsey	1
8330 Old Courthouse Road Suite 510 Vienna, VA 22180	
Director Sandia National Laboratories	
Attn: D. Hayes	1
J. Kennedy	1
R. E. Setchell	1
P. L. Stanton	1
Technical Library	1
P. O. Box 5800 Albuquerque, NM 87115	
Honeywell Defense	
Attn: P. DiBona	1
600 2nd Street N. Hopkins, MN 55343	
Library of Congress	
Attn: Gift and Exchange Division	4
Washington, DC 20540	

	Copies
Maxwell Laboratories, Inc.	
Attn: J. Devoss	1
P. Elliot	1
8835 Balboa Avenue	
San Diego, CA 92123	
Department of Electrical Engineering	
Bell Hall	
Attn: A. Gilmour, Jr.	1
State University of New York at Buffalo	
Buffalo, NY 14214	
Georgia Institute of Technology	
Georgia Tech. EES; RAIL/RED	
Attn: D. Ladd	1
Atlanta, GA 30332	
AVCO Everett Research Laboratory	
Attn: C. Pike	1
2385 Revere Beach Parkway	
Everett, MA 02149	
Physics Internation Company	
Attn: J. N. Benford	1
R. F. Johnson	1
A. Rutherford	1
2700 Merced Street	
San Leandro, CA 94577	
Enig Associates	
Attn: J. Enig	1
13230 Ingleside Drive	
Beltsville, MD 20705	
Science Applications International Corporation	
Attn: E. T. Toton	1
1710 Goodridge Drive	
McLean, VA 22102	
Zernow Technical Services, Inc.	
Attn: L. Zernow	1
425 W. Bonita Avenue	
Suite 208	
San Dimas, CA 91773	

	Copi
CETR	
New Mexico Tech	
Attn: P. Anders Persson	
Socorro, NM 87801	
New Mexico Tech	
TERA	
Attn: M. Lamar Kempton	
Socorro, NM 87801	
British Embassy	
Attn: R. Kelly	
British Defence Staff	
3100 Massachusetts Ave., N.W.	
Washington, DC 20008	
Royal Ordnance Ammunition	
Attn: P. R. Lee	
Euxton Lane	
Euxton, Chorley, Lancs.,	
PR7, 6AD UK	
Atomic Weapons Research Establishment	
Attn: C. Beck	
G. Eden	
G. Foan	
D. Grief	
Aldermaston, Reading,	
BERKS, RG7 4PR, UK	
Atomic Weapons Research Establishment	
Attn: H. R. James	
Foulness Island, Southend-on-Sea	
Essex, UK	
Royal Armament Research and Development Establishment	
Attn: J. Connor	1
I. Cullis	1
P. Haskins	1
G. Hooper	1
C. Hutchinson	1
M. Nash	1
Fort Halstead	
Sevenoaks, Kent, UK	

Copies

Royal Armament Research and Development Establishment
Attn: K. Bascombe 1
J. Jenkins 1
D. Mullenger 1
A. Owen 1
B. Hammant 1
A. Kosecki 1
Waltham Abbey, Powdermill Lane
Essex EN9 1BP, UK

Defence Research Information Center
Attn: Technical Library 1
St. Mary Cray, Kent, UK

University of Wales, Aberystwyth
Attn: H. Edwards 1
G. Thomas 1
Department of Physics
Wales, UK

Washington State University
Attn: R. Fowles 1
Y. Gupta 1
Pullman, WA 99164-2814

Oak Ridge National Laboratory
Attn: O. H. Crawford 1
P. O. Box X
Oak Ridge, TN 37831 1

Internal Distribution

E231 9
E232 3
F (R. T. Ryland) 1
F53 (E. Nolting) 1
G13 (D. Dickinson) 1
G22 (D. Brunson) 1
(W. Mock) 1
(S. Waggener) 1
R10A 1
R10B 1
R10C 1
R10D 1
R10F 1
R10J 1

	Copies
R11	
R11 (T. Hall)	
(E. Anderson)	
R11 (J. Short)	
R12	
R12 (J. Erkman)	
(W. Filler)	
(L. Montesi)	
(P. Spahn)	
R13	
R13 (R. D. Bardo)	
(A. R. Clairmont)	
(C. S. Coffey)	
(N. L. Coleburn)	
(D. L. Demske)	1
(W. L. Elban)	1
(J. W. Forbes)	1
(B. C. Glancy)	1
(R. Granholm)	1
(S. J. Jacobs)	1
(H. D. Jones)	1
(P. Gustavson)	1
(K. Kim)	1
(E. R. Lemar)	1
(R. J. Lee)	1
(T. P. Liddiard)	1
(P. J. Miller)	1
(D. Price)	1
(C. Richmond)	1
(H. W. Sandusky)	1
(M. Smith)	1
(G. Sutherland)	1
(D. G. Tasker)	10
(J. W. Watt)	1
(F. J. Zerilli)	1
R14	1
R14 (J. Gaspin)	1
(D. O'Keefe)	1
(D. Lehto)	1
R15	1
R15 (W. Faux)	1
(G. Hammond)	1
(W. Smith)	1
(R. Tussing)	1
(W. Smith)	
R16	